ARCHIVES OF ACOUSTICS
11, 1, 3-12 (1986)

REACTION DELAY TIME IN THE PROCESS OF DETECTION AND DISCRIMINATION OF ACOUSTIC SIGNALS*

ANDRZEJ RAKOWSKI, ANTONI JAROSZEWSKI

F. Chopin Academy of Music
00-368 Warszawa, ul. Okólnik 2

Reaction delay times in listeners with musical training to auditory stimuli at a level near the threshold of hearing were determined. Listeners were to detect these stimuli (detection) or state whether successive stimuli have the same or different pitch (discrimination). Reaction times in listeners in discrimination were distinctly longer than in detection tasks. Reaction delay time provide information about the relative difficulty of the task.

Introduction

In 1940 Rene Chocholle [3] proved that the auditory reaction time can be used as an evaluation criterion of sound loudness. This idea was then applied by Stebbins and Miller [18], Kohfeld [7], Moody [10], [11], O'Connor *et al.* [12], Pfingst *et al.* [13], [14], Stebbins and Miller [18] and Stebbins [19] in investigations of the threshold of hearing and of the loudness of signals with people and animals. It was also used by Beaton and Miller [1] and Miller *et al.* [8], [9] in research on the response of single neurons, and by Sidley *et al.* [18] in investigations of visual reactions.

It seems obvious that, as Pfingst *et al.* [13] state, the dependence of the time of reaction to auditory stimuli on the sound pressure level and frequency "*illustrates the characteristic properties of the organ of hearing*". It should be emphasized though, that until now the greater part of research on auditory reaction times was concerned with the simplest reaction forms connected with functioning of the organ of hearing, mostly detection. In this case

* Research was conducted in the framework of an Interdepartamental Programme MR. I. 24.

the reaction time consists mainly of the delay of the motor reaction in relation to the acoustic stimulus. But measurements of the reaction time can also be applied in more complex tasks related to the functioning of the organ of hearing, such as comparison, discrimination and recognition of auditory stimuli. These tasks require the engagement of qualitatively different functions of the auditory perception system (e. g. memory) and it may take a much longer time. It seems that the time neccessary to fulfill these tasks should be in such a case referred to not as the "*reaction time*" but "*time of auditory processing*". This notion results from the following argumentation. The reaction time in a listener consists of two components: "*time of the motor reaction*" and "*time of data processing*". It can be assumed (although the confirmation of this thesis in respect to detection and discrimination processes requires separate research) that the motor reaction time depends in a very small extent on the type of task. This component dominates in the simplest, detection type, tasks; therefore the term – "*reaction time*" seems appropriate in that case for the definition of the total time between the stimulus and reaction. In more and complicated tasks, concerning auditory discrimination for example, longer and longer part of the time between the stimulus and reaction is taken up by the process of analysing and data processing. For this reason the total reaction time may be more accurately referred to as the signal "*processing time*" or "*auditory processing time*".

The aim of this paper is the presentation to what extent, and how, the auditory processing time of signals at a level near the threshold of hearing increases with the rise of the difficulty of a task; from simple signal detection to detection of progressively decreasing differences of their pitchs, in particular. The experiment was conducted in certain correlation to the experiment by CARDOZO [2], who investigated the detection and discrimination of short sound pulses. However, a different measurement methodology was applied; better trained listeners participated in the experiment, and first of all together with the correctness level of response of the listeners, the reaction time was noted, what allowed the comparison of these two characteristics of the response to a given task. Experimental results show that the time of reaction to auditory stimuli can provide a measure of task difficulty in the detection process as well as in the discrimination process.

1. Procedure

The experimental procedure comprised a cyclic presentation of two sinusoidal pulses with 1500 ms duration, separated by a 700 ms interval, to the listeners. Pulse duration was long enough to ensure optimum evaluation of the sound pitch. The duration of the interval between the pulses was chosen, to fulfill two conditions at the same time: a) strong enough

memory trace of the pitch of the first pulse in the moment of appearance of the second pulse, with which the first pulse was compared and b) lack of an influence of the first pulse on the second pulse, that would cause a pitch shift of the latter due to poststimulatory masking [16]. Repetition periods of presented pulse pairs were randomly arranged in such a way that the begining of every following pair was separated from the begining of the preceeding pair by a $n \cdot 6250$ ms time interval, where n was a natural number changing randomly in a range from 1 to 4. Therefore, listeners did not know in which moment of the observation time of a maximal span of 4×6250 ms the signal to be detected or discriminated will appear.

The signal frequency in the first pulse of every presented pair equalled always 1000 Hz, while every second pulse was subjected to the following randomization procedure: In detection tasks it was completely damped in randomly chosen pairs and in pitch discrimination tasks it was detuned in relation to the first pulse by a certain frequency difference $\pm \Delta f$ in randomly chosen pairs. The number of pairs in which the second pulse was completely damped or detuned in relation to the first pulse always constituted 50% of the total number of pulses in a series, while the number of pulses detuned positively $(+\Delta f)$ equalled the number of pulses detuned negatively $-\Delta f$. The pulse frequency difference in a pair, Δf, was 9, 3 and 1Hz in individual tasks.

The time, Δt, between the begining of the second pulse in a pair and the signalling by the listener of a decision was taken as the measure of the reaction time (auditory signal processing). The decision was signalled by pressing a button and it could mean

a) in detection tasks: "*I heard that the second pulse* ***was present***"

b) in discrimination tasks: "*I heard that the second pulse* ***differed from the first one***".

Listeners were instructed to press the button as quickly as possible, but only when they were sure that:

a) in detection: the second signal was present

b) in discrimination: the sceond signal was different.

The reaction time values and the values of the percentage level of correct answers in every experimental series was read of digital clocks, which were switched on with the begining of the second pulse and stopped by the decision signal. Every presented test consisted of a series of 100 pairs of signals.

Experiments were carried out in a silenced chamber with the use of a *QUAD* electrostatic loudspeaker. In detection tasks stimuli were presented at the threshold level (*sensation level* 0 dB *SL*) and at levels: 2.5, 5.0 and 7.5 dB *SL*. In discrimination tasks stimuli were presented at levels: 5, 10 and 15 dB *SL*. Sound pressure levels corresponding to the given dB *SL* values were determined separately for every listener at the begining of every session. Individual thresholds of hearing were determined using the method of limits.

2. Listeners

Two men and two women-students of the Academy of Music, aged 24–27, with an otologically normal audition, made up the group of listeners. They were chosen from a group of 25 students from the same school, as they achieved best results in the initial tests of pitch discrimination. Three persons from the group have previously taken part in psycho-acoustic experiments, the remaining three persons passed additional training, so the results achieved by all listeners in the described experiment were similar. Two listeners had the same response time to visual stimuli, equalling 160 ms. All listeners were paid for the participation in the experiment and were therefore strongly motivated.

Prior to the begining of measurements every listener stayed in an acoustically isolated, silenced chamber for at least 10 min in order to stabillize the threshold of hearing. Moreover, listeners were informed that they should give up the participation in measurements in case of a bad psychophysical disposition.

3. Results

Fig. 1 presents results of detection experiments, expressed as medialn values of the percentage of correct answers at various signal sensation levels.

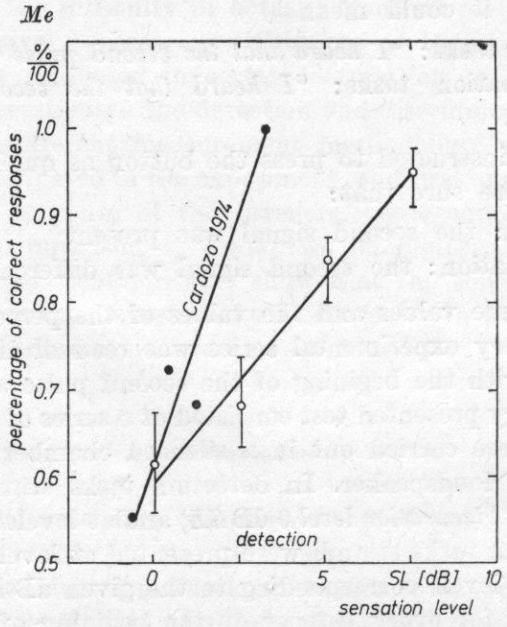

Fig. 1. Psychrometric curves for signal detection. Results obtained by B. L. CARDOZO (filled-in circles) are shown for comparison

Each of the four data points represents a median calculated from 120 hundred individual decisions made by the group of four persons. Vertical bars mark the dispersion of results, determined as interquarter intervals.

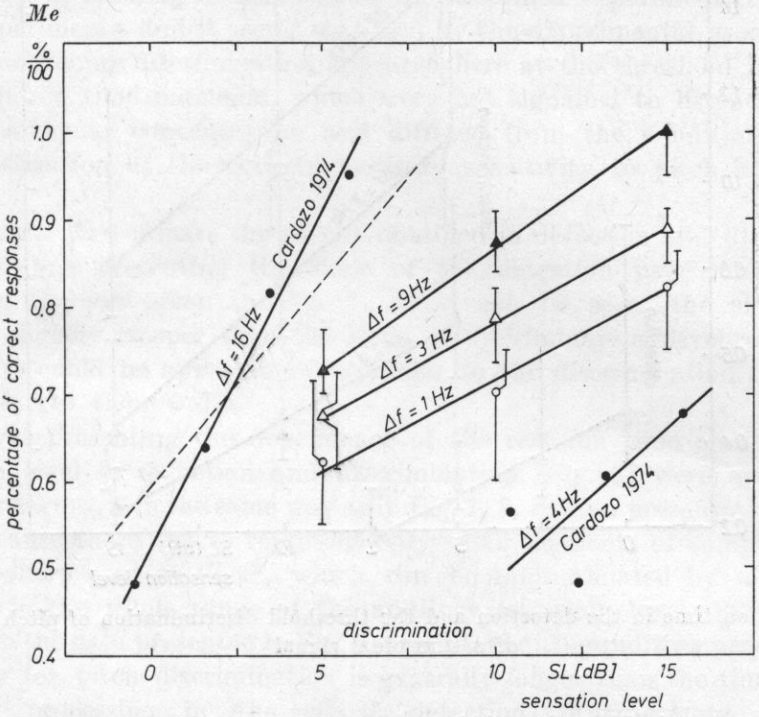

Fig. 2. Psychrometric curves for signal frequency threshold discrimination. Signals with varying frequency intervals Δf. Results obtained by B. L. CARDOZO (filled-in circles) are shown for comparison. Dashed line marks the slope of the psychrometric curve durin signal detection (according to Fig. 1)

Fig. 2 presents medians of percentage levels of correct answers in near the threshold pitch discrimination experiment. Vertical bars mark the dispersion of the results, determined as interquarter intervals. Each data point is determined by 120 hundred (at $\Delta f = 9$ and 3 Hz) or 80 hundred (at $\Delta f = 1$ Hz) individual decisions of listeners. Measurements obtained by CARDOZO [2] for $\Delta f = 16$ and 4 Hz are given for comparison. However, it has to be noted that the results by Cardozo presented here for comparison are based on a significantly smaller number of observations (50 decisions for data point) than the results of the experiments presented here.

Fig. 3 shows the values of response times of the group of listeners in the described above detection and discrimination experiments. The median values are given and the dispersion as intraquarter intervals.

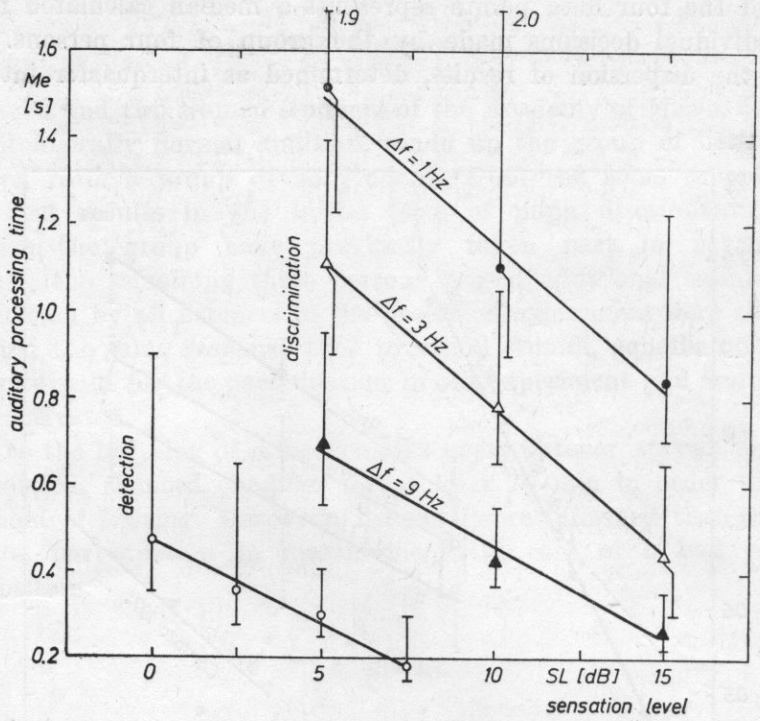

Fig. 3. Reaction time in the detection and the threshold discrimination of pitch in pulses of a sinusoidal signal

4. Discussion of the results and conclusions

A comparison of results obtained in the detection experiment (Fig. 1) with CARDOZO'S results [2] proved that psychrometric curves obtained here are less steep. This can be caused by the fact that the tasks of CARDOZO'S listeners were slightly different. They were informed in which time moments pulses for detection or discrimination can appear.

While data obtained in thes present experiments concerning the percentage level of correct answers in the signal detection (Fig. 1) approximately correspond with the values encountered in CARDOZO'S papers [2], data concerning the precision of pitch discrimination (Fig. 2) differ from the data published previously. In comparison with the data obtained by Cardozo it can be observed that our listeners had higher efficiency in pitch discrimination. This is due to the applied procedure (longer duration of pulses), as well as most probably to the differences in the predispositions and experiences of listeners.

If the results of pitch discrimination presented here were to be compared with the results of different experiments published previously by the authors of this

paper [4–6], 15, 17 the situation would 100 k differently. This confrontation shows that listeners in the described experiment demonstrated lower sensitivity to pitch differences. This is partially caused by a slightly lower level of training of listeners in the described experiment, than in previous experiments, and it seems that also by the experimental procedure used. Signal undergoing discrimination appeared here at the threshold level in randomly chosen time moments, which were not signalled to listeners. This required particular concentration and differed from the conditions in which the investigation of the extreme auditory sensitivity to pitch differences is possible.

In order to compare the results obtained in detection and discrimination a dashed line presenting the slope of the detection psychrometric curve from Fig. 1, was given in Fig. 2. As it can be seen, the slope of this curve is slightly steeper than the slope of discrimination psychrometric curves and it cuold be approximately similar to the discrimination curve if the Δf was larger than 9 Hz.

Curves presenting the dependence of the reaction time on the auditory sensation level in detection and discrimination (Fig. 3) were approximated by line ar segments in the same way as in Fig. 1, 2. Such a presentation was possible, because these curves represent only small segments of complete "*curves of the auditory reaction time*", which can be approximated by a hyperbolic function in the whole range of the auditory sensation levels [13].

From the data presented in Fig. 3 it results that the auditory processing time necessary for pitch discrimination is generally longer than the time of simple auditory processing in the signal detection. Furthermore, the auditory processing time depends on: a) the difficulty of the task, b) the auditory sensitivity level in the region near the threshold. From the comparison of detection and discrimination curves done in Fig. 3 it results that in the experimental conditions of the described investigation the reaction time in the detection of a signal at a threshold level, 0 dB *SL*, corresponds approximately to the auditory processing time in the discrimination of pitch in pulses differing by $\Delta f = 9$ Hz presented at the 10 dB *SL* level or pulses differing by $\Delta f = 3$ Hz presented at the 15 dB *SL* level.

Vertical bars mark interquarter intervals corresponding to each data point. As it can be seen, the dispersion like the reaction time, increases with increase of the task difficulty. A similar features characterize the intraindividual variability not marked in the figure, what is consistent with the general rules of the detection theory.

Data shown in Fig. 1–3 were obtained in the course of the same experiments and are complementary. Therefore, it can be evaluated for each data point to what extent the auditory processing time is related to the obtainment of a specific percentage level of correct answers,

P_c. Fig. 4 shows the relationship between the percentage level of correct answers and corresponding values of the auditory processing time in various tasks.

Dependences shown in Fig. 4 illustrate indirectly the relationship between the degree of difficulty of an auditory task and the time, in which

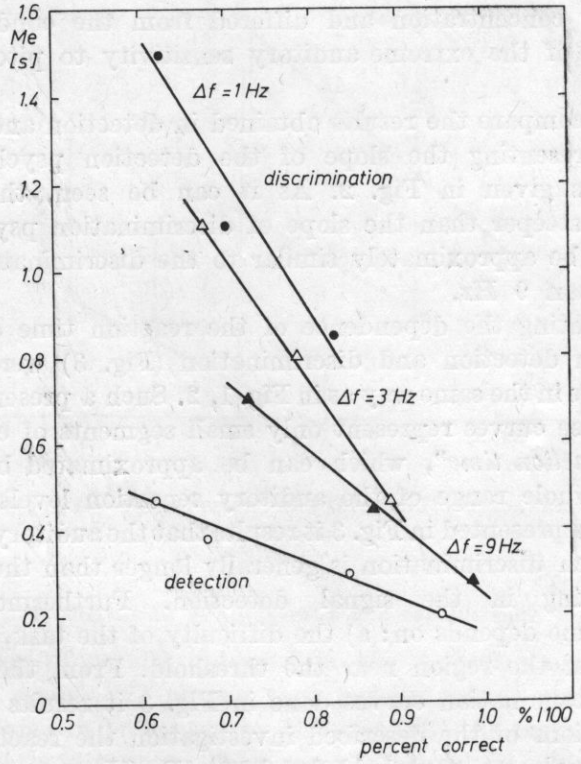

Fig. 4. Relation between the degree of performance correctness and the auditory reaction time in the of detection and threshold discrimination of acoustic signals

this task can be performed. Assuming a definite percent correct level of answers, the auditory reaction time (alias auditory processing time) can provide a difficulty measure of a task.

References

[1] R. Beaton, J. Miller, *Effects of behavioral manipulations on the activity of single units in the auditory cortex of the rhesus monkey*, 80–th Ann. Conv. AM. Psychol. Assoc. (1972).

[2] B. L. Cardozo, *Some notes on frequency discrimination and masking*, Acustica, **31**, 330–336 (1974).

[3] R. CHOCHOLLE, *Variation des temps de reaction auditifs en fonction de l'intensité à diverses frequences*, Am. J. Psychol., **41**, 65–124 (1940).

[4] A. JAROSZEWSKI, A. RAKOWSKI, *Pitch shifts in poststimulatory masking*, No 815, 8th ICA, London 1974. Published: Acustica, **34**, 220–223 (1976).

[5] A. JAROSZEWSKI, *A new method for determination of frequency selectivity in post-stimulatory masking*, H-40, 9th ICA, Madrid 1977. Published: Acustica, **41**, 327–333 (1979).

[6] A. JAROSZEWSKI, *Effects of feedback and masking on the data from psychoacoustical experiment*, J. Acoust. Soc. Am. (submitted for print).

[7] D. L. KOHFELD, *Stimulus intensity and adaptation level as determinants of simple reaction time*, J. Exp. Psychol., **76**, 468–473 (1968).

[8] J. M. MILLER, M. GLICKSTEIN, W. C. STEBBINS, *Reduction of response latency in monkeys by a procedure of differential reinforcement*, Psychonomic Sci., 177–178 (1966).

[9] J. M. MILLER, D. SUTTON, B. PFINGST, A. RYAN, R. BEATON, G. GOUREVITCH, *Single cell activity in the auditory cortex of rhesus monkeys: behavioral dependency*, Science, **177**, 449–451 (1972).

[10] D. B. MOODY, *Reaction time as an index of sensory function*, in: Animal Psychophysics, Stebbins, W. C. Ed., Appleton Centry Crofts, N. York, 277–302 (1970).

[11] D. B. MOODY, *Behavioral studies of noise-induced hearing loss in primates: loudness recruitment*, Adv. Oto-Rhino-Laryngol., **20**, 82–101 (1978).

[12] T. O'CONNOR, R. HIENZ, J. MILLER, *Reaction time as a measure of threshold and suprathreshold hearing III. The effects of stimuls duration*, J. Acoust., Soc. Am. **55**, 451 A (1974).

[13] B. E. PFINGST, R. HIENZ, J. KIMM, J. MILLER, *Reaction – time procedure for measurement of hearing I. Suprathreshold functions*, J. Acoust. Soc. Am., **57**, 421–430 (1975a).

[14] B. E. PFINGST, R. HIENZ, J. MILLER, *Reaction – time procedure for measurement of hearing II. Threshold functions*, J. Acoust. Soc. Am., **57**, 431–436 (1975b).

[15] A. RAKOWSKI, *Pitch discrimination at the threshold of hearing*, 20 H6-, 7th ICA, Budapest (1971).

[16] A. RAKOWSKI, I. J. HIRSH, *Poststimulatory pitch shifts for pure tones*, J. Acoust. Soc. Am., **68**, 467–472 (1980).

[17] A. RAKOWSKI, A. JAROSZEWSKI, *Analysis of some factors influencing frequency discrimination*, K-2, 95th JASA Meeting, Providence, Rhode Island 1978, J. Acoust. Soc. Am. 63, Suppl. No **1**, 29–30 (1978).

[18] N. A. SIDLEY, H. G. SPARLING, E. W. BEDARF, R. H. HISS, *Photopic spectral sensitivity in the monkey: methods for determining and initial results*, Science, **150**, 1837–1839 (1965).

[19] W. C. STEBBINS, J. MILLER, *Reaction time as a function of stimulus intensity for the monkey*, J. Exp. Anal. Behav., **1**, 309–312 (1964).

[20] W. C. STEBBINS, *Auditory reaction time and the deviation of equal loudness countours for the monkey*, J. Exp. Anal. Behav., **9**, 135–142 (1966).

Received on 13 October, 1984; revised version on 7 June 1985.

ARCHIVES OF ACOUSTICS
11, 1, 13-24 (1986)

THEORY OF THE REFLECTIVE LOCALIZATION OF SOUND SOURCES

GUSTAW BUDZYŃSKI

Department of Sound Engineering of the Telecommunication Institute Gdańsk Technical University, Poland

In order to explain the mechanism of distance localization of sound sources with hearing, a hypothesis was stated that a *"situation analyzer"* exists in the man central nervous system. The analyzer is capable of perceiving not only the direction of direct and reflected sounds reaching the listener, but also the position of reflecting surfaces, distance of the reflection points and corresponding angles, for the so-called early reflected sounds.

On the basis of the above mentioned hypothesis, and considering certain acoustic situations and some visual analogies, foundations for a new theory of the reflective localization of sound sources have been created. Suggestions important for the psychoacoustics in general as well as for room – acoustics and studio – technique applications have been outlined.

1. Introduction

The ability of sound source localization is an important property of the sense of audition. Binaural audition allows the precise localization of the direction of a sound source in the space surrounding the listener with an angular inaccuracy below 1° to 20°, depending on the position of the source in respect to the listeners head. It also allows the estimation of the distance between the sound source and listener in rooms with walls reflecting sounds, with a good accuracy.

The mechanism of stereophonic audition is based on the properties of binaural hearing. With the application of a pair of spaced loudspeakers supplied with adequate signals apparent sources are formed, which are localized in the sound image similarily as the real sources, although generally with lower accuracy. Stereophonic hearing is of great practical importance to the technique of stereophonic systems. That is why there is a wide and constant interest in the theories of directional hearing, manifested by many

publications concerned with this subject. For example, in BLAUERT'S monography [5] over six hundred papers concerned partially and in the whole with directional hearing, have been mentioned.

2. Former theories

The two oldest theories of the directional source localization are: the theory of the differences of the sound intensity on the entry to the left and right ear, and the theory of differences of signal access times to the left and right ear; both coming from RAYLEIGH, from the years 1877 and 1907.

A series of later theories is in reality only complements and expansions of the intensity and phase theories, which with these complements exist up to now, describing two parallely acting mechanisms of the source directional localization with the aid of audition. Mentioning here all individual theories, presented in detail in the literature [4] — [7], [9], would occupy too much place.

It should be noticed, that although the mechanism of the directional localization was thoroughly investigated theoretically and certain details were determined as goals of further research, the mechanism of the distance localization was not explained. Though there are several theories of the distance localization, still none of them explains the localization inaccuracies reaching up to about ten to twenty per cent.

The accessible in literature experimental data concerning the thresholds of directional localization in specific research situations, come mostly from experiments conducted under a free acoustical field conditions, e. g., in an anechoic chamber or in an articifially modelled field. These experiments are not fully competent in relation to the real conditions, especially in the view of the influence of reflected sounds on the localization mechanism.

3. Theory of reflective localization

The *law of the first wave front* formulated by CREMER in 1948, or the *precedence effect*, so-called by WALLACH in 1949, soon found a practical confirmation in experiments conducted by HAAS and drove the attention away from the influence of reflected sounds on source localization. For it was generally acknowledged, that only the direct sound from the source was the signal, which makes subjective localization possible, blocking at the same time out the sensitivity of the localization mechanism to following reflected sounds coming from this source during the time of the HAAS constant, that is about 20–50 ms.

However, cases of a lack of blocking in the time range of the HAAS constant were soon stated [8]. Informations appeared about a better localiza-

tion ability in rooms with reflecting walls, than in rooms with completely absorbing walls. Similar observations were made especially in the 60-ties in the course of determining the ability of directional localization of sound sources under water. This was done by free divers in not silenced pools [3]. It was found, that the threshold of angular localization, equalling about 10° in a highly damped, almost anechoic pool, decreased to about 5° for experiments in a pool with well reflecting walls.

The above mentioned informations showed the possible share of reflected sounds in the localization mechanism, however, they were not applied to generalizations. Lately, BENADE [2] drew attention to the fact, that the sequences of first reflections, reaching the listener in a room, some how increase his ability of localizing sound sources.

Auditory localization of sources in a half-open space e. g. in two street situations can easily convince us of the influence of reflections. The first situation is, when the street surfaces and objects in the street are not attenuated, and the second one when the same street covered with a thick layer of freshly fallen, fluffy snow. Source localization in a snow covered street is distinctly more difficult, just because for the lack of reflected sound.

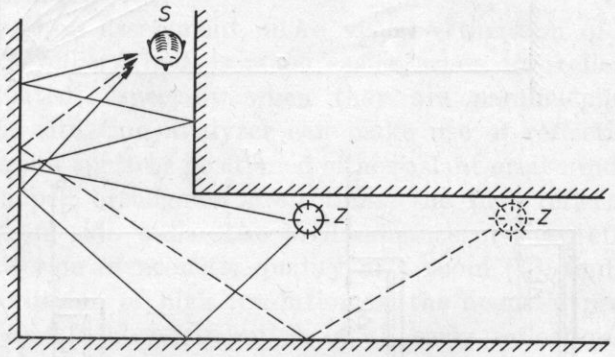

Fig. 1. Localization example without any application of a direct sound

The results of considerations of cases, where the direct sound does not reach the listener at all, are an argument against the theory, stating that the first front of a direct sound has a decisive importance for localization. A *L*-shaped corridor can be an example (Fig. 1). No direct sound, or single reflected sound reaches the listener *S*. However, as experiments show, the listener correctly localizes the moving source of sound emitted by a person moving in the corridor. So, the sounds reflected from walls two, three and may be more times and then reaching the listener from different directions, are responsible for the subrequent localizations.

Therefore a hypothesis can be made, that the above mentioned blocking mechanism does not exist and that reflected sounds have a contribution in

the localization mechanism. This hypothesis will not be contradictory to the law of the first wave front, if we assume that the sensory situation analyzer localizes not only the direction of the first and any following wave reaching the listener, but also it determines every time the position of the source on the basis of earlier perceived positions of the reflecting surfaces and the current evaluation of the directions from the point of reflection to the source (Fig. 2).

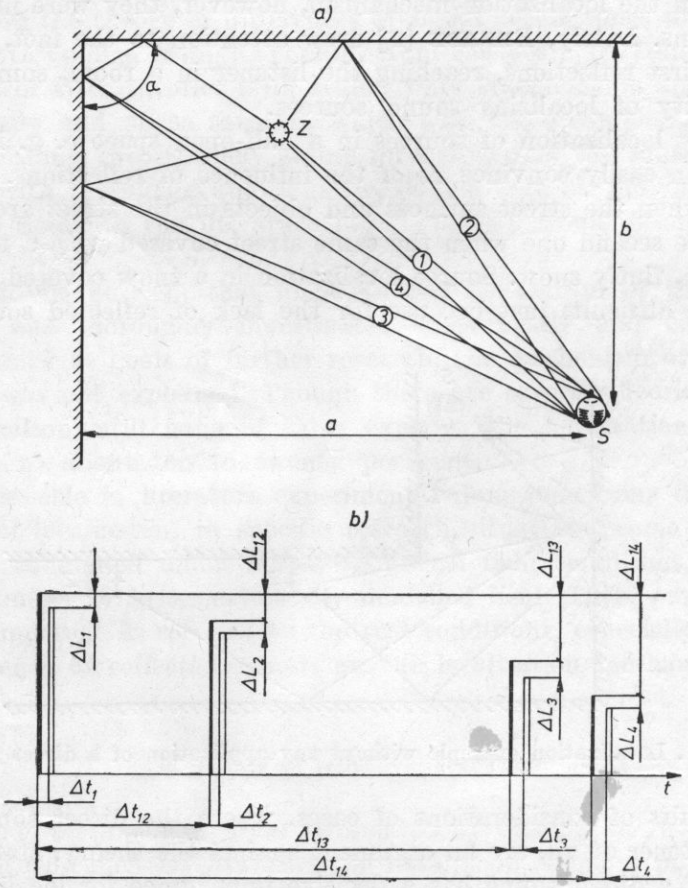

Fig. 2. Diagram of the contribution of reflected sounds in the localization of source Z: a) situation example; b) echogram of sounds reaching listener S: ⊥ to the left ear, ⫠ to the right ear

According to the previous theories, information about the directional localization of source Z, supplied to the listener, is based exclusively on the binaural difference, Δt_1 and ΔL_1. Meanwhile the information concerning the complete localization of source Z, supplied to the situation analyzer of the

listener, according to the reflective theory, consists of a set of values of the main delays and attenuations of reflections: Δt_{12}, ΔL_{12}, Δt_{13}, ΔL_{13}, Δt_{14}, ΔL_{14}, the binaural values fo delays and attenuations: Δt_1, ΔL_1, Δt_2, ΔL_2, Δt_3, ΔL_3, Δt_4, ΔL_4, and the earlier perceived distances to walls a, b and their angle α.

The assumption, that the positions of reflecting surfaces and objects are perceived earlier is obvious, because the room in which the localization is conducted is usually "*aurally known*", and mostly also known visually by the listener. This facilitates the estimation of the direction from point of reflection to the source. It should be presumed, that the mentioned here "*situation analyzer*" acts like a unit of the central nervous system, common to all man's senses. The work efficiency of the analyzer, working on the basis of the perceived acoustical signals, can be indirectly estimated, taking into account the localization accuracy of obstacles attained by blind.

The results of source localization on the basis of the first wave are compared in the situation analyzer with the localization results obtained on the basis of subsequent reflections, what increases the localization accuracy. The different directions of reflected waves, especiatly being at right angles to each other provides for the increase of the localization accuracy, due to the trigonometric relationships.

The aural direction assessment, alike visual estimation of the direction of reflections, e. g., billiard ball, is much easier, when the reflecting surfaces are regularily situated, especially when they are parallelepipedly shaped. In such a case the situation analyzer can make use of reflections of higher order, than in a case of surfaces positioned either aslant or at random. In rooms parallelepipedly shaped orthogonal projections, the first reflections come in the greater part from side walls. The predominance of side reflections, treated lately as a criterion of acoustic quality of a room [1], finds here an explanation as the criterion of high resolution of the acoustic perspective.

The assumption of the contribution of all early reflections in the process of sound source localization, that is the nonexistance of the reflection blocade, forces us to interpret the HAAS constant in a new way. Previously it was approximated at 20 to 50 ms, but practically it has a greater dispersion of values. According to the theory of reflective localization, the Haas constant finds a simple interpretation. It is the time in which the situation analyzer is still able to use the results of the analyzis of the reaching it reflected waves as informations on source localization. Waves reaching the situation analyzer after a longer period of time mostly after multiple reflections, are too difficult to analyze and do not give information on source localization. Subsequent waves do not improve the localization and give an impression of a reverberant sound without discrete localization.

The quantity of subsequent wave reflections which the auditory analyzer is able to reproduce and utilize is limited great. For a typical value of the HAAS constant $T_H \cong 50$ ms assuming the mean free path in the room

to be equal to $d_m \cong 8.5$ m, the analyzer is able to utilize waves reflected n times, where

$$n = \frac{T_H c}{d_m} = \frac{50 \cdot 10^{-3} \cdot 340}{8.5} \cong 2.$$

Therefore in cases concerning typical rooms, waves giving information about the localization, are reflected once, or twice at the very most.

It is worth noticing, that the localized sources are either stationary or slowly moving. Thus the situation analyzer can take advantage of the localizations registered in earlier analysis.

The contribution of all early reflections in the localization process corresponds quite naturally to their share in the subjective integration of the loudness impression which in general lasts up to several, tens, or even hundred, miliseconds.

4. Optical analogies

In the course of examining possibilities of subconscious evaluation of the direction of reflections, visual analogies have to be considered. With the application of a mirror a person localizes seen objects not in the direction of sight, i. e., behind the minor, but in their real direction, determined on the basis of other observations. It is generally known, how precisely the direction and in consequence — the distance can be evaluated by a car driver using a rear-view mirror, or by a bus driver using single and dual mirrors. The "*acquaintance*" with the position of the mirror is a condition for a correct evaluation; what is an analogy to the initial "*sound familiarization*" with the room.

An increase of the localization accuracy by sight is obtained by superimposing results of the optical localization of the object, obtained from multiple path observations with the application of mirrors, shadows, cameras with picture monitors, etc. Analogously sound sources can be localized by hearing an improved accuracy due to well reflecting surfaces in a rectangle room without a roof.

5. Reflections and distance localization

"*Little is known, as far, about the mechanism of distance localization*" POTTER and STEINBERG wrote in the 50-ties in the introduction to a paper which dealt with the properties of audition [10].

Also not too much was explained in the further period of time.

Meanwhile the reflection mechanism of directional localization (described in p. 3) at the same time acts as a mechanism of distance localization due

to simple trigonometric dependencies. In order to examine the quantity of the incremental sensitivity threshold of distance localization, resulting from this mechanism, the typical value φ for the incremental sensitivity threshold of angular localization in a horizontal plane passing through the ears of the

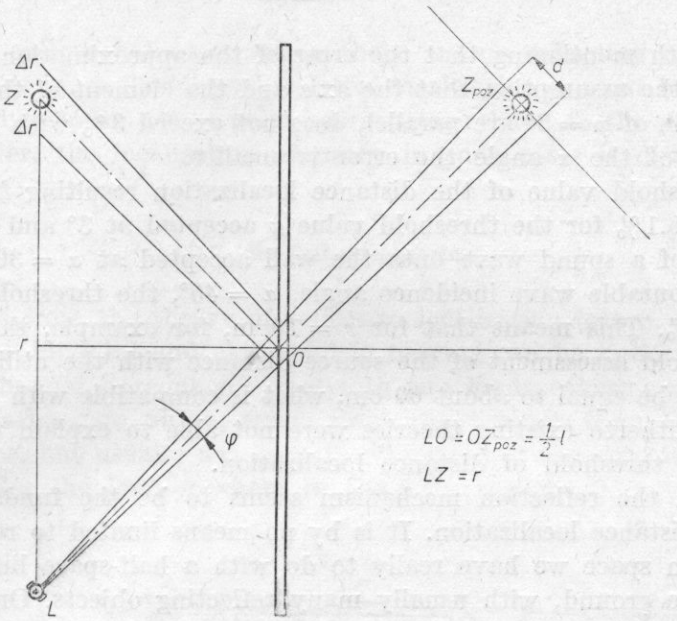

Fig. 3. The dependence of the threshold of accuracy of distance localization, Δr, on the value of the threshold of the directional localization, φ, at a given position of source Z and listener S with respect to the reflecting surface

listener has to be taken into account. For a straight ahead direction, φ equals about 3°, assuming that the listener turns his head, as it is in reality.

The neccessary trigonometric dependencies can be easily determined with the application of an apparent source Z_{poz} in a situation (Fig. 3), where source Z and the listener, at a distance r from it, are located near the reflecting plane, onto which a wave incides under an angle α.

$$\frac{1}{2}r = \frac{l}{2}\sin\alpha, \tag{5.1}$$

$$d = l\,\mathrm{tg}\,\frac{\varphi}{2}, \tag{5.2}$$

$$\Delta r \cong \frac{d}{\cos\alpha}. \tag{5.3}$$

From equations (5.1)–(5.3) it results that

$$\frac{\Delta r}{r} \cong 2 \frac{\operatorname{tg} \frac{\varphi}{2}}{\sin 2\alpha}. \tag{5.4}$$

It is worth mentioning that the error of the approximation in (5.3), resulting from the assumption that the axis and the element of the cone, with the apex angle of $\varphi = 3°$ are parallel, does not exceed 3% with $\alpha = 45°$. For other values of the α angle the error is smaller.

The threshold value of the distance localization resulting from formula (5.4), equals 6.1% for the threshold value φ accepted at 3° and for the incidence angle of a sound wave onto the wall accepted at $\alpha = 30°$. While for the most favourable wave incidence angle, $\alpha = 45°$, the threshold value equals only 5.2%. This means that for $r = 10$ m, for example, the inaccuracy of the threshold assessment of the source distance with the utilization of reflections, will be equal to about 60 cm, what is compatible with practical observations. Hitherto existing theories were not able to explain this value of the accuracy threshold of distance localization.

Therfore, the reflection mechanism seems to be the fundamental mechanism of distance localization. It is by no means limited to rooms. In the so-called open space we have really to do with a half-space limited by the surface of the ground, with usually many reflecting objects. Only the mentioned above case with snowfall approximates such a half-space to a case of an almost anechoic chamber.

Discussing the influence of reflections on localization, the role of reflections has to be mentioned in the precise distance localization mechanism which functions not only with sea mammals and bats, but also with blind people.

6. Relative localization

Until now in discussions on directional hearing in literature and in experiments, a polar coordinate system with the begining at the point of the head of the listener, was generally used. Meanwhile man projects the surroundings by means of his senses in a local cartesian coordinate system rather, related to characteristic reflecting objects in these surroundings. He chooses instinctively the best directions of the main axes for such a system. This is the reason for man's predilection for rectangular rooms, which facilitate the localization of inside objects by the means of sight and hearing.

In the mentioned local system the relative localization takes place. It consists in determining the position of the source in relation to objects localized before, when the current position of his head in this system is known

to the listener beforehand. Relative localization was surely developed in the course of the species evolution in order to compensate the mobility of the observer in the surroundings, especially of his eyes and ears, in relation to the objects and localized sources. Current localizations, remembered impressions and earlier general experiences of the observer form the image of the surroundings.

Only in exceptional cases, when there are no reflecting objects in the surroundings (e. g., a flat desert), relative localization can not be applied and we are forced to make use of polar coordinates related to the position of our head. However, the localization accuracy in such cases is distinetly lower.

7. Stereophonic hearing

It results from the theory of reflective localization (see p. 3), that localization in the binaural and stereophonic hearing can be uniformly interpreted. A two-channel stereophony base with two loudspeakers gives the possibility of radiating two waves, which reach the listener from the loud speakers directions, but usually not form the direction of the apparent source occuring between the loud speakers in the base region.

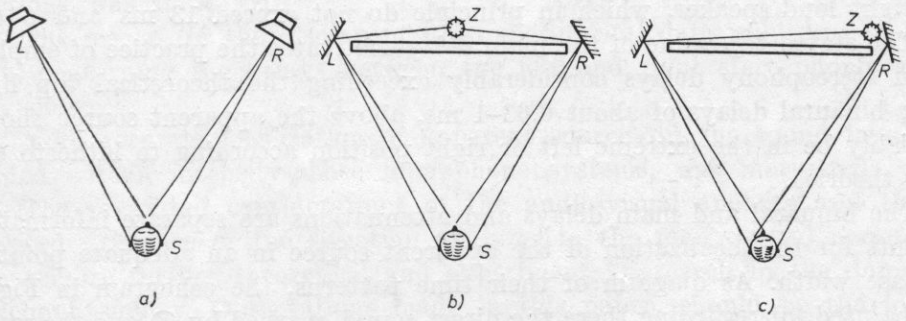

Fig. 4. Diagram of stereophonic hearing, taking into account the theory of reflective localization: a) audio monitoring system; b) equivalent system with a midpositioned source in the centre of the base; c) as above, but with the source in a side position

The two waves from the loud speakers, which reach the listener (Fig. 4a), can be treated as waves travelling from a real source located in place of an apparent source, reaching the listener after being reflected in the spots in which the loud-speakers are located (Fig. 4b). In the above reasoning an assumption was made that the listener is not reached by any direct wave from the source, just as if the base would be an insulating baffle. The midposition of an apparent source corresponds to a simultaneous attainment of the lis-

tener by both reflected waves (Fig. 4b). Whereas, an extreme side position of the apparent source (Fig. 4c), means that the left wave will reach the listener with a delay resulting from the difference of the paths $(\overline{ZL}+\overline{LS})-\overline{RS} = \overline{ZL}$. In practice for a base spacing of $d_B = 3$ m, the delay is $\Delta t_s = d_B/c = 3/340 \cong 8.8$ ms, while for $d_B = 4.5$ m the delay increases to 13 ms. Greater base spacing is not applied, because for $\Delta t_s > 13$ ms both reflections would be heard as separate sound impressions. The path difference for extreme positions of the source is equal to the base spacing. This difference has to be taken into account when the level difference of reflections reaching the listener is determined. Under the assumption of the spherical radiation of the source, a six decibel drop of the loudness level can be accepted for every doubling of the distance. As in a typical stereo monitoring configuration (Fig. 4) $\overline{ZL} = \overline{LS}$ and $\overline{LS} = \overline{RS}$ while $\overline{ZL}+\overline{LS} = 2\overline{RS}$, so the reflection with the possibly greatest delay is weakened by about 6 dB.

Intermediate positions of the apparent source can be localized with the application of adequately delayed and weakened loud speaker signals, reproducing delay and attenuation values, which would appear on the path from the source, through the reflection points near the loud speakers, to the listener. In order to conduct a correct stereophonic localization, binaural delays and attenuations reaching the left and right ear of the listener have to be preserved, as well as the main signal delays and attenuations of the left and right loud speaker, which in principle do not exceed 13 ms and 6 dB.

The stated top value of the main delay motivates the practice of employing in stereophony delays considerably exceeding the theoretical top limit of the binaural delays of about 0.63–1 ms, above the apparent source should invariably be in the extreme left or right position according to hitherto existing theories.

The binuaral and main delays and attenuations are separate information elements for the localization of the apparent source in an adequate point of the base width. As diagram of their time patterns, the echogram in Fig. 2 may be used, disregarding there the direct sound, marked by ① and the sound reflected twice, marked by ④.

The regard to the influence of reflections on the process of stereophonic localization leads to the neccessity of applying an intensity-phase microphone system where the spacing of microphones should be kept equal to the spacing of loud speakers in the monitoring system. This constraint and the difficulty of preserving the conformity of localization information from main and binaural delays and attenuations can make the practical application of reflective localization in stereophony difficult.

Nevertheless, the disregarding of main delays, i. e. delays between the subsequent reflections, has led in hitherto existing theories of stereophonic hearing to misunderstandings, concealments [4], or even to the questioning of generally recognized publications of experimental data [11].

8. Conclusions

The presented theory widens the konwledge of the properties of binaural hearing and explains the mechanism of subjective source localization, which up to now was presented in the psychoacoustic literature in a not quite clear and incomplete way. The theory makes possible a more effective solution of several problems of room acoustics, sound recording techniques and other applications of the psychoacoustic knowledge.

A systematic presentation of all resulting conclusions of this work has to be postponed to a separate publication. However, several more important achievments and consequences of the theory of reflective localization of sound sources are worth summing up in brief.

The mechanism of auditory distance localization of sound sources, functioning especially in rooms has been presented for the first time. If explains theoretically the localization accuracy achieved practically.

A new interpretation of the HAAS constant was given.

A common mechanism of the directional and distance localization was pointed out, as well as the contribution of early reflections in the increase of the localization accuracy.

The advantages of rectangular concert-halls were motivated by the influence of side reflections on the improvement of the discrimination of sound plans on the stage. The advantage of flat side walls in the region of first reflections was indicated.

The reason for the discrepancy of experimental data published in literature, concerning the delays between the left and right stereophonic signals was shown.

More accurate localization of apparent sources in the sound image, recorded withan intensity-phase microphone systems, was motivated.

The presented considerations of the audio-visual analogy and the postulated existence of the situation analyzer in the man central nervous organ require further theoretical and experimental research in the domain of psychophysiology. Observations made in this paper, should be the foundation for thorough investigations.

It is obvious that the presented theory can not be neither proved nor refuted with ad hoc conducted experiments. The theory of the reflective localization of sound sources can not be assessed before sufficiently numerous experimental results, will be obtained, critically checked and widely discussed.

References

[1] M. BARRON, *The subjective effects of first reflections in concert halls – the need for lateral reflections*, J. of Sound and Vibrations, **15**, 4 (1971).

[2] A. H. BENADE, *From Instrument to Ear in a Room: Direct or via Recording*, J. Audio Eng. Soc., **33**, 4 (1985).

[3] P. B. BENNETT, D. H. ELLIOTT, *Physiology and Medecine of Diving*, Bailliere and Tindall, London 1975.

[4] J. BLAUERT, *Räumliches Hören*, Hirzel, Stuttgart 1974.

[5] N. I. DURLACH, *Binaural Signal Detection: Equalization and Cancellation Theory* (in: Foundation of Modern Auditory Theory, ed. J. V. TOBIAS), Academic Press, New York 1972.

[6] N. V. FRANSSEN, *Stereofonie*, Philips, Centrex, Eindhoven 1963.

[7] L. A. JEFFRES, *Binaural Signal Detection: Vector Theory* (in: Foundations of Modern Auditory Theory, ed. J. V. TOBIAS), Academic Press, New York 1972.

[8] H. KIETZ, *Der echte und ein falscher Haas-Effekt*, III ICA Congress, Liege (in: Proceedings, ed. L. CREMER), Stuttgart 1959.

[9] A. W. MILLS, *Auditory Localization* (in: Foundations of Modern Auditory Theory, ed. J. V. TOBIAS), Academic Press, New York 1972.

[10] R. K. POTTER, J. C. STEINBERG, *Speech and Hearing, Depth Localization*, Technical Aspects of Sound, **1**, 4 (1953).

[11] G. THEILE, *Neue Erkenntnisse zur Wahrnehmung der Richtung und Entfernung von Phantomschallquellen und Konsequenzen für die stereofone Aufnahmepraxis*, Verband Deutscher Tonmeister – Information, **5**, 6 (1984).

Received on 4 July, 1985; revised version on 11 November, 1985.

ARCHIVES OF ACOUSTICS
11, 1, 25-38 (1986)

METHOD OF CALCULATING THE ACOUSTICAL WAVE REFLECTION COEFFICIENT FROM A NOT-SHARP BOUNDARY OF TWO MEDIA

MAREK HAGEL

Institute of Automatics of the Silesion Technical University
44-100 Gliwice, ul. W. Pstrowskiego 16

The paper presents a numerical calculation method of the reflection coefficient of a plane, longitudinal acoustical wave from a plane-parallel, non-homogeneous transient layer (not-sharp boundary) positioned between two homogeneous, half-spatial media. Changes in the physical properties of the transient layer, determined by the changes in its material parameters, occur along its thickness and can by described by arbitrary one-variable functions.

Results of theoretical calculations of the reflection coefficient were given for chosen cases of material parameter changes in the transient layer and they were compared with results of measurements conducted on a physical model.

The presented method is accurate, universal and simple. It can be useful for the choice of ultrasonic wave frequency and for the measurement accuracy evaluation in certain applications of ultrasonic level meters, as well as for the determination of the shape of an ultrasonic pulse reflected from a not-sharp transient layer.

1. Introduction

The echo method is one of the methods of level measurement (determination of the position of the boundary of two media in space) applied in the ultrasonic technique. It is based on the measurement of the ultrasonic pulse transition time on the path: sending head – measured level – receving head. This method can be applied only when the pulse is reflected from the boundary of two media. Hence, the reflection coefficient of an acoustical wave from the studied media boundary is an important factor, which influences the choice of the construction parameters of ultrasonic level meters. Calculations of the reflection coefficient are not difficult in the case of a sharp boundary between the media, i. e. there is a discontinuous change of the phy-

sical properties on the boundary [11]. However, in certain cases one medium passes into the second through a non-homogeneous transient layer, called further on a not-sharp boundary [4]. Such cases can be encountered e. g. during the measurements of sediment levels, investigations of the bottom of water reservoirs and in medicine. The problem of calculating the wave reflection coefficient from a not-sharp boundary of two media has been undertaken in several papers [2], [3], [7], [8], [10]. However, all these publications do not contain the confirmed experimentally general analytical expressions allowing the calculation of the wave reflection coefficient for arbitrary parameters of the transient layer. Therefore, this paper presents a numerical method of calculating the of coefficient reflection from a not-sharp boundary of two media, for a case of a perpendicular incidence of a plane, longitudinal wave on a plane-parallel transient layer. Changes of the physical properties of this layer are determined by the changes of its material parameters (density and elasticity coefficients), take place along its thickness and can be described by arbitrary one variable functions. Measurements of the reflection coefficient on a physical model were done in order to check the obtained calculation results.

2. A mathematical model of the reflection of an acoustical wave from a not-sharp boundary of media

In order to calculate the acoustical wave coefficient of reflection from a not-sharp boundary of media it was accepted, that between two half plane, continuous, homogenous, non-dispersive and lossless media A and C a plane-parallel transient layer B exists. It differs from media A and C, because its material parameters (density and elasticity coefficients) can change along its thickness in an arbitrary manner.

The wave equation in layer B, for a linear, one-dimension problem, with neglect of the body force, is [6]:

$$\varrho_B(x)\left|\frac{\partial^2 u_B(x,\ t)}{\partial t^2}\right. = \frac{\partial}{\partial x}\left\{[\lambda_B(x)+2\mu_B(x)]\frac{\partial u_B(x,\ t)}{\partial x}\right\}, \tag{1}$$

where $u_B(x,\ t)$ — displacement of medium particles, $\varrho_B(x)$ — density, $\lambda_B(x)$, $\mu_B(x)$ — Lamé coefficients, t — time, x — linear coordinate.

Let us assume that in medium A a continuous, plane, sinusoidal and longitudinal acoustical wave A_A propagates in a direction opposite to axis x, and at the same time perpendicularily to the boundary of media A and B (Fig. 1).

Part of the incident wave A_A is reflected from layer B (wave A_{A1}) and a part of it passes to medium C (wave A_C). Displacements of medium parti-

cles in waves A_A, A_{A1}, A_C can be presented in a complex form:

$$u_A(x, t) = U_A e^{j\omega(x-d)/c_A} e^{j\omega t},$$
$$u_{A1}(x, t) = U_{A1} e^{-j\omega(x-d)/c_A} e^{j\omega t}, \tag{2}$$
$$u_C(x, t) = U_C e^{j\omega x/c_C} e^{j\omega t},$$

where U_A, U_{A1}, U_C – displacement amplitudes in the incident, reflected and transmitted waves, ω – pulsation, c_A, c_C – wave phase velocities in media A and C, d – thickness of the transient layer.

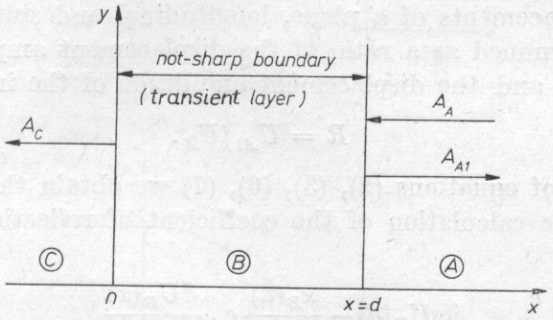

Fig. 1. Reflection of an acoustical wave from a not-sharp transient layer

Because initial phase displacements can occur in the incident, reflected and transmitted waves, the displacement amplitudes U_A, U_{A1} and U_C are complex numbers in a general case. The particle displacements in layer B can be expressed by [8]:

$$u_B(x, t) = U_B(x)\, e^{j\omega t}. \tag{3}$$

Placing equation (3) in (1) we obtain:

$$\frac{d^2U_B(x)}{dx^2} = -\frac{1}{\varkappa_B(x)} \frac{d\varkappa_B(x)}{dx} \frac{dU_B(x)}{dx} - \omega^2 \frac{\varrho_B(x)}{\varkappa_B(x)} U_B(x), \tag{4}$$

where

$$\varkappa_B(x) = \lambda_B(x) + 2\mu_B(x).$$

In order to reach a full mathematical description of the not-sharp boundary, equation (4) has to be supplemented by the continuity conditions for displacements and stresses, for $x = 0$ and $x = d$:

for $x = 0$

$$u_B(0, t) = u_C(0, t),$$
$$\varkappa_B(0) \left.\frac{\partial u_B(x, t)}{\partial x}\right|_{x=0} = \varkappa_C \left.\frac{\partial u_C(x, t)}{\partial x}\right|_{x=0}, \tag{5}$$

for $x = d$

$$u_B(d, t) = u_A(d, t) + u_{A1}(d, t),$$

$$\varkappa_B(d) \frac{\partial u_B(x, t)}{\partial x}\bigg|_{x=d} = \varkappa_A \frac{\partial}{\partial x}[u_A(x, t) + u_{A1}(x, t)]\bigg|_{x=d}, \tag{6}$$

where

$$\varkappa_A = \varkappa_A + 2\mu_A, \quad \varkappa_C = \lambda_C + 2\mu_C,$$

λ_A, λ_C, μ_A, μ_C – Lamé coefficients in media A and C.

The coefficient of reflection R, from not-sharp boundary between media A and C for displacements of a plane, longitudinal and sinusoidal acoustical wave can be determined as a ratio of the displacement amplitude of the reflected wave U_{A1}, and the displacement amplitude of the incident wave U_A:

$$R = U_{A1}/U_A. \tag{7}$$

On the basis of equations (2), (3), (6), (7) we obtain the general expression leading to the calculation of the coefficient of reflection R from a not sharp boundary:

$$R = \frac{j\omega U_B(d) - \dfrac{\varkappa_B(d)}{\varkappa_A} c_A \dfrac{dU_B(x)}{dx}\bigg|_{x=d}}{j\omega U_B(d) + \dfrac{\varkappa_B(d)}{\varkappa_A} c_A \dfrac{dU_B(x)}{dx}\bigg|_{x=d}}. \tag{8}$$

3. Calculation of the reflection coefficient

The calculation of the reflection coefficient R was conducted numerically. A linear second order differential equation in the form (4) was solved with the function coefficients and boundary conditions expressed by equations (5) and (6). Equation (4) was integrated numerically along coorinate x, begining from the boundary condition for $x = 0$. The integration Runge-Kutt procedure was applied. The results, in the form of values $U_B(d)$ and $dU_B(x)/dx|_{x=d}$, were put in equation (8). The following functions describing changes of material parameters, $\varrho_B(x)/\varrho_C$ and $\varkappa_B(x)/\varkappa_C$ in medium B (Fig. 2), were accepted in the course of calculations:

a. $$p(x) = 1 + (a-1)\frac{x}{d},$$

b. $$r(x) = \frac{1}{2}\left[1 + a - (a-1)\cos\frac{\pi}{d}x\right],$$

c. $$s(x) = a - (a-1)\cos\frac{\pi x}{2d},$$

d. $$t(x) = \sqrt{a},$$

where a – ratio of the values of material parameters in medium A and C:

$$a_\varrho = \varrho_A/\varrho_C, \quad a_\varkappa = \varkappa_A/\varkappa_C,$$

ϱ_A, ϱ_C – densities of media A and C.

The calculation programme was written in language FORTRAN 1900.

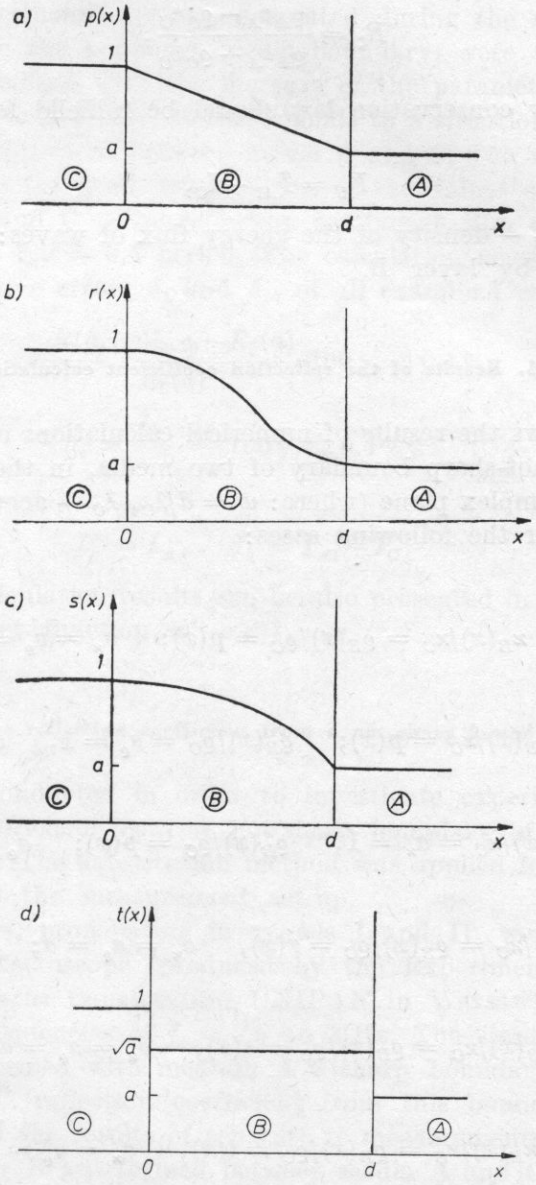

Fig. 2. Changes of material parameters in a transient layer, described by function: a. $p(x)$, b. $r(x)$, c. $s(x)$, d. $t(x)$

The physical significance and the accuracy of numerical calculations was controlled with the application of two methods:

a) when the width of the transient layer d decreaces to zero, then the value of the reflection coefficient R should tend to the values of the reflection coefficient R_ζ for a sharp boundary between two media:

$$R_\zeta = \frac{\varrho_A c_A - \varrho_C c_C}{\varrho_A c_A + \varrho_C c_C}, \tag{9}$$

b) the energy conservation law should be fulfielld for waves A_A, A_{A1}, A_C, i. e.,

$$I_A = I_{A1} + I_C, \tag{10}$$

where I_A, I_{A1}, I_C – density of the energy flux of waves: incident, reflected and transmitted by layer B.

4. Results of the reflection coefficient calculation

Fig. 3a-f shows the results of numerical calculations of the reflection coefficient from a not-sharp boundary of two media, in the form of diagrams $R(a, w)$ in the complex plane (where: $w = d/\lambda_C$, λ_C – acoustical wave length in medium C), for the following cases:

a. case $P1$

$$\varkappa_B(x)/\varkappa_C = \varrho_B(x)/\varrho_C = p(x); \quad a_\varkappa = a_\varrho = a;$$

b. case $P2$

$$\varkappa_B(x)/\varkappa_C = p(x); \quad \varrho_B(x)/\varrho_C = a_\varrho = 1, \quad a_\varkappa = a;$$

c. case $P3$

$$\varkappa_B(x)/\varkappa_C = a_\varkappa = 1, \quad \varrho_B(x)/\varrho_C = p(x); \quad a_\varrho = a;$$

d. case $P4$

$$\varkappa_B(x)/\varkappa_C = \varrho_B(x)/\varrho_C = r(x), \quad a_\varkappa = a_\varrho = a;$$

e. case $P5$

$$\varkappa_B(x)/\varkappa_C = \varrho_B(x)/\varrho_C = s(x), \quad a_\varkappa = a_\varrho = a;$$

f. case $P6$

$$\varkappa_B(x)/\varkappa_C = \varrho_B(x)/\varrho_C = t(x), \quad a_\varkappa = a_\varrho = a;$$

The analysis of obtained diagrams shows, that the coefficient of reflection from a not-sharp boundary of two media is a complex quantity and its

values depend on the ratio of the width of the transient layer to the length of the acoustical wave in medium C, the ratio of the values of material parameters on media A and C, and on the functions describing the changes of material parameters in layer B. In cases $P1$–$P5$ the values of the modules of the reflection coefficient rapidly decrease to zero with the increase of the value of parameter w (for $w \approx 1$, so $\lambda_C \approx d$, $|R(a, w)| = 0.1-0.3\ R_\zeta(a)$). The values of phase displacements φ(a, w), generated during the reflection of the acoustical wave from the not-sharp media boundary, were in an $(0-\pi)$ interval and were stabilized with the increase of the parameter w value.

Case P6 is a particular case. It corresponds to a situation in which a homogeneous layer B is present between media A and C. The values of its material parameters are the geometrical means of the values of material parameters of media A and C – the reflection coefficient $R(a, w)$ is then a periodic function with a $w = 0.5$ period. The calculation accuracy determined on the basis of relative errors δ_1 and δ_2, of all examined cases, was:

$$\delta_1 = \frac{R(a, w)|_{w\to 0} - R_\zeta(a)}{R_\zeta(a)} 100\,\% \leqslant 0.1\,\%, \tag{11}$$

$$\delta_2 = \frac{I_p - I_0}{I_0} 100\,\% \leqslant 0.4\,\%, \tag{12}$$

where

$$I_p = I_A, \qquad I_0 = I_{A1} + I_C.$$

The obtained calculation results can be also presented in a different form e. g. as a parameter function $w' = d/\lambda_A$.

5. Measurements of the reflection coefficient from a not-sharp boundary of two media

Research was conducted in order to investigate experimentally values of the reflection coefficient from a not-sharp boundary of two media calculated theoretically. The substitution method was applied for measurements [9]. Fig. 4 presents the measurement set-up.

Ultrasonic pulses, propagating in vessels I and II, were generated by a *UNIPAN* 511 defectoscope (produced by the Experimental Department for Scientific Apparatus Construction UNIPAN in Warsaw) and ultrasonic heads with rated frequencies of $f_z = 0.5$–10 MHz. The standard was placed in vessel I and it formed with medium A a sharp boundary reflecting the ultrasonic wave. The reflection coefficient from this boundary was calculated on the basis of the results of separate te measurements. In vessel II a model transient layer B was formed between media A and C, where the top edge of the standard and the transient layer were theoretically at the same distance from the ultrasonic head. Layers A, B and C were made from ge-

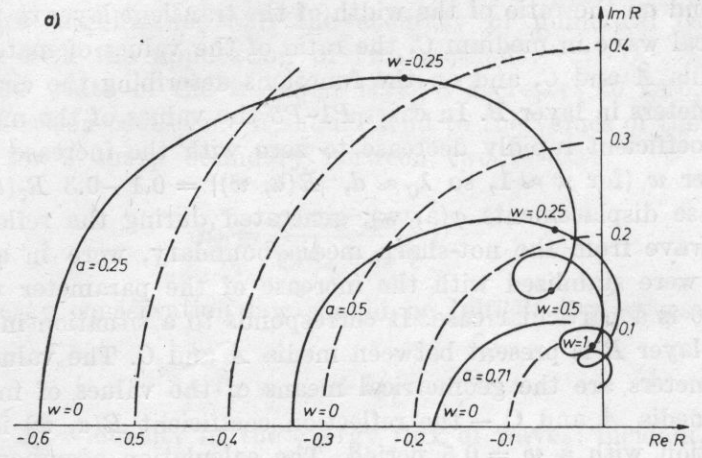
a)
Im R
0.4
0.3
0.2
0.1
w = 0.25
w = 0.25
w = 0.5
w = 1
a = 0.25
a = 0.5
a = 0.71
w = 0
w = 0
w = 0
-0.6
-0.5
-0.4
-0.3
-0.2
-0.1
Re R

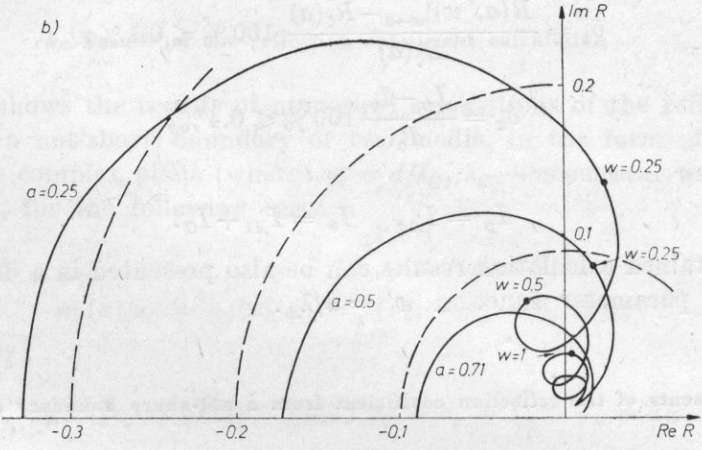
b)
Im R
0.2
0.1
w = 0.25
w = 0.25
w = 0.5
w = 1
a = 0.25
a = 0.5
a = 0.71
-0.3
-0.2
-0.1
Re R

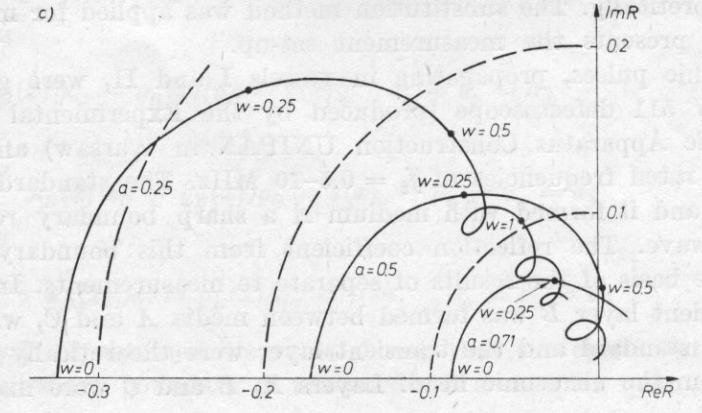
c)
Im R
0.2
0.1
w = 0.25
w = 0.5
w = 0.25
w = 1
w = 0.5
w = 0.25
a = 0.25
a = 0.5
a = 0.71
w = 0
w = 0
w = 0
-0.3
-0.2
-0.1
Re R

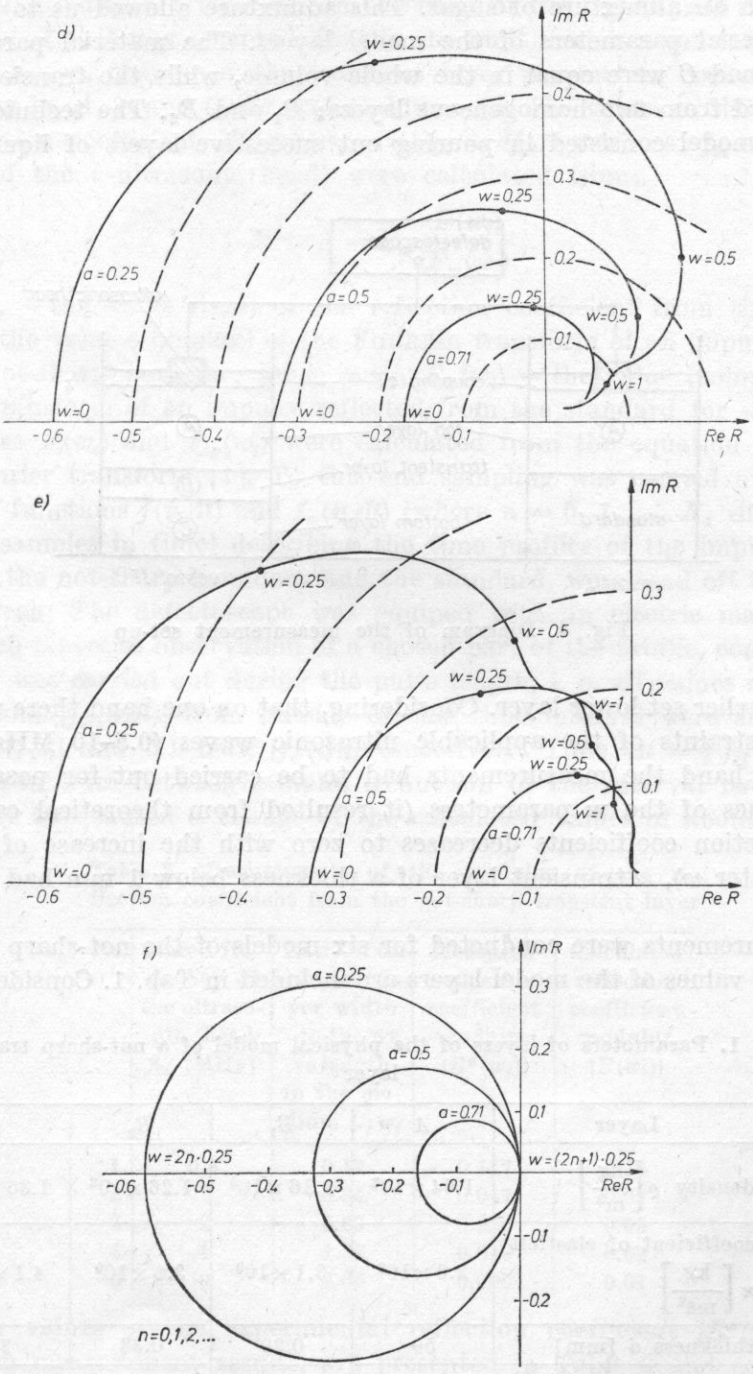

Fig. 3. Results of numerical calculations of the reflection coefficient $R(a, w)$ for cases: a. $P1$, b. $P2$, c. $P3$, d. $P4$, e. $P5$, f. $P6$

latine with an admixture of sugar. This admixture allowed us to obtain various material parameters of the model layers. The material parameters of media A nad C were equal in the whole volume, while the transient layer B was formed from two homogeneous layers: B_1 and B_2. The technique of making the model consisted in pouring out successive layers of liquid gelatine

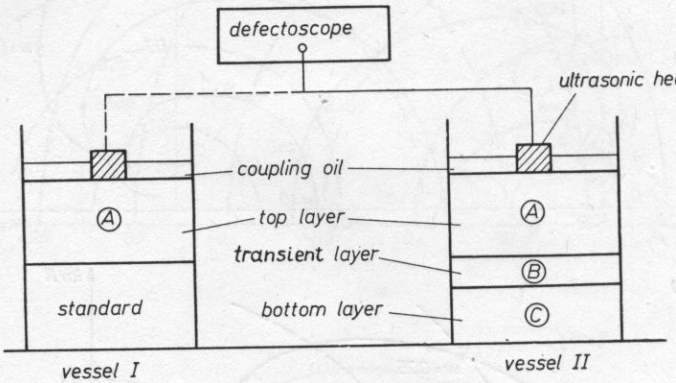

Fig. 4. Diagram of the measurement set-up

onto an earlier set lower layer. Considering, that on one hand there were apparatus constraints of the applicable ultrasonic waves (0.5–10 MHz), and on the other hand the measurements had to be carried out for possibly small (0–2) values of the w parameters (it resulted from theoretical calculations, that reflection coefficients decreases to zero with the increase of the value of parameter w), a transient layer of a thickness below 1 mm had to be modelled.

Measurements were conducted for six models of the not-sharp boundary. The mean values of the model layers are included in Tab. 1. Considering parti-

Table 1. Parameters of layers of the physical model of a not-sharp transient layer

No	Layer	A	B_1	B_2	C
1	density $\varrho\left[\frac{\text{kg}}{\text{m}^3}\right]$	1.04×10^3	1.16×10^3	1.26×10^3	1.35×10^3
2	coefficient of elasticity $\varkappa\left[\frac{\text{kg}}{\text{ms}^2}\right]$	2.6×10^9	3.1×10^9	3.6×10^9	4.1×10^9
3	thickness d [mm]	50	0.29	0.33	77
4	logarythmic damping decrement Λ (for $f = 0 - 10$ MHz)	< 0.06	< 0.06	< 0.06	<0.06

cle diffusion between layers and on the basis of the logarithmic damping decrement $\Lambda \ll 1$, it was accepted, that in the built models a continuous, approximately linear, change of the transient layer parameters occurs and damping in media A, B and C are neglectably small. The values of the experimental reflection coefficient $R^*(w_i)$ ($w_i = d/\lambda_{Ci} = df_{zi}/c_C$, where: f_{zi} — rated frequency of the i ultrasonic head) were calculated from:

$$R^*(w_i) = R_w \frac{F(w_i)}{F_w(w_i)}, \tag{13}$$

where R_w — the value (real) of the reflection coefficient from the standard, $F(w_i)$ — the value (complex) of the FOURIER transform of an impulse reflected from a not-sharp boundary for $w = w_i$, $F_w(w_i)$ — the value (complex) of the Fourier transform of an impulse reflected from the standard for $w = w_i$.

Values $F(w_i)$ and $F_w(w_i)$ were calculated from the equation of the discrete Fourier transform [1]. To this end sampling was carried out, i. e. the values of functions $f(n\,\Delta t)$ and $f_w(n\,\Delta t)$ (where $n = 0, 1, \ldots, N$, Δt — interval between samples in time) describing the time profiles of the impulses reflected from the not-sharp boundary and the standard, were read off the defectoscope screen. The defectoscope was equiped with an electric magnifier, through wich a precise observation of a chosen part of the profile, could be done. Sampling was carried out during the pulse length, i. e. all values of functions $|f(n\,\Delta t)|$ and $|f_w(n\Delta t)|$ from outside of this time interval were smaller than 0.1 max $|f(t)|$ and 0.1 max $|f_w(t)|$, respectively. Time $\Delta t = \frac{1}{4} f_{zi}$ was taken to be the interval between samples (reduction of the interval between samples Δt by two caused a change of the calculated values of about 0.5 %).

Table 2. Measurements of the modulus of the reflection coefficient from the not-sharp transient layer

No	Rated frequency of the ultrasonic head f_{zi} [MHz]	Ratio of the transient layer width to the wave length in the medium C; w_i	Measured reflection coefficient modulus $\lvert R^*(w_i)\rvert$	Calculated reflection coefficient modulus $\lvert R(w_i)\rvert$
1	0.5	0.17	0.117	0.14
2	1	0.34	0.047	0.07
3	2	0.68	0.026	0.03
4	4	1.36	0.010	0.02
5	6	2.06	0.006	0.01

Mean values of the experimental reflection coefficient $|R^*(w_i)|$, calculated from measurement results, are presented in Table 2 and compared to the results of numerical calculations done for a linear change of the material parameters in the transient layer for $a_\varrho = 0.77$ and $a_\varkappa = 0.63$.

Taking into account the difficulty of building a physical model (small thickness of the transient layer), its departure from the theoretical model (among others: approximately linear change of the material parameters of the transient layer, nonplanar wave front), as well as the low accuracy of the measurements (several percent), it can be said, that the experimental results are qualitatively consistent with the results of numerical calculations, despite fairly considerable differences in the numerical values.

The values $\varphi^*(w_i)$ (calculated from equation (13)), of the phase shift $\varphi(w)$, generated during the reflection of the acoustical wave from a not-sharp boundary, were contained in the range $(\pi, -2.5\pi)$ rad. On the other hand it has to be taken into account, that the inaccuracy of the ultrasonic head setting in respect to the reflecting boundary (approximated at ± 0.5 mm), could cause phase shifts of the same order of magnitude. For this reason the measured values of the phase shifts were not presented.

6. Conclusions

The presented here numerical method of calculating the coefficient of reflection from a not-sharp boundary of two media is accurate, universal and simple. The diagrams of the reflection coefficient, calculated with its application, can be used for the selection of optimal rated frequencies of ultrasonic heads for level meters, measuring the level determined by a not-sharp boundary of media; for the analysis of their indication accuracy as well as for the determination of the shape of an ultrasonic pulse reflected from a not-sharp boundary between media [5].

References

[1] R. BRACEWELL, *Fourier Transform and its Application*, WNT, Warszawa 1968, pp. 148–150 (in Polish).

[2] G. CANÉVET, G. EXTRÉMET, M. JESSEL, *Propagation du son dans un dioptre flou*, Acoustica **26**, 2, 102–107 (1972).

[3] D. H. DAMERON, *An Inhomogeneous Media Model for the Determination of Acoustic Parameters in Tissues*, IEEE Transactions on Sonics and Ultrasonics **SU-27**, 5, 244–248 (1980).

[4] M. HAGEL, *Reflection of an ultrasonic wave from a not-sharp boundary of two media*, Proc. Open Seminar. Acous., Gliwice 1981, pp. 56–59 (in Polish).

[5] M. HAGEL, *Application of the model of ultrasonic wave reflection effects, for the construction of an instrument for the measurements of sediment levels in liquids*, Dissertation, Dept. Autom. and Inform. Silesian Technical University, Gliwice 1984, pp. 87–114 (in Polish).

[6] I. MALECKI, *The Theory of Waves and Acoustical Systems*, PWN, Warszawa 1964, pp. 556 (in Polish).

[7] H. E. MORRIS, *Bottom Reflection Loss Model with a Velocity Gradient*, The Journal of the Acoustical Society of America **48**, 5 part 2, 1198–1202 (1970).

[8] C. B. OFFICER, *Introduction to the Theory of Sound Transmission*, McGraw Hill Book Comp. Inc., New York, Toronto, London 1958, pp. 201–207.

[9] J. PIOTROWSKI, *Elements of Metrology*, PWN, Warszawa 1976, p. 160 (in Polish).

[10] V. I. VOLOVOV, A. N. IVAKIN, *Otrazenije zwuka ot dna s gradientami skorosti zvuka i plotnosti*, Akusticeskij Zurnał XXVI, 2, 194–199 (1980).

[11] J. WEHR, *Measurements of the Velocity and Damping of Ultrasonic Waves*, PWN, Warszawa 1972, p. 22 (in Polish).

Revised on 16 May, 1985; revised version on 16 October, 1985.

ARCHIVES OF ACOUSTICS
11, 1, 39-52 (1986)

ACOUSTICAL IMPEDANCE OF A CIRCULAR MEMBRANE VIBRATING UNDER THE INFLUENCE OF A FORCE WITH A UNIFORM SURFACE DISTRIBUTION*

WITOLD RDZANEK

Institute of Physics,
Higher Pedagogical School
35-310 Rzeszów, ul. Rejtana 16a

The problem of acoustic impedance was analyzed for a circular membrane being acted on by a time-harmonic surface force with constant density. The membrane is innuersed in a lose-loss gaseous medium and the edges of the membrane are assumed to be rigid and fixed. Emploing the integral HUYGENS-RAYLEIGH formulas the exact formulae were obtained for the acoustic pressure and power. These formulae are especially convinient for digital computer calculations in the situation where the propagation velocity of the wave on the membrane surface is much smaller than the velocity of the acoustic wave propagation through the surronnoling medium. The acoustic impedance is presented as a function of an interference parameter.

1. Introduction

Although the problems connected with the acoustical field of a vibrating circular membrane are clasical problems of acoustics, up to now they have not been analyzed theoretically in detail with the application of mathematical methods. Among others a comprehensive analysis of the acoustical impedance of a circular membrane vibrating harmonically under the influence of a force with a konwn surface distribution, is lacking.

The knowledge of the acoustical impedance of a circular piston with a uniform distribution of the vibration velocity [6] and a piston with a nonuniform velocity distribution [5], is not sufficient to infer about the impedance of a circular membrane.

---

* This investigation was carried out within the problem MR. I. 24.

Skudrzyk [9] presented the problem of acoustical power radiated by a membrane for a determined vibration mode, but only for small interference parameters.

In paper [7] the author conducted an analysis of the acoustical pressuer in the far field of a circular membrane vibrating harmonically under the influence of a force with a uniform surface distribution.

The investigation of the radiation impedance of a vibrating membrane, done in this paper, is the next stage of the study on the acoustical properties of a vibrating membrane. The expression for the vibration velocity [2], [7], obtained by solving the non-uniform vibration equation for not damped and harmonic in time effects, was used. It was assumed, that a membrane is stretched on the circumference and placed in a perfectly rigid and flat acoustical baffle, and the gascous medium, in which it radiates, is non-dissipative. The exact expression for the radiation impedane was reached here on the grounds of the integral HUYGENS-RAYLEIGH equation. Obtained equations were given a thorough analysis in the domain of small interference parameters. Calculation resuls have been also presented graphically.

Notation

a – membrane radius,
b – radius of the central membrane surface, effected by a non-zero normal component of the exciting force,
c – propagation velocity of a wave in a fluid medium,
c_M – propagation velocity of a wave in the membrane,
f – surface density of the force exciting vibrations (1),
f_0 – time independent constant density of the force forcing vibrations,
J_m – m-order BESSEL function,
k – $\omega\sqrt{\frac{\eta}{T}}$,
k_0 – $2\pi/\lambda$,
M – characteristic function of the source (A7),
N – acoustical power radiated by the membrane (A3),
N_m – m-order NEUMANN function,
p – acoustical pressure (A4),
r_0 – radial variable of the membrane surface point in a polar coordinate system,
S_n – n-order STRUVE function,
T – force stretching the membrane, related to a unit length,
t – time,
U – function described by formula (A22),
v – normal component of the vibration velocity of the points on the surface of the membrane,
$\langle|v|^2\rangle$ – value of the quadratic mean of the vibration velocity (A2),
Z – mechanical impedance (A1),

a – function described by formula (17),
ζ – normalized relative impedance (A8),
η – surface density of the membrane,
Θ – normalized relative resistance (A8),
λ – wave length in a fluid medium,
ξ – transverse displacement of the membrane surface points,
ϱ_0 – rest denisty of the fluid medium,
σ_0 – membrane surface,
χ – normalized relative reactance (A8),
ω – angular frequency of the force forcing vibrations.

2. Analysis assumptions

A circular membrane, stretched with an equal force on circumference of a raduis a, is placed on a plane forming a rigid acoustical baffle, in an unlimited, ideal fluid medium with a rest density ϱ_0. The membrane is excited to vibrate transversally by an axially-symmetrical force (e. g. with the aid of two flat circular electrodes with a raduis, b parallel to the membrane surface), having the surface density equal to:

$$f(r,\ t) = \begin{cases} f_0 e^{i\omega t} & \text{for} \quad 0 < r < b, \\ 0 & \text{for} \quad b < r < a, \end{cases} \tag{1}$$

where f_0 is a constant, r – radial variable in a polar coordinate system, t – time, ω – angular frequency of the force forcing vibrations, b – radius of the circular membrane surface, on which the non-zero normal component of the force forcing vibrations acts.

The equation of the circular membrane vibrations [3] is as follows:

$$T\frac{1}{r}\frac{\partial}{\partial r}\left(r\frac{\partial \xi(r,\ t)}{\partial r}\right) - \frac{\partial^2 \xi(r,\ t)}{\partial t^2} = -f(r,\ t), \tag{2}$$

where ξ is the distribution of the transverse vibrations of the membrane surface, $T = c_M^2 \eta$ – force stretching the membrane, related to a unit length, η – membrane surface density, c_M – wave propagation velocity on the membrane, f – surface density of the axially-symmetrical force forcing vibrations.

The solution of equation (2) for a membrane excited to vibrate by force (1) has the form [2], [7]

$$\xi_1(r,\ t) = \frac{f_0}{\eta\omega^2}\left\{\frac{\pi kb}{2}\left[\frac{N_0(ka)}{J_0(ka)}J_1(kb) - N_1(kb)\right]J_0(kr) - 1\right\}e^{i\omega t} \tag{3}$$

for $0 < r < b$,

$$\xi_2(r,\ t) = \frac{f}{\eta\omega^2}\frac{\pi kb}{2}J_1(kb)\left[\frac{N_0(ka)}{J_0(ka)}J_0(kr) - N_0(kr)\right]e^{i\omega t} \tag{4}$$

for $b < r < a$, where $k = \omega\sqrt{\eta/T}$, J_m – the Bessel function, N_m – Neumann function, both (m-order). The solution presented here satisfies the boundary condition $\xi_2(a, t) = 0$ and the conformity conditions $\xi_1(b, t) = \xi_2(b, t)$ and

$$\frac{\partial \xi_1(r, t)}{\partial r} = \frac{\partial \xi_2(r, t)}{\partial r} \quad \text{for } r = b.$$

The normal component of the vibration velocity is obtained after taking into account, that

$$v(r, t) = \frac{\partial \xi(r, t)}{\partial t}, \tag{5}$$

while

$$\xi(r, t) = \xi_0(r) e^{i\omega t}.$$

3. Exact calculation of the radiation impedance

The characteristic function (A7) for a circular membrane which vibrates according to dependences (3) and (4), is equal to:

$$M(\vartheta) = \int_0^b v_1(r_0) J_0(k_0 r_0 \sin\vartheta) r_0 dr_0 + \int_b^a v_2(r_0) J_0(k_0 r_0 \sin\vartheta) r_0 dr_0. \tag{6}$$

We use the formula for a indefinite integral [11]

$$\int w J_0(hw) Z_0(lw) dw = \frac{1}{h^2 - l^2} [hw J_1(hw) Z_0(lw) - lw J_0(hw) Z_1(lw)], \tag{7}$$

where Z_n is a cylindrical m-order function. We obtain

$$M(\vartheta) = \frac{i f_0 b^2}{\eta\omega} \frac{1}{1 - \left(\frac{k_0}{k}\right)^2 \sin^2\vartheta} \left[\frac{J_1(kb)}{kb} \frac{J_0(k_0 a \sin\vartheta}{J_0(ka)} - \frac{J_1(k_0 b \sin\vartheta)}{k_0 b \sin\vartheta} \right] \tag{8}$$

taking into account the Wronskian [11]

$$J_1(x) N_0(x) - J_0(x) N_1(x) = \frac{2}{x}. \tag{9}$$

The value of the quadratic mean of the vibration velocity, $\langle |v|_0^2 \rangle$, occuring in the formulas for the relative impedance, is determined for a case, when the distribution of the force forcing vibrations is not equal zero (uniform) on the whole membrane surface, so $0 \leqslant r \leqslant a$. This also means, that the relative impedance is normalized in such a way, that its real component tends to one when the wave number $k_0 = 2\pi/\lambda$ tends to an infinitelly great value

and the whole membrane surface is excited to vibrate. In formulas (3) and (4) we accept $a = b$ and apply the definition (5), and then $v_2(r_0, t)|_{b=a} = 0$ and

$$v_1(r_0, t)|_{b=a} = v_0(r_0, t) = \frac{if_0}{\eta\omega}\left[\frac{J_0(kr_0)}{J_0(ka)} - 1\right]e^{i\omega t}. \tag{10}$$

On the basis of definition (A2) we achieve

$$\langle|v_0|^2\rangle = \left(\frac{f_0}{a\eta\omega}\right)^2 \int_0^a \left[\frac{J_0(kr_0)}{J_0(ka)} - 1\right]^2 r_0 dr_0. \tag{11}$$

Taking into account formulas [11] for indefinite integrals

$$\int J_0(hw)\, w\, dw = \frac{w}{h} J_1(hw), \tag{12}$$

$$\int J_0^2(hw)\, w\, dw = \frac{1}{2} w^2 [J_0^2(hw) + J_1^2(hw)], \tag{13}$$

we obtain

$$\langle|v_0|^2\rangle = \left(\frac{f_0}{\eta\omega}\right)^2 \left[1 + \frac{1}{2}\frac{J_1^2(ka)}{J_0^2(ka)} - \frac{2}{ka}\frac{J_1(ka)}{J_0(ka)}\right]. \tag{14}$$

Exact expressions for the relative impedance will be reached by placing the calculation results of the characteristic function $M(\vartheta')$, $M(\vartheta'')$ and the quadratic mean of the vibration velocity $\langle|v_0|^2\rangle$ in formulas (A9) and (A12). So

$$\Theta = (k_0 b)^2 \left(\frac{b}{a}\right)^2 \alpha^{-1} \int_0^{\pi/2} \left\{ \frac{1}{1 - \left(\frac{k_0}{k}\right)^2 \sin^2\vartheta'} \left[\frac{J_1(kb)}{kb} \frac{J_0(k_0 a \sin\vartheta')}{J_0(ka)} - \right.\right.$$

$$\left.\left. - \frac{J_1(k_0 b \sin\vartheta')}{k_0 b \sin\vartheta'} \right]\right\}^2 \sin\vartheta' d\vartheta', \tag{15}$$

$$\chi = (k_0 b)^2 \left(\frac{b}{a}\right)^2 \alpha^{-1} \int_0^{\pi/2} \left\{ \frac{1}{1 - \left(\frac{k_0}{k}\right)^2 \frac{1}{\sin^2 y}} \left[\frac{J_1(kb)}{kb} \frac{J_0\left(\frac{k_0 a}{\sin y}\right)}{J_0(ka)} - \right.\right.$$

$$\left.\left. - \frac{\sin y}{k_0 b} J_1\left(\frac{k_0 b}{\sin y}\right)\right] \frac{1}{\sin y}\right\}^2 dy, \tag{16}$$

where

$$\alpha = 1 + \frac{1}{2}\frac{J_1^2(ka)}{J_0^2(ka)} - \frac{2}{ka}\frac{J_1(ka)}{J_0(ka)}. \tag{17}$$

4. Radiation impedance at resonance frequencies

In a particular case, when the frequency of radiated waves is equal to the frequency of free vibrations of the membrane, the resonance effect occurs. At resonance frequencies $ka = x_n$, where quantities x_1, x_2, $x_3 = 2.4048 \ldots$, $5.5201 \ldots$, $8.6557 \ldots$ are the not of equation $J_0(x_n) = 0$. If $ka \to x_n$, $kb = (b/a)ka \to (b/a)x_n$,

$$\lim_{ka \to x_n} \alpha = \lim_{ka \to x_n} \frac{1}{2} \frac{J_1^2(x_n)}{J_0^2(ka)}, \tag{18}$$

then the radiation impedance (15), (16) are of the form

$$\lim_{ka \to x_n} \Theta = \Theta_n' = 2 \left(\frac{k_0 a}{x_n} \right)^2 \left[\frac{b}{a} \frac{J_1(kb)}{J_1(x_n)} \right]^2 \int_0^{\pi/2} \frac{J_0^2(k_0 a \sin \vartheta') \sin \vartheta'}{\left[1 - \left(\frac{k_0 a}{x_n} \right)^2 \sin^2 \vartheta' \right]^2} d\vartheta', \tag{19}$$

$$\lim_{ka \to x_n} \chi = \chi_n' = 2 \left(\frac{k_0 a}{x_n} \right)^2 \left[\frac{b}{a} \frac{J_1(kb)}{J_1(x_n)} \right]^2 \int_0^{\pi/2} \frac{J_0^2 \left(\frac{k_0 a}{\sin y} \right)}{\left[1 - \left(\frac{k_0 a}{x_n} \right)^2 \frac{1}{\sin^2 y} \right]^2} \frac{dy}{\sin^2 y}. \tag{20}$$

The obtained expressions present the radiation resistance and radiation reactance of a circular membrane of a radius a, excited by a force with uniform distribution on its central circular surface of a radius b.

If we then put $b = a$, we reach expressions:

$$\Theta_n = 2 \left(\frac{k_0 a}{x_n} \right)^2 \int_0^{\pi/2} \frac{J_0^2(k_0 a \sin \vartheta') \sin \vartheta'}{\left[1 - \left(\frac{k_0 a}{x_n} \right)^2 \sin^2 \vartheta' \right]^2} d\vartheta' \tag{21}$$

and

$$\chi_n = 2 \left(\frac{k_0 a}{x_n} \right)^2 \int_0^{\pi/2} \frac{J_0^2 \left(\frac{k_0 a}{\sin y} \right)}{\left[1 - \left(\frac{k_0 a}{x_n} \right)^2 \frac{1}{\sin^2 y} \right]^2} \frac{dy}{\sin^2 y} \tag{22}$$

which are known from paper [8] and are the formulae for the radiation impedance of a circular membrane, excited to vibrate axially-symmetrically, so for $a(0, n)$ vibration mode.

5. Radiation resistance in a particular case

The radiation resistance is easier to analyze, when $k_0/k < 1$ and $b = a$. In such a case approximate formulae can be used.

For $(k_0/k)^2 \ll 1$, a reduction can be applied

$$\left[1-\left(\frac{k_0}{k}\right)^2 \sin\vartheta'\right]^{-2} \simeq 1+2\left(\frac{k_0}{k}\right)^2 \sin^2\vartheta' \tag{23}$$

and including $b = a$

$$\Theta' = \frac{(k_0 a)^2}{\alpha}\int_0^{\pi/2}\left[1+2\left(\frac{k_0}{k}\right)^2\sin^2\vartheta'\right]\left[\frac{J_1(ka)}{ka}\,\frac{J_0(k_0 a\sin\vartheta')}{J_0(ka)} - \frac{J_1(k_0 a\sin\vartheta')}{k_0 a\sin\vartheta'}\right]^2 \sin\vartheta'\,d\vartheta'. \tag{24}$$

The obtained expression for the radiation resistance is expressed by a sum of intefrals calculated from formulas (A17), (A19), (A20), (A21) and (A22). After integrating

$$2\alpha\Theta' = 1-\frac{J_1(2x)}{x}-\frac{2}{y}\,\frac{J_1(y)}{J_0(y)}[1-J_0(2x)]+(2\varepsilon)^2\left\{-\frac{J_1(2x)}{x}-\frac{J_1(y)}{yJ_0(y)}U(x)+\left[1+\frac{1}{2}\,\frac{J_1^2(y)}{J_0^2(y)}\right][J_0(2x)+U(x)]\right\}, \tag{25}$$

where

$$x = k_0 a,\ y = ka, \qquad \varepsilon = x/y = k_0/k, \qquad U(x) = \frac{\pi}{2}[J_1(2x)S_0(2x)-J_0(2x)S_1(2x)].$$

In formula (25) only the small terms of second order with respect to ε have been taken into account.

6. Example and conclusions

The diagrams of the radiation resistance and reactance of a circular membrane excited to vibrate by a force with a uniform surface distribution are shown in Fig. 1. $k_0/k = c_M/c = 1$ was taken, so the propagation velocity of a wave in a fluid medium is equal to the wave propagation velocity on the membrane.

Fig. 2 presents diagrams of radiation resistance fo r$k_0/k = 1, 2$ and 4, while Fig. 3 for $k_0/k = 1/2$.

In the analyzed example it was supposed that a non zero uniform distribution of the force forcing vibrations occurs on the whole surface of the membrane.

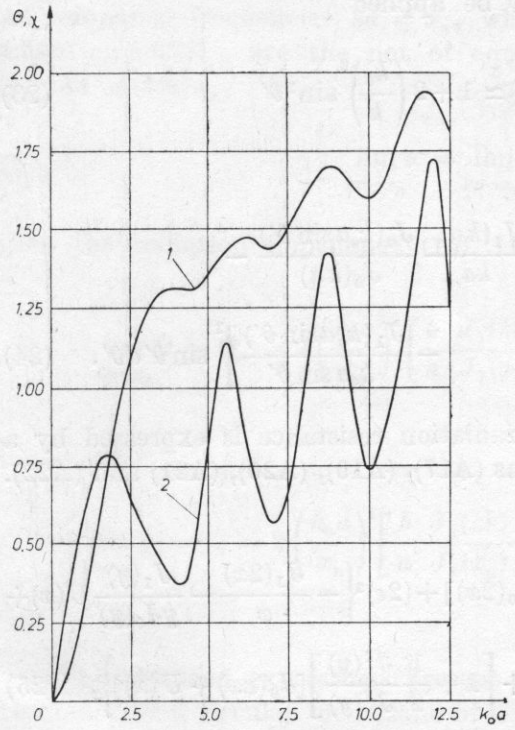

Fig. 1. Normalized impedance (15), (16) versus interference parameter k_0a, for $k_0/k = 1$, $b = a$; *1* — resistance, *2* — reactance

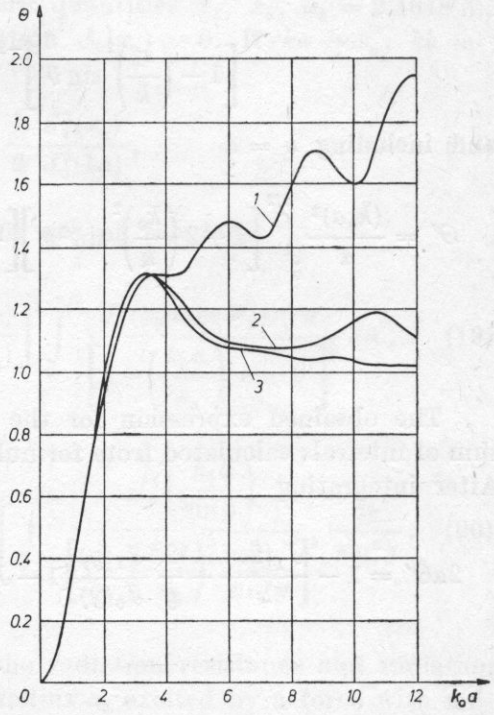

Fig. 2. Normalized resistance (15) versus interference parameter k_0a, for $b = a$; *1* — $k_0/k = 1$, *2* — $k_0/k = 2$, *3* — $k_0/k = 4$

The radiation impedance of a circular membrane depends above all on the interference parameters

$$ka = \frac{\omega}{c_M}a, \qquad k_0a = \frac{\omega}{c}a$$

and at fixed dimensions of the membrane (fixed diameter a) on the frequency of the radiated waves, the propagation velocity in the fluid medium and the propagation velocity of a wave on the membrane.

Unfavourable radiation conditions take place for $c_M/c_0 < 1$. Maximum values of the real component of the radiation impedance are lower from the corresponding resistance values for $k_0/k = 1$. Also such values of the k_0a parameter occur, for which radiation with the employment of the real impedance imponent is not present (Fig. 3).

It results from the above analysis that the radiation impedance is of a finite value for every quantity of the interference parameter $k_0 a$. The acoustical radiation power and vibration velocity for the analyzed membrane were infinitely high for resonance frequencies.

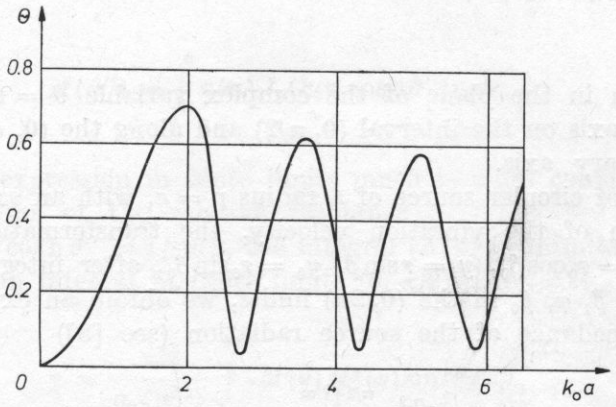

Fig. 3. Normalized resistance (15) versus interference parameter $k_0 a$, for $k_0/k = 1/2$, $b = a$

Appendix A

The calculation of the mechanical impedance of a vibrating membrane is calculated in accordance to definition [10]

$$Z = \frac{N}{\langle |v|^2 \rangle}, \tag{A1}$$

where

$$\langle |v|^2 \rangle = \frac{1}{2\sigma} \int_{\sigma} v^2(r)\, d\sigma \tag{A2}$$

is the quadratic mean value of the vibration velocity, while

$$N = \frac{1}{2} \int_{\sigma} p(\vec{r})\, v^*(\vec{r})\, d\sigma \tag{A3}$$

s the expression for the acoustical power radiated by the membrane v^* marks the value conjugated to the complex quantity of the vibration velocity v.

The acoustical pressure [6]

$$p(\vec{r}) = \frac{ik_0 \varrho_0 c}{2\pi} \int_{\sigma_0} V(\vec{r}_0)\, \frac{e^{-ik_0 |\vec{r} - \vec{r}_0|}}{|\vec{r} - \vec{r}_0|}\, d\sigma_0 \tag{A4}$$

— radiated by the membrane — is rearranged with the application of the Fourier expansion [8]

$$\frac{e^{-ik_0|\vec{r}-\vec{r}_0|}}{|\vec{r}-\vec{r}_0|} = \frac{-ik_0}{2\pi}\int_0^{\pi/2+i\cdot\infty} \exp\{-ik_0\sin\vartheta[(x-x_0)\cos\varphi+(y-y_0)\sin\varphi]\}\sin\vartheta\, d\vartheta\, d\varphi. \tag{A5}$$

Integration in the plane of the complex variable $\vartheta = \vartheta' + i\vartheta''$ is done along the real axis on the interval $(0, \pi/2)$ and along the $(0, \infty)$ line, parallel to the imaginary axis.

In a case of circular source of a radius $r = a$, with an axially-symmetrical distribution of the vibration velocity, the transformation coordinates: $x = r\cos\beta$, $x_0 = r_0\cos\beta_0$, $y = r\sin\beta$, $y_0 = r_0\sin\beta_0$, after integrating over angular variables β, φ, β_0 in the $(0, 2\pi)$ limits, we obtain an expression for the mechanical impedance of the source radiation (see [8])

$$Z = \varrho_0 c\frac{\pi k_0^2}{\langle|v|^2\rangle}\int_0^{\pi/2+i\cdot\infty} M(\vartheta)M^*(\vartheta)\sin\vartheta\, d\vartheta, \tag{A6}$$

where

$$M(\vartheta) = \int_0^a v(r_0)J_0(k_0 r_0\sin\vartheta)r_0\, dr_0 \tag{A7}$$

is the characteristic function of the source.

The relative impedance is

$$Z/\varrho_0 c\sigma_0 = \zeta = \Theta + i\chi, \tag{A8}$$

where Θ, χ are the relative resistance and reactance, respectively, c — wave propagation velocity in a fluid medium, and $\sigma_0 = \pi a^2$.

The real component of the relative impedance, i. e., the relative resistance, is acquired from expression (A6), when the integration in the complex variable $\vartheta = \vartheta' + i\vartheta''$ is performed on the interval on the real axis ϑ' in the $(0, \pi/2)$ limits, i. e.,

$$\Theta = \frac{\pi k_0^2}{\sigma\langle|v|^2\rangle}\int_0^{\pi/2} M(\vartheta')M^*(\vartheta')\sin\vartheta'\, d\vartheta'. \tag{A9}$$

In order to isolate the imaginary component of the relative impedance in formula (A6), calculations have to be limited to the calculation of the integral over a half-line parallel to the imaginary axis in the complex variable plane, $\vartheta = \vartheta' + i\vartheta''$. Accepting $\vartheta' = \pi/2$, we obtain $\vartheta = \pi/2 + i\vartheta''$, $0 \leqslant \vartheta'' < \infty$,

and then

$$\chi = \frac{\pi k_0^2}{\sigma \langle |v^2| \rangle} \int_0^\infty M(\vartheta'') M^*(\vartheta'') \cos h\vartheta'' d\vartheta'' \tag{A10}$$

while

$$M(\vartheta'') = \int_0^a v(r_0) J_0(k_0 r_0 \cosh \vartheta'') r_0 dr_0. \tag{A11}$$

An integral expression in finite limits much is more convenient for numerical calculations of the relative reactance.

Substituting $\cosh \vartheta'' = 1/\sin y$, the integral (A10) in infinite limits $(0, \infty)$ is converted to an integral in finite limits $(0, \pi/2)$, i. e.,

$$\chi = \frac{\pi k_0^2}{\sigma_0 \langle |v|^2 \rangle} \int_0^{\pi/2} M(y) M^*(y) \sin^{-2} y \, dy, \tag{A12}$$

where

$$M(y) = \int_0^a v(r_0) J_0 \left(\frac{k_0 r_0}{\sin y} \right) r_0 dr_0. \tag{A13}$$

Appendix B

In order to determine the value of the integral

$$A_{10} = \int_0^{\pi/2} J_0(x \sin t) J_1(x \sin t) dt \tag{A14}$$

the product of two Bessel function is expanded into a series [4], [11]

$$J_p(u) J_q(u) = \sum_{n=0}^{\infty} (-1)^n \frac{(2n+p+q)! (\frac{1}{2}u)^{2n+p+q}}{n!(n+p)!(n+q)!(n+p+q)!} \tag{A15}$$

and, putting $p = 0$, $q = 1$, $u = x \sin t$ we have

$$J_0(x \sin t) J_1(x \sin t) = \sum_{n=0}^{\infty} (-1)^n \frac{(2n+1)! (\frac{1}{2} x \sin t)^{2n+1}}{(n!)^2 [(n+1)!]^2}. \tag{A16}$$

The alternating series (A16) is substituted in the integral in expression (A14). Integrating term by term we obtain

$$A_{10} = \sum_{n=0}^{\infty} (-1)^n \frac{(2n+1)!(\frac{1}{2}x)^{2n+1}}{[n!(n+1)!]^2} \int_0^{\pi/2} \sin^{2n+1} t\,dt$$

$$= \frac{1}{2x} \sum_{n=0}^{\infty} (-1)^n \frac{x^{2n+2}}{[(n+1)!]^2} = \frac{1}{2x}[1 - J_0(2x)], \quad \text{(A17)}$$

where the intagrate property was applied

$$\int_0^{\pi/2} \sin^{2n+1} t\,dt = \frac{1}{2} \frac{\Gamma(n+1)\sqrt{\pi}}{\Gamma(n+3/2)} = \frac{2^{2n}(n!)^2}{(2n+1)!}. \quad \text{(A18)}$$

In a similar way the other integrals, essential for the radiation resistance analysis, can be calculated. Most of them is considered in papers [1] and [4]:

$$A_{00} = \int_0^{\pi/2} J_0^2(x\sin t)\sin t\,dt = \frac{1}{2x} \int_0^{2x} J_0(t)\,dt$$

$$= J_0(2x) + \frac{\pi}{2}[J_1(2x)S_0(2x) - J_0(2x)S_1(2x)], \quad \text{(A19)}$$

where S_n is the n-order STRUVE function.

$$A_{11} = \int_0^{\pi/2} \frac{J_1^2(x\sin t)}{\sin t}\,dt = \frac{1}{2}\left[1 - \frac{J_1(2x)}{x}\right], \quad \text{(A20)}$$

$$B_{10} = \int_0^{\pi/2} J_1(x\sin t)J_0(x\sin t)\sin^2 t\,dt = \frac{\pi}{4x}[J_1(2x)S_0(2x) -$$

$$- J_0(2x)S_1(2x)], \quad \text{(A21)}$$

$$B_{11} = \int_0^{\pi/2} J_1^2(x\sin t)\sin t\,dt = J_0(2x) - \frac{J_1(2x)}{x} +$$

$$+ \frac{\pi}{2}[J_1(2x)S_0(2x) - J_0(2x)S_1(2x)]. \quad \text{(A22)}$$

It is convenient to introduce function

$$U(x) = \frac{\pi}{2}[J_1(2x)S_0(2x) - J_0(2x)S_1(2x)] \quad \text{(A23)}$$

which can be approximated for $x \ll 1$ by the expression

$$U(x) \simeq \frac{2}{3}x^2\left(1 + \frac{3}{10}x^2\right) \quad \text{(A24)}$$

if we use the approximate formulae for the STRUVE and BESSEL functions [4]:

$$S_0(x) \simeq \frac{2}{\pi} x\left(1-\frac{x^2}{9}\right), \quad S_1(x) \simeq \frac{2}{3\pi} x^2\left(1-\frac{x^2}{15}\right), \tag{A25}$$

$$J_0(x) \simeq 1-\frac{x^2}{4}, \quad J_1(x) \simeq \frac{x}{2}\left(1-\frac{x^2}{8}\right). \tag{A26}$$

References

[1] J. S. GRADSZTEJN, I. M. RYŻYK, *Integral, sum and series tables*, PWN, Warszawa 1964 (in Polish).

[2] T. HAJASAKA, *Elektroakustika*, Mir, Moskwa 1982.

[3] I. MALECKI, *The theory of waves and acoustic systems*, PWN, Warszawa 1964 (in Poilsh).

[4] N. W. MCLACHLAN, *Bessel functions for engineers*, PWN, Warszawa 1964 (in Polish).

[5] D. T. PORTER, *Self- and mutual – radiation impedance and beam patterns for flexural disks in a rigid plane*, JASA, **36**, 6, 1154–1161 (1964).

[6] J. W. S. RAYLEIGH, *Theory of sound*, MACMILLAN, London 1929.

[7] W. RDZANEK, *Directional characteristic of a circular membrane vibrating under the influence of a force with a uniform surface distribution*, Arch. Acoust.

[8] W. RDZANEK, *Mutual acoustic impedance of circular membranes and plates with Besel axially – symmetric vibration velocity distributions*, Arch. of Acoust., **5**, 3, 237–250 (1980).

[9] E. SKUDRZYK, *Simple and complex vibratory systems*, University Press, University Park and London 1968.

[10] C. E. Wallace, *Radiation resistance of a rectangular panel*, JASA, **51**, 3(2), 946–952 (1972).

[11] G. N. Watson, *Theory of Bessel functions*, 2nd ed., University Press, Cambridge 1966.

Received on 23 November, 1984; revised version on 4 December, 1985.

ARCHIVES OF ACOUSTICS
11, 1, 53-60 (1986)

ULTRASONICS ABSORPTION MEASUREMENTS OF A LIQUID WITH BACKED TRANSDUCER

V. N. BINDAL T. K. SAKSENA, J. N. SOM

National Physical Laboratory, New Delhi, India

An effect of backing of the transducer on the measured value of absorption of a liquid have been shown using shock excited system. The resulting deviation in the measured value of absorption from the accepted value has been observed to be large as 40%, depending on the damping produced. A mechanism to explain the observed variation of the measured value of absorption with backing has been put forward. Implication of the work in characterisation of ultrasonic probe have been discussed.

1. Introduction

While working on the measurement of ultrasonic absorption in liquids [1], the authors observed that appreciable error in measurement is introduced if the transducer is highly damped, even if usual precautions [2, 4] in the absorption measurement are taken. This phenomenon has not been discussed earlier in the literature. This led the authors to investigate whether this observation can be used to throw light on the damping of a transducer. Damping of the transducer is required to prevent ringing which is important for acheiving high resolution for analysing the defects close together and also with respect to the transducer. It finds application in transducers used for *NDT*, medical diagnostic and ultrasonic spectroscopy.

Present studies concern the measurement of absorption in a non-relaxational liquid using transducers having backing of various acoustic impedances. The dependence of the measured value of absorption on the damping characteristic of the transducer as studied by observing the ringing pattern, has been discussed. Measurements of absorption are also carried out with

a number of normal *NDT* probes to examine this phenomenon. It has been attempted to explain the mechanism lying behind it and experimentally to verify it by examining the wave shape of the acoustic pulse.

2. Experimental

Ultrasonic absorption in liquids were measured with an ultrasonic flaw detector using backed and unbacked transducers. These transducers were prepared with piezoelectric ceramic *NPLZT-5A* [5] disc of diameter (D) 20 mm, and thickness (t) 0.6 mm using araldite and tungsten powder loaded araldite as backings which were cemented to the ceramic dise with salol for taking measurements with same disc. Ultrasonic pulses were sent into the liquid and the amplitude was noted. By varying the acoustic path length, the diminuation of echo height was measured from which absorption coefficient α/ν^2 was evaluated. The parallelism between the transducers face and the reflector was assured by adjusting the reflector-platform maximum echo height

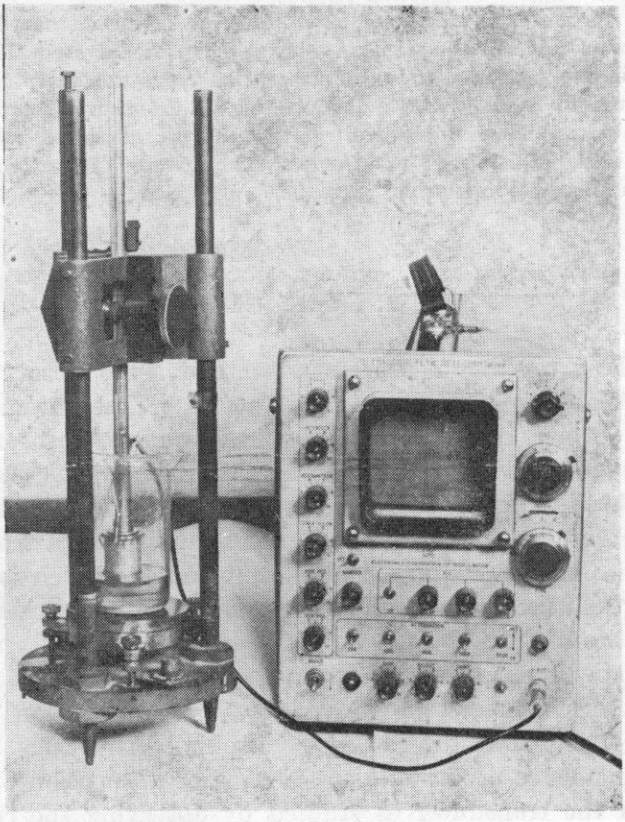

Fig. 1

and diffraction effects were avoided by working in the Fresnel region. An air backed thin stainless steel plate having thickness 0.4 mm was used as a reflector which was kept fixed at the bottom of the liquid cell (Fig. 1).

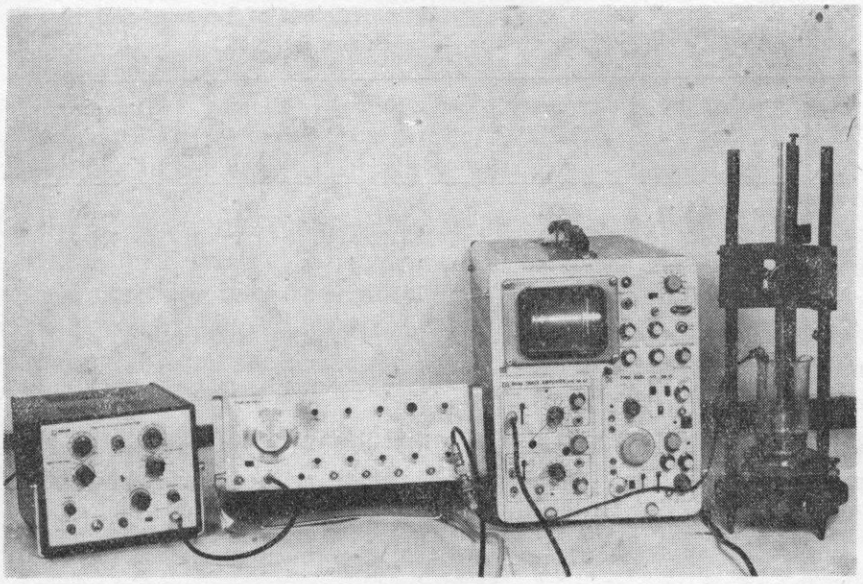

Fig. 2

Ringing characteristics of these transducers were studied using a pulsed *R. F. System* (Fig. 2) in which a sinusoidal continuous wave signal was modulated by pulses from a square wave generator to produce gated signals of known duration. The response of the transducer to the signal was monitored on an oscilloscope.

Examination of the waveshape of the acoustic pulse generated by these transducers was made using a wideband probe hydrophone in an unechoic water tank.

3. Results

The absorption coefficient α/ν^2 of benzene (L. R. GRADE) was measured at first with an airbacked transducer (ceramic dise diameter 20 mm, and thickness 0.9 mm) to test the performance of the set up. α/ν^2 of benzene was observed to be $\sim 990 \times 10^{-17}$ np cm^{-1} sec^2 which is close to the value reported in literature [3], [4]. After that, with the backed transducers α/ν^2 of benzene was measured. The results are shown in the Table 1. The maximum scatter in measurements for a given absorption value is within 4%. From the Table 1, it is seen that there is a large deviation $\sim$ (40%) in the measured value

of absorption when tungdten-loaded araldite backing is used. Thus damping of the transducer introduced by the backing is seemed to affect the measured value of absorption.

Table 1. Measured values of absorption coefficient of benzene and ringing time of the transducers at 25°C

Sl. No.	Type of backing	Frequency ν [MHz]	$\alpha/\nu^2 \times 10^{17}$ [np cm^{-1} sec^2]	Ringing time [μs]	Damping coefficient $k \times 10^{-5}$
1	Air Backing	3.93	990	2.1	4.76
2	Araldite Backing	3.90	1312	1.4	7.14
3	Tungsten loaded Araldite Backing	3.89	1370	0.56	17.8

Damping of the transducer is studied with the measurement of the ringing time. The typical ringing patternsof the transducers are shown in Fig. 3. Using the equation

$$Y = Y_0 e^{-kt} \cos \omega t \tag{1}$$

the ringing time $\tau = 1/k$ has been evaluated from these patterns.

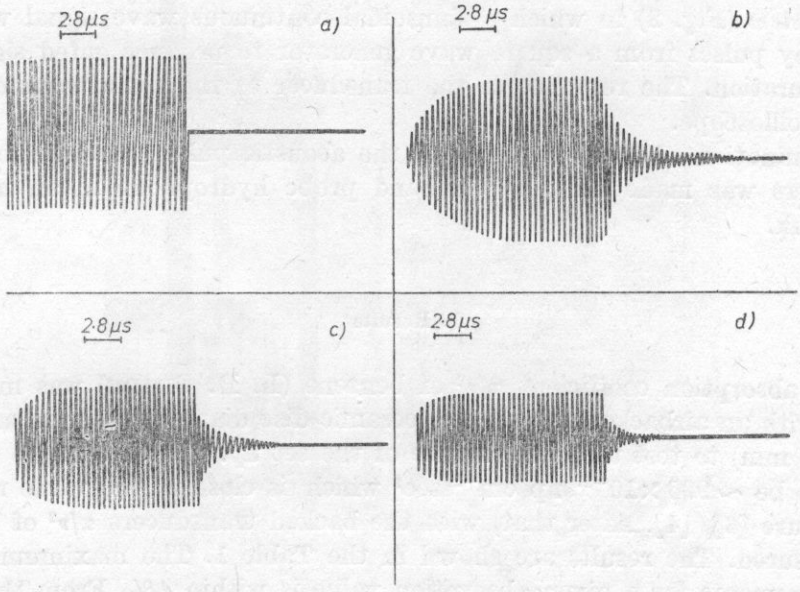

Fig. 3

Here k is the damping coefficient and τ is defined as the time in which the sound amplitude is reduced to $1/e$ of its initial value. The value of τ and k are ahown in the Table 1. It is seen from the Table 1 that as the backing is changed the ringing time τ is shortend and the measured value of absorption of the liquid increases, thus indicating a close correlation between the two.

4. Discussions

The deviation in measured value of absorption of the liquid observed in the present work can not be explained in terms of mechanical, acoustical or electronic causes as they have been taken into account at the time of measurement. PELLAM and GALT [2] and NOZDREV [3] however, discussed the effect of pulse width on the measurement of absorption of a liquid. According to them, error in absorption measurement can be occured if a short pulse is used and fractional error in absorption, $\Delta\alpha$, can be correlated with frequency spread, $\Delta\nu$, as:

$$\Delta\alpha/\alpha = [\Delta\nu/(2\nu_0)]^2, \tag{2}$$

where ν_0 is the resonant frequency of the transducer.

But using a long pulse, error due to above cause can be eliminated. In the present case, the authors suggest the following mechanism to explain the observed results. The flaw detector generates a transient pulse to shock excite the transducer. The Fourier transform of this pulse has got a wide spectrum in the frequency domain. The air-backed transducer has got a sharper resonance and excited into a narrower range of frequency while heavily bac-

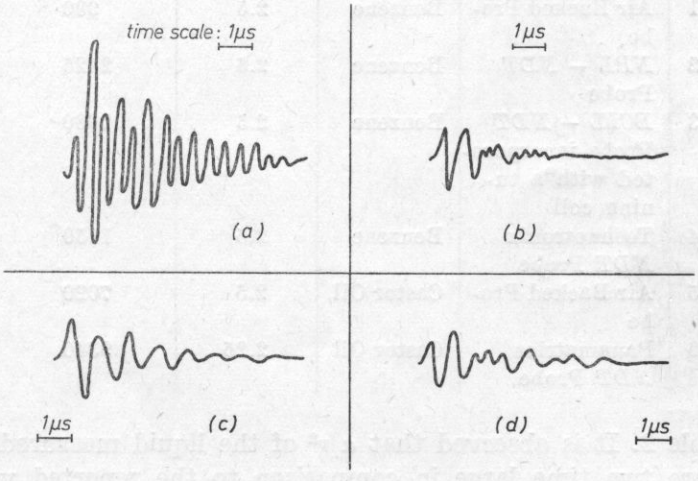

Fig. 4

ked one has a broader resonance curve and excited into wider range of frequency. The frequency spread $\Delta\nu$ in the later is larger than in the former depending upon the backing and hence the error in measurement of α will occur because the individual frequency component of the spectrum is attenuated in different degree since the absorption has a frequency dependence.

The experimental evidence that a marked frequency spread is produced in the transducer is shown in the Fig. 4. From the hydrophone response of the acoustic pulse generated by an airbacked transducer due to shock excitation (Fig. 4a), it is seen that there is a given pulse containing a number of cycles with no frequency change where as in that of the backed transducer (Fig. 4b) there is a broading of cycles in the pulse which is due to superposition of various vibration in different frequency range. Also acoustic pulses of other commercial probes are shown in Figs 4c and 4d.

5. Concluding Remarks

The application of this work is visualised in the characterisation of *NDT* probe. These probes use a high degree of backing which can result in significant changes in the measured value of absorption coefficient of the liquid. Some results which are obtained with different *NDT* commercial probes are

Table 2. Measured value of absorption coefficient of liquids using NDT probes at room temperature 25°C

Sl. No.	Probe	Liquid	Frequency ν MHz	$\alpha/\nu^2 \times 10^{17}$ [np cm^{-1} sec^2]
1	Air Backed Probe	Benzene	2.5	990
2	*NPL – NDT* Probe	Benzene	2.5	2425
3	*ECIL – NDT* Probe incorporated with a tuning coil	Benzene	2.5	1680
4	Technotronix *NDT* Probe	Benzene	2.5	1650
5	Air Backed Probe	Castor Oil	2.5	7020
6	Panamatrios *NDT* Probe	Castor Oil	2.25	9340

shown in Table 2. It is observed that α/ν^2 of the liquid measured with these transducers are two time large in comparison to the reported value in the literature (in the case of benzene). The magnitude in deviation of α/ν^2 can

thus be used as an indication of the degree of damping due to the backing. The method is novel in approach and involves no complicated instrumentation.

References

[1] V. N. Bindal, T. K. Saksena, J. N. Som, *National Seminaron Acoustics and Ultrasonics*, cochin, 8–10th Feb., 1981.

[2] J. R. Pellam, J. K. Galt, J. Chem. Phys., 608 (1946).

[3] V. F. Nozdrev, *The Use of Ultrasonics in Molecular Physics*, Pergamon Press London, 1965.

[4] J. J. Markham, R. T. Beyer, B. R. Lindsay, *Rev. Modern Phys.*, **23**, 353 (1951).

[5] G. C. Tain, V. N. Bindal, Tanardan Singh, Ved Singh, Narayana Swami and N. C. Soni, Ind. Tr. Pure Appl. Phys., **21**, 573 (1983).

Received on 13 December, 1983; revised version on 15 September, 1985.

ARCHIVES OF ACOUSTICS
11, 1, 61-74 (1986)

REFLECTION AND TRANSMISION OF A BLEUSTEIN-GULAYEV SURFACE WAVE BY THE EDGE OF A PIEZOELECTRIC MATERIAL

P. KIEŁCZYŃSKI, W. PAJEWSKI

Laboratory of Acousto-electronics,
Institute of Fundamental Technical Research
Polish Academy of Sciences
00-049 Warsaw, Świętokrzyska 21

The paper presents an analysis of the effect of reflection and transmission of a BLEUSTEIN-GULAYEV transverse surface wave by an edge of a piezoelectric area formed by two mechanically free and electrically shorted planes intersecting at an angle θ. The fundamental properties of the *B-G* waves have been discussed, as well as the possibilities of their application. A method of calculating the coefficients of reflection, A_R, and transmission, A_T, for a *B-G* wave by a metallized piezoelectric edge of a 6 mm symmetry, has been presented schematically. The values of coefficients $|A_R|^2$ and $|A_T|^2$ were measured in $LiJO_3$ crystal samples. Suggestions concerning further research on the analyzed effect have been inducted in the conclusions.

Introduction

The former research has shown, that transverse surface waves do not exist in homogeneous elastic materials [1]. BLEUSTEIN'S discovery in 1968 [2] and independantly GULAYEV'S discovery of transverse surface waves in homogeneous piezoelectric materials was a certain surprise to the scientists. BLEUSTEIN-GULAYEV type surface waves can propagate on a mechanically free surface of a piezoelectric, which has a two-fold axis of symmetry [4]. LOVE type surface transverse waves have one non-vanishing component of the mechanical displacement and can propagate in elastic materials having a non-homogeneous subsurface layer [5]. As opposed to them BLEUSTEIN-GULAYEV waves, except for the transverse component of the mechanical displacement U_2 (Fig. 1), have an electric potential φ, induced by the piezoelectric effect of the foundation [9]. For this reason BLEUSTEIN-GULAYEV waves are cal-

led acoustoelectric waves. In agreement with the state of research, the BLEUSTEIN-GULAYEV waves do not exhibit dispersion, what has a significance in the measurements of their velocities with the application of the PAPADAKIS' reflection method [6]. In the last years a hypothesis was put forward, stating that the position of a metallic layer on the surface of a piezoelectric causes the formation of a subsurface intermediate layer with decreased piezo-

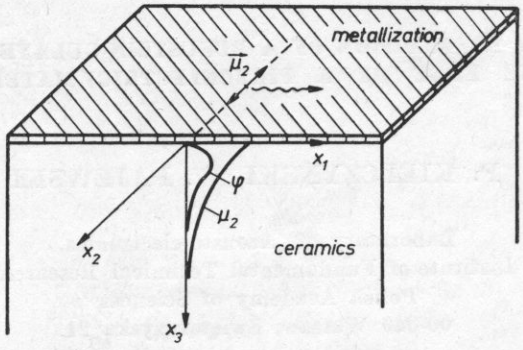

Fig. 1. Mechanical displacement U_2 and electric potential of a BLEUSTEIN-GULAYEV wave propagating on a metallized surface of a piezoelectric with a diad axis $\| x_2$

electric properties [7]. If this hypothesis would prove itself true, this would radically change the understanding of the essence of the BLEUSTEIN-GULAYEV waves, which in this case should be dispersive and exhibit a multimodal structure. Hitherto existing research results do not solve this problem finally [7], [8].

The research of effect of reflection and transmission of a BLEUSTEIN-GULAYEV wave by an edge is of great theoretical significance, because up to now there an accurate method of solving this problem does not exist [10], [11]. Furthermore the knowledge of the coefficient of reflection and transmission of a *B-G* wave by an edge is of fundamental significance in the construction of acoustoelectric devices for analogue processing of telecommunication signals: delay lines [12] and broad-band resonators [13]. Taking advantage of the invertibility of the diffraction effects on the investigaled edge, a new method of generating *B-G* waves with the aid of volume transverse SH waves falling from the inside of the medium onto the studied edge, was given in paper [14].

This paper is concerned with the theoretical and experimental study of the effect of reflection and transmission of a *B-G* type transverse surface wave by a metallized egde of a piezoelectric with a 6 mm, 4 mm symmetry, or of piezoelectric ceramics. This effect was also investigated experimentally for piezoelectric crystals with a 6 symmetry [15].

Theory

The piezoelectric material covers an area limited by two planes: $x_3 = 0$ and $\xi_3 = 0$, intersecting under an angle Θ (Fig. 2). The two intersecting planes are unbounded mechanically free and electrictrically shorted (infinitely thin layer of an perfect conductor). A *B-G* wave propagating on surface $x_3 = 0$ in the $+x_1$ direction encounters a strong geometrical discontinuity of the surface — the

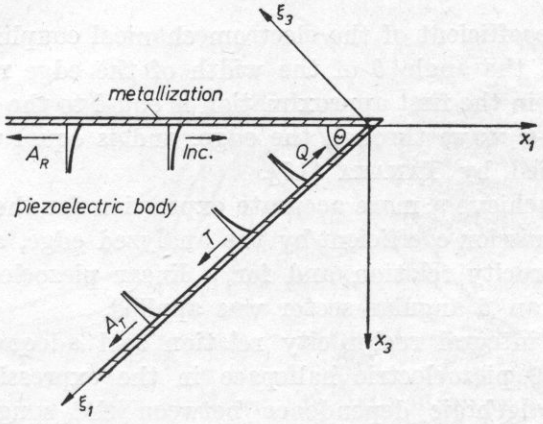

Fig. 2. Schematic diagram of an incident (i), reflected (r), transmitted (t) and produced by auxiliany sources (T, Q) BLEUSTEIN-GULAYEV wave in an edge area of an θ angle of flare

edge area of an angle θ. Therefore, two *B-G* waves appear: reflected, propagating in direction $-x_1$, and passing through, propagating in direction $+\xi_1$, on the surfaces limiting the edge region. The rest of the incident wave energy is changed into a volume transverse wave radiated into the material in the angular sector Θ.

Further on the method will be presented of calculating the coefficient of reflection and transmission of a *B-G* type plane wave by the edge of a piezoelectric. This method is presented in detail in paper [15].

A *B-G* wave, incident on the investigated region edge, fulfills the (zero) boundary conditions for the stress tensor component τ_{23} and electric potential φ, only on the guiding surface $x_3 = 0$. Components τ_{23} and φ of the incident wave are not zeroed on the reflecting surface $\xi_3 = 0$. In order to fulfil the zero boundary conditions on surface $\xi_3 = 0$, an assumption was done, that on this surface auxiliary sources of stress and electric potential act, which together with τ_{23} and φ of the incident wave satisfy the zero boundary conditions on this surface. Introduced auxiliary sources generate on surface $\xi_3 = 0$ two *B-G* type plane waves with amplitudes T and Q, propagating in directions $+\xi_1$ and $-\xi_1$, respectively. Amplitudes T and Q (LAMB problem for

a piezoelectric halfspace $\xi_3 \geqslant 0$), calculated with the application of the methods of the FOURIER analytical functions and transformations [26], [16], are expressed by the following formulae:

$$T = \frac{k_{15}^2}{k_{15}^2 + j\operatorname{ctg}(\theta/2)}, \tag{1}$$

$$Q = j\frac{k_{15}^2}{1+k_{15}^2}\operatorname{ctg}(\theta/2), \tag{2}$$

where k_{15} is the coefficient of the electromechanical coupling of the piezoelectric material and the angle θ of the width of the edge region.

Amplitude T in the first approximation is equal to the of coefficient transmission of the *B-G* wave through the edge, and is equal to the transmission coefficient obtained by TANAKA [17].

In order to achieve a more accurate expression for the *B-G* wave for reflection and transmission coefficient by the analyzed edge, a double integrated form of the reciprocity relation and for a linear piezoelectric material [18] in the region of an θ angular sector was applied.

Placing the integral reciprocity relation and adequate Green function [19] for a $x_3 \geqslant 0$ piezoelectric halfspace in the expression, we obtain the following linear algebraic dependence between the sought reflection, A_R, and transmission, A_T, coefficients:

$$A_R = R + Q(T + A_T), \tag{3}$$

where R is the reflection coefficient in the first approximation and is expressed by the following formula:

$$R = \frac{1}{2}\frac{k_{15}^2}{k_{15}^2 + j\operatorname{ctg}\theta}\frac{\sin\theta + jk_{15}^2\cos\theta}{\sin\theta - jk_{15}^2\cos\theta}. \tag{4}$$

The application of the reciprocity relation and the GREEN function for the $\xi_3 \geqslant 0$ piezoelectric halfspace, leads to another linear algebraic dependence between coefficients A_R and A_T

$$A_T = T + Q(R + A_R). \tag{5}$$

Solving a system of two algebraic equations, (4) and (5), in relation to A_R and A_T, we reach the final form of the expressions of the coefficients of reflection and transmission of a *B-G* wave by a metallized edge of a piezoelectric:

$$A_R = \frac{1+Q^2}{1-Q^2}R + \frac{2Q}{1-Q^2}T, \tag{6}$$

$$A_T = \frac{1+Q^2}{1-Q^2}T + \frac{2Q}{1-Q^2}R, \tag{7}$$

where amplitudes T, Q and R are expressed by formulas (1), (2) and (4), respectively.

The functional discussion of the dependence of the reflection A_R, and transmission, A_T, coefficients on the electromechanical coupling coefficient k_{15} and the θ angle, on the basis of expressions (6) and (7) is rather inconvenient. To this

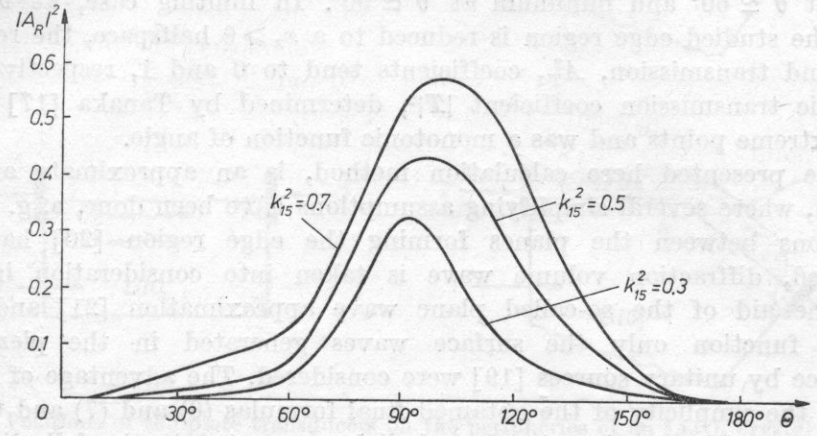

Fig. 3. Calculated reflection energy coefficient $|A_R|^2$ of a BLEUSTEIN-GULAYEV wave as a function of angle θ. Electromechanical coupling coefficient k_{15} is a parameter

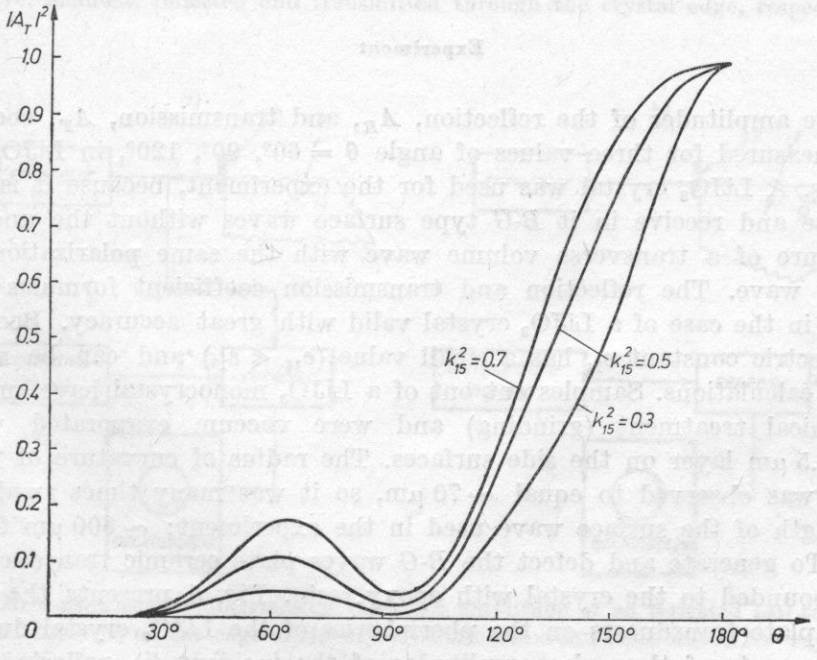

Fig. 4. Calculated transmission energy coefficient $|A_T|^2$ of a BLEUSTEIN-GULAYEV wave as a function of angle θ. Electromechanical coupling coefficient k_{15} is a parameter

end, expressions (6) and (7) were tabularized with the aid of a computer and the calculation results are presented in Fig. 3 and 4. These figures show, that with the increase of the electromechanical coupling coefficient k_{15}, the values of the energetic coefficients of reflection, $|A_R|^2$, and transmission, $|A_T|^2$, increase for the whole θ angle range. Furthermore, coefficient $|A_T|^2$ has a maximum at $\theta \simeq 90°$, while coefficient $|A_T|^2$ has two extreme values, i. e. maximum at $\theta \simeq 60°$ and minimum at $\theta \simeq 90°$. In limiting case, at $\theta \simeq 180°$, when the studied edge region is reduced to a $x_3 \geqslant 0$ halfspace, the reflection, $|A_R|^2$ and transmission, A_T^2, coefficients tend to 0 and 1, respectively. The energetic transmission coefficient $|T|^2$, determined by Tanaka [17] did not have extreme points and was a monotonic function of angle.

The presented here calculation method, is an approximate analytical method, where several simplifying assumptions have been done, e. g. multiple reflections between the planes forming the edge region [20] have been neglected, diffraction volume wave is taken into consideration indirectly with the aid of the so-called plane wave approximation [21] and in the GREEN function only the surface waves generated in the piezoelectric halfspace by unitary sources [19] were considered. The adventage of this method is the simplicity of the obtained final formulas (6) and (7) and the good conformity with experiment, what shall be presented in the following parts of the paper.

Experiment

The amplitudes of the reflection, A_R, and transmission, A_T, coefficients were measured for three values of angle $\theta = 60°$, 90°, 120°, in $LiJO_3$ crystal samples. A $LiJO_3$ crystal was used for the experiment, because it is easy to generate and receive in it *B-G* type surface waves without the undesirable admixture of a transverse volume wave with the same polarization as the surface wave. The reflection and transmission coefficient formulas (6) and (7) are in the case of a $LiJO_3$ crystal valid with great accuracy. Because its piezoelectric constant e_{14} has a small value ($e_{14} \ll e_{15}$) and can be neglected in the calculations. Samples cut out of a $LiJO_3$ monocrystal have undergone mechanical treatment (grinding) and were vaccum evaporated with an Al ~ 0.5 μm layer on the side surfaces. The radius of curvature of the edge region was observed to equal ~ 70 μm, so it was many times smaller than the length of the surface wave used in the experiment: ~ 600 μm for $f \simeq 4$ MHz. To generate and defect the *B-G* waves plate ceramic transducers were used, bounded to the crystal with epoxy resin. Fig. 5 presents the position of the plate transducers on the pheripheries of the $LiJO_3$ crystal during the measurements of the pulse amplitudes of the incident (i), reflected (r) and

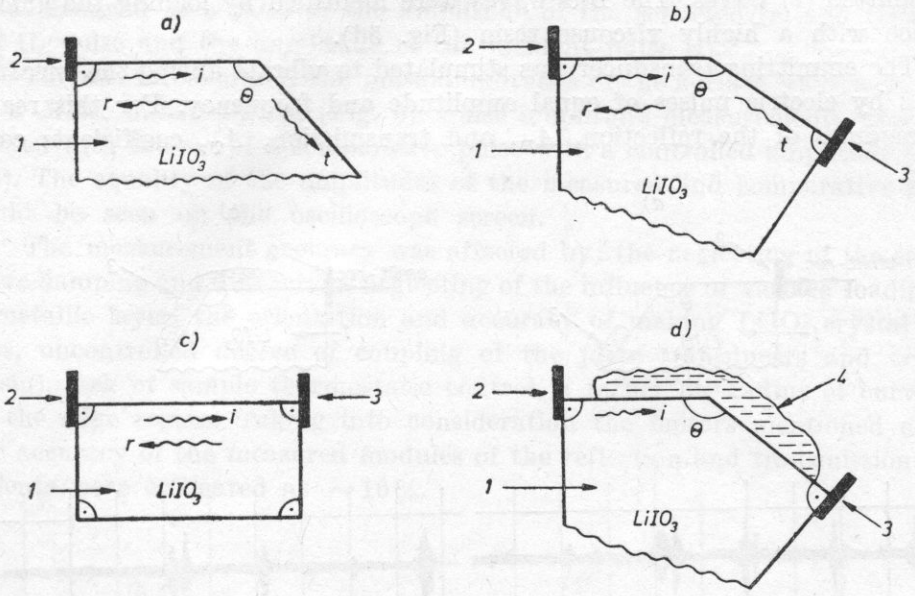

Fig. 5. Positions of the plate transducers on the peripheries of an $LiJO_3$ crystal during the measurements of the pulse amplitude of the *a*) reflected, *b*) transmitted, *c*) incident BLEUSTEIN-GULAYEV wave. Resin applied to the crystal surface (*d*). *1* — $LiJO_3$ crystal sample, *2*, *3* — plate transducers, *4* — resin layer, *i*, *r*, *t* — impulses of the BLEUSTEIN-GULAYEV wave, incident, reflected and transmitted through the crystal edge, respectively

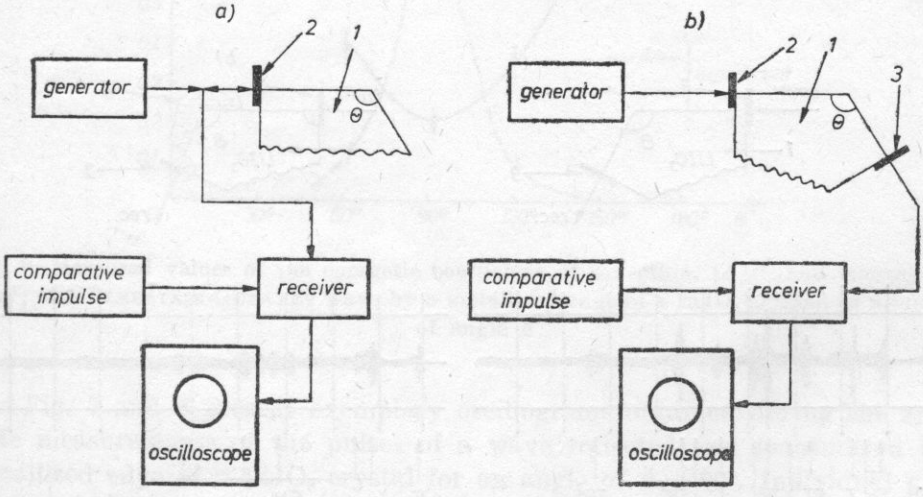

Fig. 6. Measuring set for determining the pulse amplitude of an reflected (*a*), transmitted (*b*) and incident (*c*) on the edge of the crystal BLEUSTEIN-GULAYEV wave. *1* — crystal sample, *2* — emmitting-receinving transducer, *3* — receiving transducer

transmitted (t) waves. The *B-G* waves were identified by loading the guiding surface with a highly viscouse resin (Fig. 5d).

The emmitting transducer was stimulated to vibrate during the measurements by electric pulses of equal amplitude and frequency. For this reason the modules of the reflection, A_R, and transmission, A_T, coefficients could

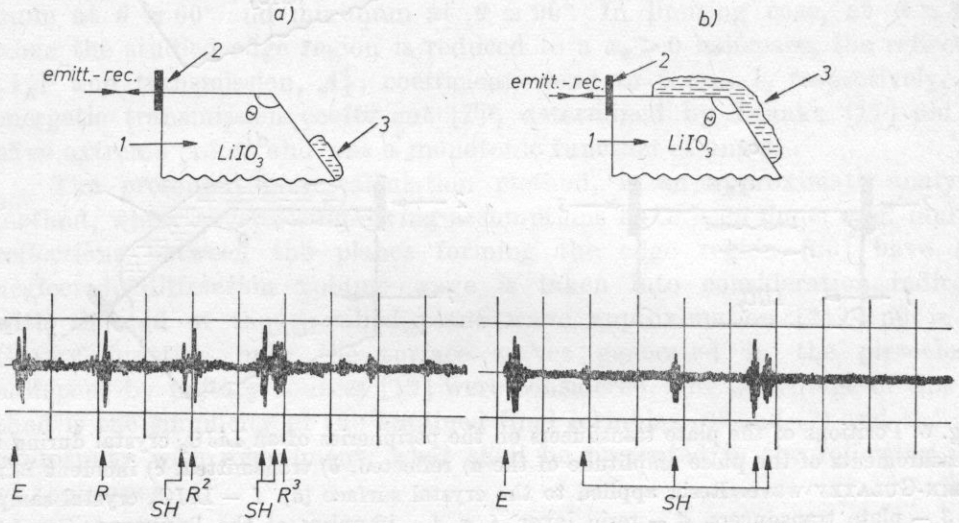

Fig. 7. Oscillograms of impulses of a BLEUSTEIN-GULYEV wave reflected from the edge of a $LiJO_3$ crystal, for an angle $\theta = 90°$. The crystal surface with resin (b) and without resin (a). *1* — $LiJO_3$ crystal sample, *2* — emmitting-receiving transducer, *3* — resin layer

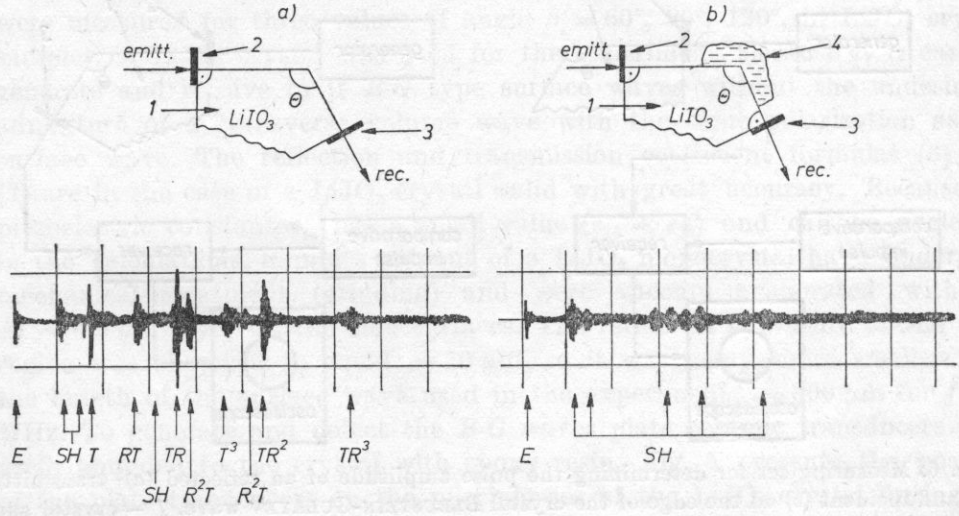

Fig. 8. Oscillograms of impulses of a BLEUSTEIN-GULAYEV wave transmitted by a $LiJO_3$ crystal edge. The crystal surface with out resin (a) and with resin (b). $\theta = 90°$

be determined as a ratio of the amplitude of the reflected (r) and transmitted (t) pulse and the amplitude of the incident pulse (i).

The measurements of the pulse amplitudes of the surface wave were done on a *Matec* measuring set (Fig. 6). Pulse amplitude measurements were conducted with the aid of a comparative pulse with a controlled amplitude (± 0.2 dB). The equality of the amplitudes of the measured and comparative pulses could be seen on the oscilloscope screen.

The measurement accuracy was affected by: the neglecting of the surface wave damping and diffraction, neglecting of the influence of surface loading by a metallic layer, the orientation and accuracy of making $LiJO_3$ crystal samples, uncontrolled degree of coupling of the plate transducers and crystal, (resin), lack of sample thermostatic control, a rather big radius of curvature of the edge region. Taking into consideration the factors mentioned above, the accuracy of the measured modules of the reflection and transmission coefficients were estimated at $\sim 10\,\%$.

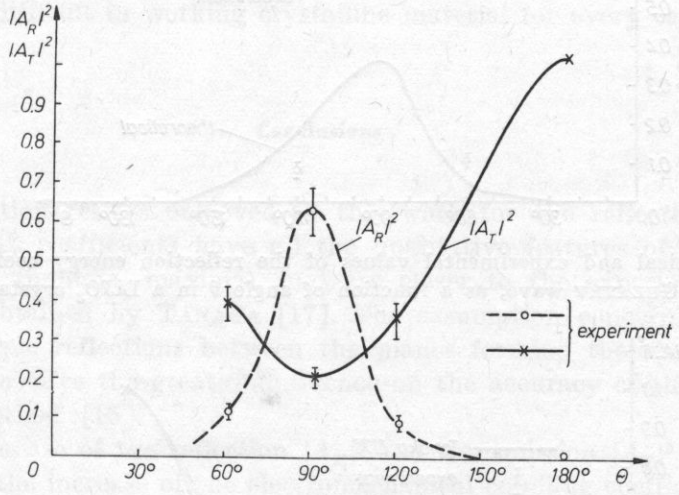

Fig. 9. Measured values of the energetic coefficient of reflection, $|A_R|^2$, and transmission, $|A_T|^2$, of a BLEUSTEIN-GULAYEV wave by a metallized edge of a $LiJO_3$ crystal, as a function of angle θ

Fig. 7 and 8 present exemplary oscillograms obtained during the amplitude measurements of the pulses of a wave reflected and transmitted by a metallized edge of a $LiJO_3$ crystal for an angle of $\theta = 90°$. Individual pulses on the oscillograms were identified as pulses of a *B-G* wave multiply passing or reflected by the crystal edge. For example, the pulse marked with symbol r^2t in Fig. 8 is a pulse which after passing through the investigated edge (t), was reflected twice from it (r^2) before reaching the receiving transducer. Sym-

bol SH marks the existing in the studied structure pulses of a transverse volume wave.

Fig. 9 shows the values of the reflection $|A_R|^2$ and transmission $|A_T|^2$ energy coefficients, measured in the described measuring set-up.

Comparison of Theoretical and Experimental Results

The maximum of the measured reflection energy coefficient, $|A_R|^2$, was localized near the angle $\theta \simeq 90°$ (Fig. 10), what is in accordance with the theoretical expectations expressed by equation (6). It is worth noting, that at an angle of $\theta \simeq 90°$ a minimum of the reflection coefficient occurs for RAYLEIGH type surface waves [22]. This can be explained by the fact, that RAY-

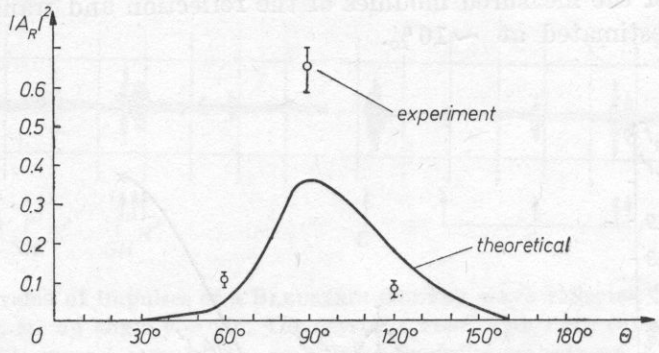

Fig. 10. Theoretical and experimental values of the reflection energy coefficient, $|A_R|^2$ of a BLEUSTEIN-GULAYEV wave, as a function of angle θ in a $LiJO_3$ crystal ($k_{15}^2 = 0.38$)

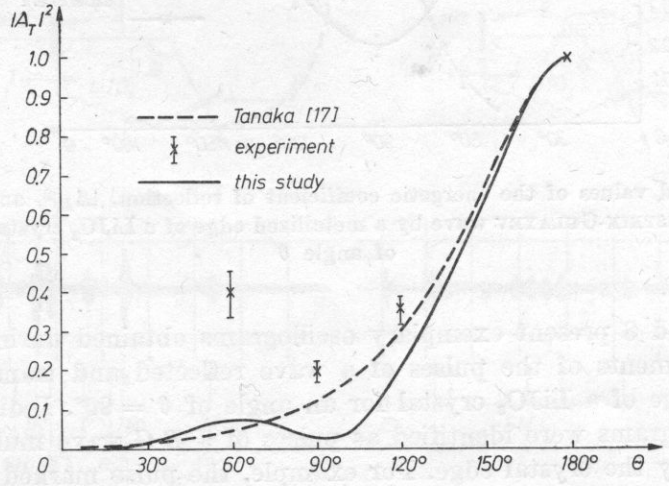

Fig. 11. Theoretical and experimental values of the transmission energy coefficient, $|A_T|^2$, of a BLEUSTEIN-GULAYEV wave, as a function of angle θ in a $LiJO_3$ crystal ($k_{15}^2 = 0.38$)

LEIGH waves are not transverse waves, but have two displacement components: SV and L.

The measured transmission energy coefficient $|A_T|^2$ has a minimum at an angle of $\theta \simeq 90°$ and a maximum at an angle of $\theta \simeq 60°$. The latter can be easily explained on the basis of simple geometrical reasoning for a wave reflected twice between the planes inclined toward each other at an angle of 60°. The profile of the measured transmission energy coefficient is in accordance with formula (7) (Fig. 11).

It is difficult to explain the discrepancies between the calculation and experiment results, due to the low accuracy of the experiment and the imperfection of the calculation method [15].

In order to fully experimentally presented in this paper verify the calculation method, the measurements of the reflection and transmission coefficients should be done for a greater amount of θ angle values, especially in its low value range ($\leqslant 60°$). But carrying out measurements for a large number of the θ angle values is very labour-consuming, because a mechanically seperate sample of considerably big dimensions (~ 3 cm) would have to be made from a difficult in working crystalline material for every case.

Conclusions

1. Calculation results achieved in this work for the reflection A_R^2 and transmission A_T^2 coefficients have all the qualitative features of the measurement results (minima, maxima), and are closer to the experiment results than results obtained by TANAKA [17]. The assumption concerning the absence of multiple reflections between the planes forming the analyzed edge region seems to have the greatest influence on the accuracy of the presented calculation method [15].

2. The increase of the reflection $|A_R|^2$ and transmission $|A_T|^2$ coefficients occuring with the increase of the electromechanical coupling coefficient, found in the work, can be an argument for the existance of a transient layer near the metallized piezoelectric surface.

3. Considering the only qualitative conformity of the calculation results, obtained with the application of existing methods, with the experiment results, a method of integral equations [23] and nummerical methods (finite element [24], boundary element [25]) can be applied in future work on the analyzed effect. These methods allow us to achieve a solution of essentially arbitrary accuracy.

4. A relatively high value of the B-G wave of coefficient reflection, $|A_R|^2$, from a rectangular edge region, enables the construction of a Fabry-Perrot resonator of a quality factor of about 5000, working in a widefrequency band.

Summarizing we have to state, that in order to sget to know fully the complicated reflection and transmission effect of a *B-G* wave by an edge, further theoretical and experimental studies have to be done.

References

[1] J. D. ACHENBACH, *Wave Propagation in Elastic Solids*, North Holland Publishing Company, 1973.

[2] J. L. BLEUSTEIN, *A new surface waves in piezoelectric materials*, Appl. Phys. Lett., **13**, 312 (1968).

[3] Ju. W. GULAJEW, *Electroacoustic surface waves in solids*, ŻETF, **9**, 63 (1969) (in Russian).

[4] E. DIEULESAINT, D. ROYER, *Ondes Elastiques dans les Solides*, Masson et C^ie, (1974), ch. 5 i 6.

[5] P. KIEŁCZYŃSKI, *Propagation of Surface SH Waves In Nonhomogeneous Media*, Journal of Technical Phys., **22**, 1, 73–78 (1981).

[6] E. P. PAPADAKIS, *Ultrasonic phase velocity by the pulse-echo-overlap method incorporating diffraction phase corrections*, JASA, **41**, 1045–1051 (1967).

[7] W. PAJEWSKI, *The excitation and selection of Bleustein-Gulayev waves on piezoelectric ceramics*, Acoustics Letters, **4**, 6, 118 (1980).

[8] W. PAJEWSKI, *Private commonication* (1982).

[9] J. A. WIKTOROW, *Acoustic surface wavesin solids*, Nauka, Moskwa (1981) (in Russian).

[10] L. J. BOND, *A computer model of the interaction of acoustic surface waves with discontinuinuities*, Ultrasonics, **17**, 2, 71 (1979).

[11] E. CAMBAGIO, F. CUPZZO, *Finite difference analysis of surface acoustic waves propagation and scattering in piezoelectric crystalls*, Journal of Computational Phys., **33**, 153 (1979).

[12] W. I. ANISIMKIN, A. I. MOROZOV, *Cyclic ultrasonic delay line with amplification on Bleustein-Gulyaev waves*, ŻETF, **2**, 9, 46 (1976) (in Russian).

[13] J. I. BUROV, C. N. THANK, N. V. ANASTASOVA, *Reflection, transmission and conversion of acoustic suriace waves incident normally onto a quartz wedge with plane Y, X-cut*, Appl. Phys. Lett. **20**, 189 (1979).

[14] W. PAJEWSKI, M. SZALEWSKI, *Reflection of a transverse surface wave from an edge*, Arch. Acoust., **8**, 3–10 (1983) (in Polish).

[15] P. KIEŁCZYŃSKI, *Reflection and transmission of a Bleustein-Gulajew wave by an edge of a space limited by two planes*, Dissertation, IFTR (1984) (in Polish).

[16] A. K. MAL, L. KNOPOFF, *Transmission of Raylegh waves at a corner*, Bulletin of the Seismological Society of America, **56**, 2, 455 (1966).

[17] K. TANAKA, Z. KAWASAKI, *Transmission characteristics of Bleustein-Gulayaev waves at a corner*, J. Appl. Phys., **48**, 9, 1778 (1977).

[18] G. DE JONG, *Integral equation formulation of piezoelectric diffraction problems*, Appl. Sci. Res., **26**, 445 (1972).

[19] I. HERRERA, *On a method to obtain a* GREEN *function for multilayered half space*, Bull. Seism. Soc. Amer., **54**, 4, 1087 (1964).

[20] J. KANE, J. SPENCE, RAYLEIGH, *Wave transmission on elastic wedges*, Geophysics, **23**, 5, 715 (1963).

[21] H. JEFFREYS, *The reflection and refraction of elastic waves*, Monthly Notices Roy. Astron. Soc., Geophysics, Suppl., **1**, 321 (1926).

[22] W. L. Pilant, L. Knopoff, F. Schwab, *Transmission and reflection of surface waves at a corner*, J. Geophys. Res., **69**, 2, 291–297 (1964).

[23] G. de Jong, *Generation of* Bleustein-Gulyaev *waves along a semiinfinite metal coated piezoelectric medium*, IEEE Trans. on Sonics and Ultrasonics, **SU-21**, 187 (1974).

[24] A. J. Jennings, G. K. Cambrell, *Refined finite-element analysis of a clad fiber acoustic waveguide*, IEEE Trans. on Sonics and Ultrasonics, **SU-29**, 5, 239–248 (1982).

[25] C. A. Brebia, *Boundary Element Methods*, Springer, N. York 1981.

[26] H. W. Wyld, *Mathematical Methods for Physics*, The Benjamin Cummings Publ. Comp., 1976.

Received on 28 December, 1984; revised version on 8 October, 1985.

ARCHIVES OF ACOUSTICS
11, 1, 75-88 (1986)

Bi-DIRECTIONAL CONTINUOUS WAVE DOPPLER FLOWMETER AND ITS APPLICATION IN INVESTIGATIONS OF DISTURBED BLOOD FLOWS

MACIEJ PIECHOCKI

Department of Ultrasonics, Institute of Fundamental Technological Research, Polish Academy of Sciences
00-049 Warsaw, ul. Świętokrzyska 21

The paper deals with a new two-way DOPPLER apparatus and with its clinical applications. A mathematical description is given of operations leading to the separation of a signal in dependence of the flow direction. Also a block diagram of an analogue realization of such a system, and a diagram of a broad-band phase shifter, which is the principal part of the system, are presented. The part of the paper dealing wth the applications shortly presents diagnostic methods and new clinical applications of flowmeters, in which the system of separating flow directions plays a significant part.

1. Introduction

This paper is concerned with a continuous wave ultrasonic flowmeter based on the DOPPLER effect, which allows the simultaneous determination of two directions of the blood flow — from and towards the ultrasonic probe. For this reason it is called a two-way flowmeter.

The method of determining the flow direction is the characteristic feature distinguishing the two-way continuous wave flowmeter from hitherto used directional flowmeters. A classical, widely applied coincidential flow detector, described by MCLEOD [5], detects the flow direction, i. e. whether it is directed from or towards the ultrasonic head, with an assumption, that the whole signal reaching the receiver is related to only one of so defined flow directions. The detection system of flow directions, applied in the two-way apparatus and described in a paper by NIPPA et al. [6], separates the received signal into two independent components. Each one is related to one flow

direction. Owing to this independent audio monitoring and flow velocity measurements for every direction are possible, even when they occur simultaneously.

A prototype of such an apparatus was constructed in the Department of Ultrasonics in 1980.

This paper contains construction principles of this flowmeter and a presentation of new diagnostic applications, enabled by this type of instrument.

2. Apparatus construction

The construction of a flowmeter, separating Doppler signals in dependence upon the flow direction, is based on a phase rotation system, described by NIPPA [6].

In the greater part of applications, the transmitting and receiving transducers are placed next to each other in the same casing, forming the so-called DOPPLER probe. The further discussion concers such a positioning of the transducers.

Let us recall the formula for the Doppler frequency of particle i, f_{di} [7]

$$\omega_i = 2(1/c)\pi f_0 v_i \cos\theta_i, \tag{1}$$

where v_i — velocity of particle i, θ_i — angle between the particle velocity and the propagation direction of an ultrasonic wave.

According as the particle dissipating the ultrasonic wave moves from or towards the transducer, what is expressed by the value of angle θ_i, the value of the Doppler frequency can be negative or positive.

Let us note the signal received by the flowmeter as the sum of three components arising from:

— dissipated waves originating from particles moving towards the transducer. In this case the Doppler frequency is positive,

$$U_+(t) = \sum_{i=1}^{N_+} A_i \cos(\omega_0 t + \omega_i t), \tag{2}$$

where A_i — amplitude of a wave dissipated from particle i, f_0 — fequency of carrier wave, f_{di} — Doppler frequency resulting from the particle velocity, according to formula (1), N_+ — quantity of particles moving towards the probe,

— scattered waves originating from particles moving away from the transducer, which have a negative Doppler frequency

$$U_-(t) = \sum_{i=1}^{N_-} A_i \cos(\omega_0 t - \omega_i t), \tag{3}$$

where N_- – quantity of particles moving away from the probe;

– so-called *"leakage"*, which is a sum of the signal transmitted directly from the transmitter to the receiver, due to electric and acoustic couplings, and the signal generated by waves reflected by fixed structures. The frequency of these signals is equal to the carrier frequency of the instrument

$$U_p(t) = D\cos\omega_0 t, \tag{4}$$

where D – resultant amplitude of the *"leakage"* signal.

The complete signal received by the flowmeter is a sum of three mentioned above components: $U_+(t) + U_-(t) + U_p(t)$.

In order to obtain the spearation of signals corresponding to the velocity of particles moving from and towards the probe, several operations have to be conducted on the received signal $U_w(t)$.

In order to investigate the course of these operations in the further part of the paper, it was assumed that the received signal originates from only two particles one moving away from the probe, with a DOPPLER frequency f_{d-} and amplitude A_-, and second, moving towards the probe, with a DOPPLER frequency f_{d+} and amplitude A_+.

Quadrature demodulation, i. e. the multiplication of signal $U_w(t)$, independently by two functions with a frequency ω_0 and phase difference 90° is the first operation.

To simplify the notation, we assume the signals as sinusoidal and cosine. We receive:

$$U_1(t) = U_w(t)\cos\omega_0 t, \qquad U_2(t) = U_w(t)\sin\omega_0 t. \tag{5}$$

Writing equation (5) in respect to signal $U_1(t)$ for example we obtain:

$$U_1(t) = \frac{1}{2} D[\cos(2\omega_0 t) + \cos 0] + \frac{1}{2}\sum_{i=1}^{N_+} A_i[\cos(2\omega_0 t + \omega_i t) + \cos(\omega_i t)] + \\ + \frac{1}{2}\sum_{i=1}^{N_-} A_i[\cos(2\omega_0 t + \omega_i t) + \cos(\omega_i t)]. \tag{6}$$

Performing the adequate summation and applying the filtration of factors related to pulsation 2_o and of the constant component we have:

$$U_1(t) = \frac{1}{2}\sum_{i=1}^{N_+} A_i\cos\omega_i t + \frac{1}{2}\sum_{i=1}^{N_-} A_i\cos\omega_i t \tag{7}$$

and similarly for $U_2(t)$

$$U_2(t) = -\frac{1}{2}\sum_{i=1}^{N_+} A_i\sin\omega_i t + \frac{1}{2}\sum_{i=1}^{N_-} A_i\sin\omega_i t. \tag{8}$$

It can be easily seen, that a 90° phase shift of one of these signals, and then summation and subtraction will cause the separation of the components related to different flow directions. After shifting the phase for signal $U_2(t)$ we obtain

$$U_1'(t) = U_1(t), \tag{9}$$

$$U_2'(t) = -\frac{1}{2}\sum_{i=1}^{N_+} A_i \sin(\omega_i t + 90°) + \frac{1}{2}\sum_{i=1}^{N_-} A_i \sin(\omega_i t + 90°)$$

so

$$U_2'(t) = \frac{1}{2}\sum_{i=1}^{N_+} A_i \cos\omega_i t - \frac{1}{2}\sum_{i=1}^{N_-} A_i \cos\omega_i t.$$

Summing and subtracting signals, $U_1(t)$ and $U_2(t)$, we achieve:

$$\begin{aligned} U_+(t) &= U_1'(t) + U_2'(t) = \sum_{i=1}^{N_+} A_i \cos\omega_i t, \\ U_-(t) &= U_1'(t) - U_2'(t) = \sum_{i=1}^{N_-} A_i \cos\omega_i t. \end{aligned} \tag{10}$$

Consequently we obtain signal $U_+(t)$ from particles moving towards the head, solely, and $U_-(t)$ from particles moving away from the probe.

The practical realization of the signal transformation according to the given above method (Fig. 1) required the construction of electronic systems

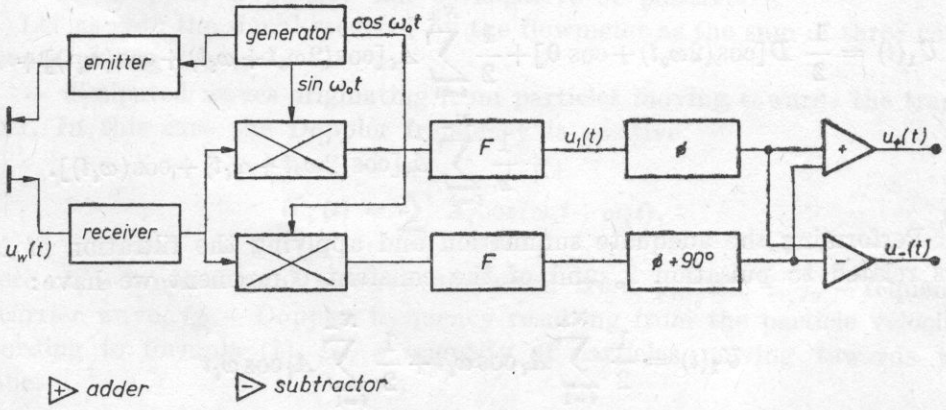

Fig. 1. Block diagram of the system separating a signal in dependence on the particle flow direction

NAD – transmitter, *ODB* – receiver, *GEN* – carrier frequency generator, *X* – multiplying systems, *F* – wide band filtres, $\left.\begin{matrix}\Phi \\ \Phi+90°\end{matrix}\right\}$ – two branches of the high frequency phase pass

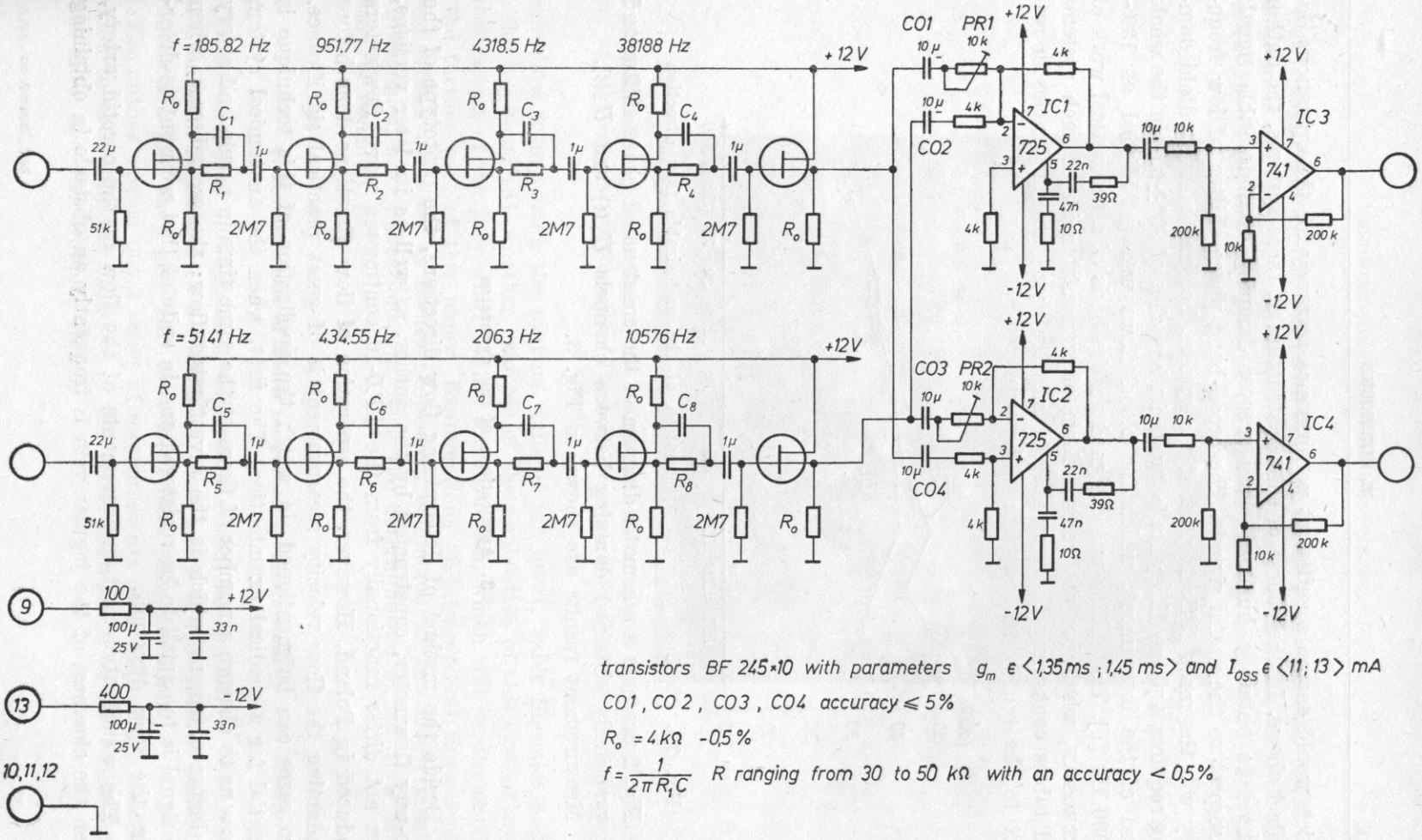

Fig. 2 A. Schematic diagram of the broad band phase shifter

which would ensure a sufficient performance accuracy for the operations described above. In the course of the construction of these systems, the author wanted to obtain a hundred times greater damping of undesirable signals in respect to the useful signals. The broad-band phase shifter of low frequency was the most difficult part of the system, because a hundredfold damping requires a phase difference between its branches of $90° \pm 0.5°$ in the whole band of the instrument, which for blood flows was established at 150 – 15000 Hz [1]. The shifter was designed on the basis of a theoretical work of BEDROSIAN, who gave the general form of transmittancies of such systems and tables containing the parameter values for these transmittancies in respect to the required bandwidth and accuracy [1].

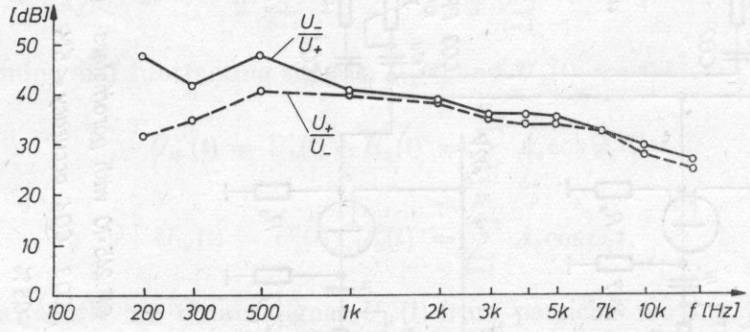

Fig. 2B. Obtained practical attenuation of the undesirable flow direction

Fig. 2 presents a schematic diagram of the constructed phase shifter and the practically obtained damping between channels $U_+(t)$ and $U_-(t)$. Measurement results are shown in Fig. 3.

3. Applications of the apparatus

Beside the method of determining flow directions, the prototype of the two-way flowmeter, constructed by the author, as well as its later versions, does not differ functionally from the *UPD*-10 continuous wave flowmeters produced in Poland. However, the separation of flow directions done before conducting the flow velocity measurement is of great practical significance. Two cases can be mentioned, in which the application of this technique is essential for a medical examination. The first, when the anatomical system forces us to observe a number of flows at the same time in a vein and artery for instance, among which is the investigated flow; the second case, when the signal is too small to be registered and in spite of that we want to determine the flow direction.

The visualization and measurements of the flow in the carotid artery, when the closeness of the jugular vein is frequently an obstacle in obtaining

correct results [10], [3], [4], can be an example of the first case. Also the flow measurements in the heart and in large blood vessels are a lot easier with the application of the two-way system, because it enables us to *"fish out"* the

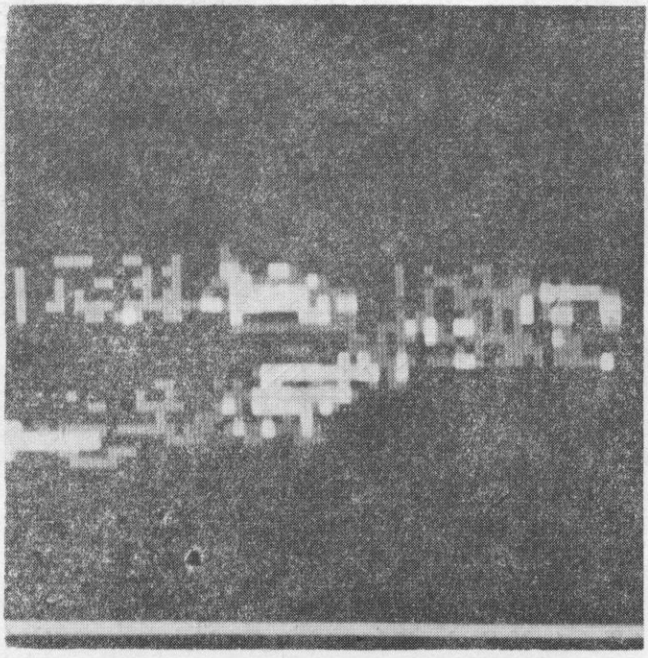

Fig. 3. Visualization of the division of the common carotid artery into the internal carotid artery and the external carotid artery. The brighter points show the flow with increased velocity

sought flow from among the moving walls of the heart, valve floccules and the flowing blood [8]. Another example of the application of this system are investigations of the flow whirl behind a contraction, which will be discussed in the further part of this paper. Examinations of intracerebral flows and investigations of flows in breast neoplasms, conducted in the Department of Ultrasonics, are applications, in which the determination of the flow direction is essential [9].

4. Investigations of whirls introduced by contractions

Observations of flows behind contractions and the published research results on such flows lead to a conclusion, that whirls can be formed behind a contraction and they give rise to a local back flow direction.

The author carried out a series of measurements on a contraction model in order to determine the influence of the vessel contraction on the character of the flow and the Doppler signal.

The use of the two-way instrument allowed the detection and measurement of the back flow velocities resulting from these whirls.

The analysis of the Doppler signal from such flows may be will enable the connection of the parameters of this signal to the vessel contraction degree. The pipe, applied for measurements, had an 8 mm diameter and had rings of 5 mm thickness and of four different internal diameters, placed half-way along its length. This way four different contractions, calculated as a proportional decrease of the flow cross-section area, were obtained. Fig. 4 shows the method of calculating the contraction.

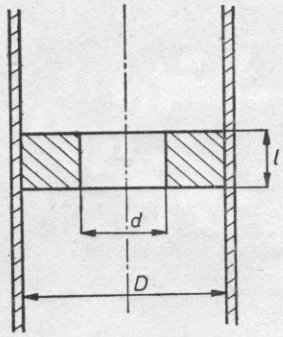

$$ZW = \frac{D^2 - d^2}{D^2} \cdot 100\,\%$$

Fig. 4. Method of determining the pipe contraction

The flow was visualized in order to determine the character of the flow behind the obstacle. To faciliate this, a 17 mm diameter pipe and a ring of 10 mm thickness were used in order to preserve the scale of the mechanism disturbing the flow. A domestic salt solution was used as the liquid and two electrodes connected to a constant voltage source, were placed in the pipe. As a consequence of electrolysis gas bubbles were liberated on one electrode. They were entrained by the flow and marked the stream path of the liquid. Fig. 5 presents a photograph of the flow with a Reynolds number $Re = 500$ and contraction $ZW = 72\,\%$ and $32\,\%$. Three characteristic regions of the flow can be noted. The laminar flow is observed before the obstacle, where paths of the liquid elements are rectilinear and are curved next to the obstacle, forming the so-called inlet effect. Close behind the contraction the outlet stream with a high velocity and whirls by the pipe walls is observed. Further on this stream is disturbed and the liquid elements move with random paths.

Separated signals from individual flow directions were registered on magnetic tape with the application of a stereophonic tape recorder *M 2403 SD*, in order to carry out their analysis.

Signals from flows were registered for four different contractions: $ZW = 75$, 61, 44 and $23\,\%$. For all of these contractions, measurements were conducted for three REYNOLDS numbers: 600, 1900 and 5300, with the signal

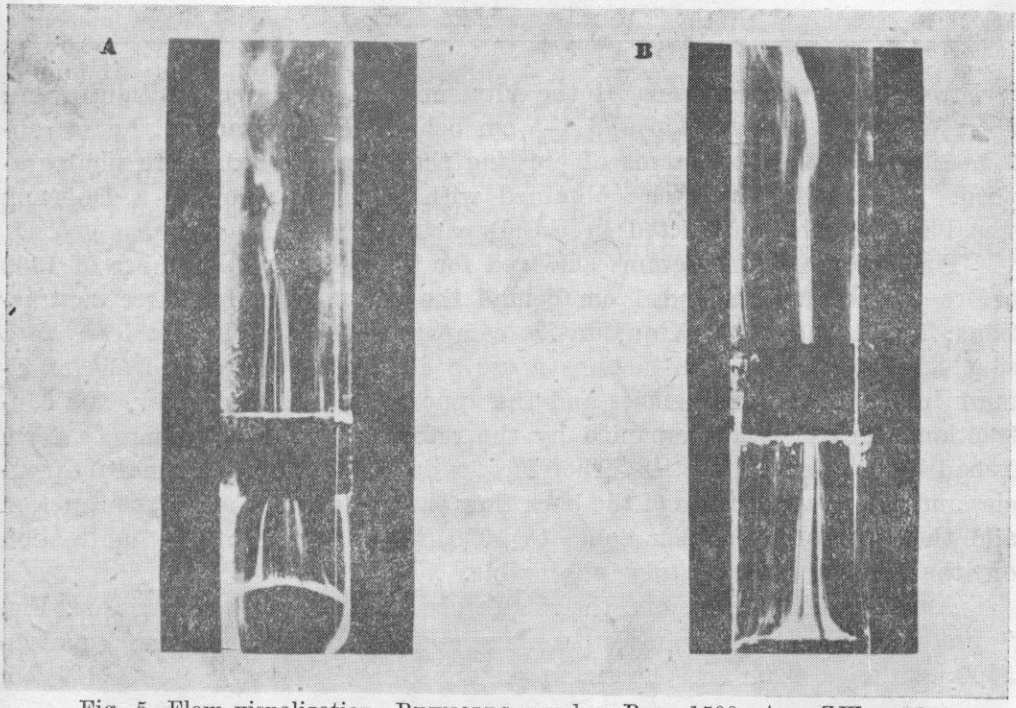

Fig. 5. Flow visualization, REYNOLDS number $Re = 1500$: A $- ZW = 72\,\%$, B $- ZW = 32\,\%$

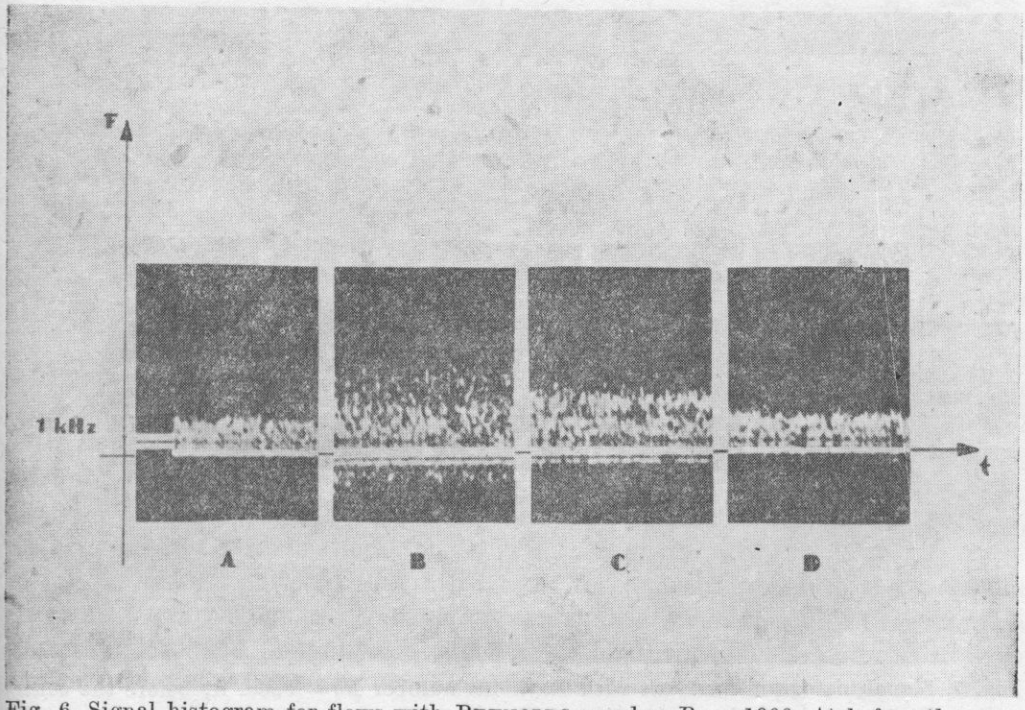

Fig. 6. Signal histogram for flows with REYNOLDS number $Re = 1900$. A) before the contraction, B) 1 cm behind the contraction, $ZW = 75\,\%$, C) 1 cm behind the contraction, $ZW = 61\,\%$, D) 1 cm behind the contraction, $ZW = 44\,\%$

registration for six positions of the ultrasonic head. These positions were: 2 cm before the contraction and 1–5 cm behind the contraction. For so obtained signals, the histograms of crossing the reference axis were photographed. These histograms were obtained with the application of a DOPPLER signal histograph constructed in the Department of Ultrasonics.

Fig. 6 presents histograms achieved for flows Reynolds number of 1900 before the contraction and 1 cm behind the contraction, for three contractions: 75, 61 and 44%. A qualitative comparison fo these images leads to a conclusion, that large contractions cause a significant increase of the maximum instantaneous frequencies and the appearance of a back flow. The contraction decrease is accompanied by the return of the histogram to a form it had before the contraction. Therefore, a decrease of the maximal frequencies and the disappearence of the back flow is observed. For a 44% contraction and the REYNOLDS number equal to 1900, the influence of the contraction on the histogram is hardly observable.

At higher flow velocities the whirls are even more clearly visible. Fig. 7 presents signal histograms from flows with REYNOLDS number equal to 5300, obtained from measurements done before the contraction and 1 cm

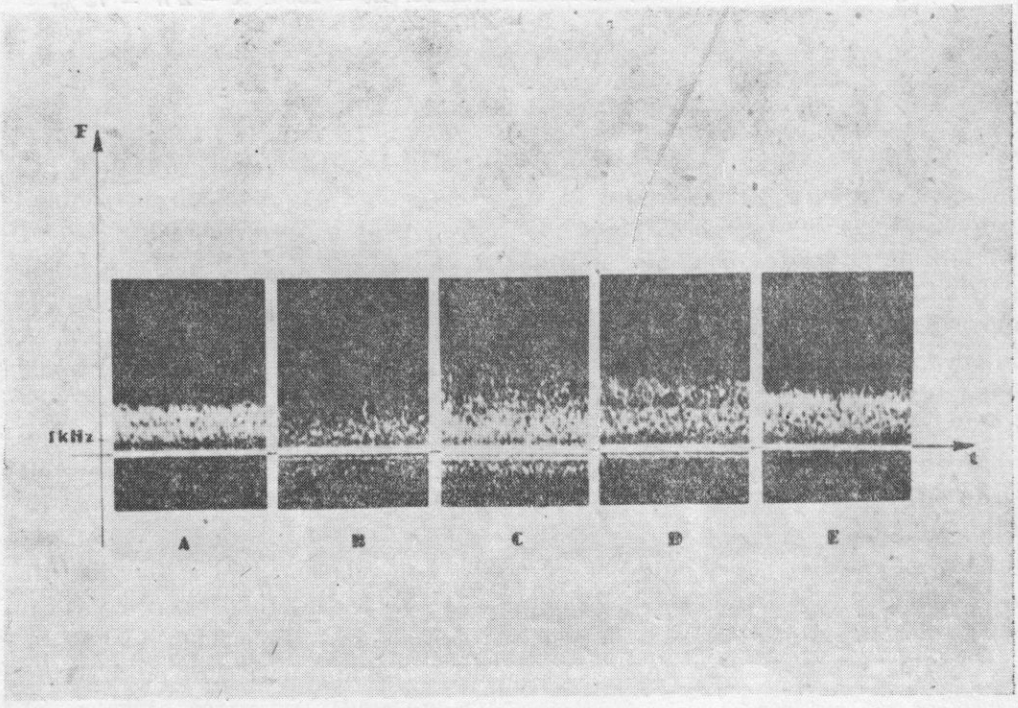

Fig. 7. Signal histogram for flows with Reynolds number $Re = 5300$. A) before the contraction, B) 1 cm behind the contraction, $ZW = 75\%$, C) 1 cm behind the contraction, $ZW = 61\%$, D) 1 cm behind the contraction, $ZW = 44\%$, E) 1 cm behind the contraction, $ZW = 23\%$

behind the contraction, for contractions: 75, 61 and 23%. These results are similar to those shown in Fig. 5. However, a 44% contraction gives a distinct back flow.

Studying the DOPPLER signal in successive points along the vessel we observe similar changes in the histogram as during the decrease of the contraction. This is shown in Fig. 8, where histograms are presented for flows

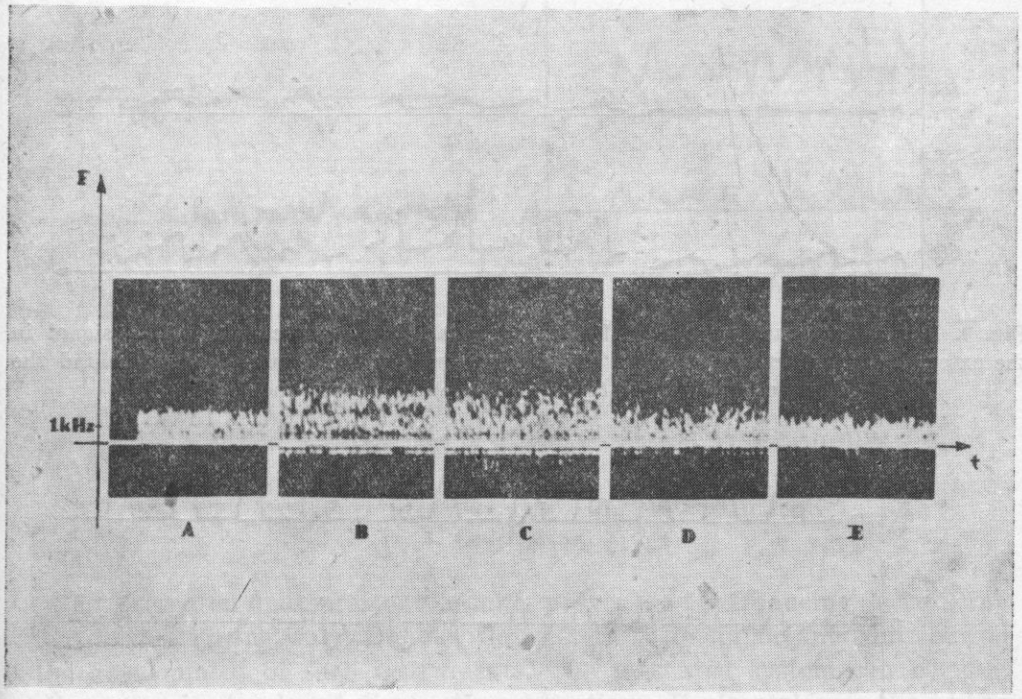

Fig. 8. Signal histograms for flows with REYNOLDS number $Re = 1900$, $ZW = 61\%$. A) before the contraction, B) 1 cm behind the contraction, C) 2 cm behind the contraction, D) 3 cm behind the contraction E) 5 cm behind the contraction

with $Re = 1900$ and in positions: before the contraction, 1, 2, 3 and 5 cm behind the contraction. Again we observe the decrease of the maximal frequencies and the decay of the back flow. This corresponds to the image obtained during the flow visualization.

It should be noticed, that histograms for a position before the contraction and 5 cm behind the contraction are similar, even though in the second case the flow was undoubtedly much more disturbed. This leads to a conclusion, that the influence of homogeneous disturbances on a signal histogram, obtained with the aid of a flowmeter with a continuous emission, is scarcely noticable in the qualitative presentation shown here. The following

conclusions can be drawn on the basis of the presented above observations of flows and histograms originating from them:

1. Flow disturbances introduced by a contraction applied in the experiment depend on the degree of contraction, but also on the distance from the contraction and flow velocity, represented by the Reynolds number in our investigations;

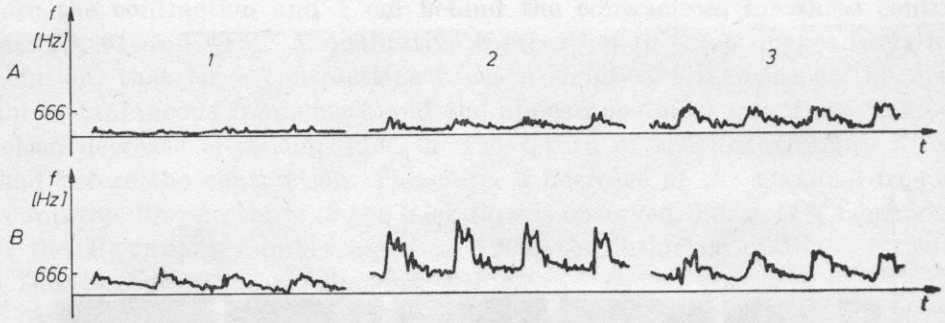

Fig. 9. Results of measurements of the average quantity of zero-crossing of a signal in the external carotid artery. a) before the contraction, b) in the contraction, c) behind the contraction, d) flow to the head, e) flow from the head

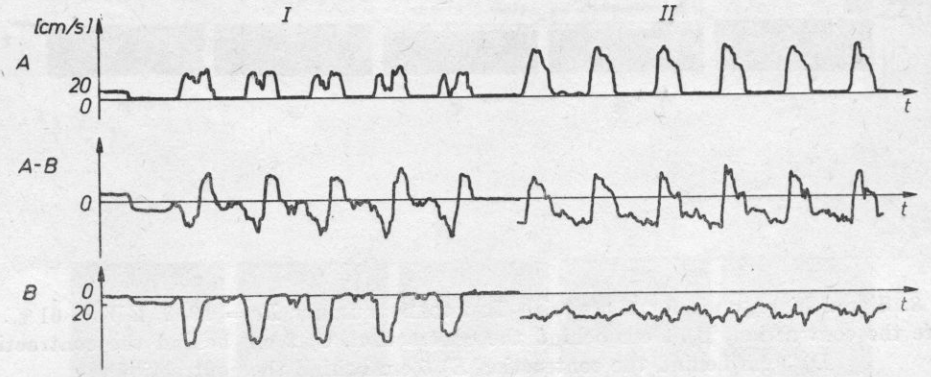

Fig. 10. Results of measurements of the average quantity of zero-crossing. I. descending aorta: A) flow to the probe (artefacts from the common carotid artery), B) folw from the head (aortic flow) A-B difference of flows (here: without practical significance). II. ascending aorta: A) flow to the head (aortic flow), B) flow from the head (artefacts from one of the veins), A-B difference of flows (without practical significance)

2. At a fixed flow velocity and fixed positioning of the probe in respect to the contraction, the degree of the contraction has a significant influence on the existance of the back flow, as well as on the shape of the histogram, what Figs. 6 and 7 prove.

The next stage of research will be concerned with the qualitative relations between the histogram parameters, the Doppler signal spectrum and the degree of the pipe contraction.

Although the flow applied in the experiment greatly strays from the flows in arteries, the obtained results correspond to the results obtained for coarctations of the carotid artery.

Fig. 9 presents the measurement results of the zero-crossing density in a carotid artery. Its Doppler visualization was shown in Fig. 3. A distinct back flow can be observed behind the contraction.

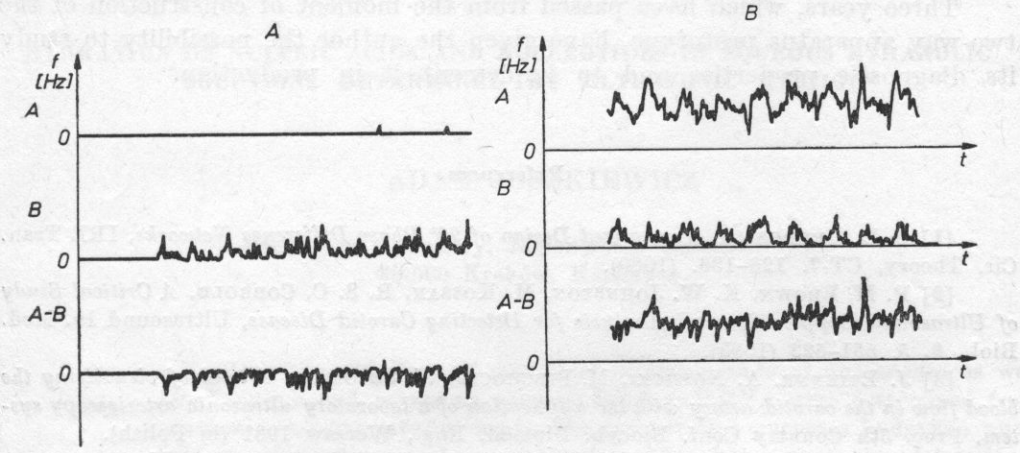

Fig. 11. Results of flow investigations in a breast neoplasm A) benign, B) malignant

5. Conclusions

The presented measurement results prove that introducing a two-way system to continuous wave Doppler flowmeters is an important contribution to the development of such instruments. The presented system can be used in all previously developed diagnostic applications. It also enlarges the utility of diagnostic DOPPLER flowmeters.

The separation of flow directions greatly facilitated the investigations of flows in the carotid artery branching, by eliminating the influence of the vein flows on the measurement results. Presented research of the flow in model contractions led to a fuller interpretation of the flow velocity records obtained practically. The experimental confirmation of the occurence of back flows behind local vessel contractions was a very important result of these investigations. The two-way system allowed the application of continuous wave flowmeters to heart and large blood vessel examinations, as well as the possibility of measuring very high flow velocities, what was impossible with the pulse Doppler apparatus.

The two-way system enabled the application of continuous wave flowmeters in heart and large blood vessel examinations, thanks to the possibility of measuring very flow velocities. The maximal flow velocity occuring

in heart defects can reach several meters per second and are the basis of determining the pressure gradient in contractions.

Stereophonic audio monitoring of the Doppler signal, resulting from the two-way system, ensures great facility of the determination of flow directions, even for very small signals, no longer possible to register with the application of zero-crossing detectors.

Three years, which have passed from the moment of construction of the two-way apparatus prototype, have given the author the possibility to study its diagnostic properties and to implement it in production.

References

[1] S. D. BEDROSIAN, *Normalized Design of 90° Phase Difference Networks*, IRE Tran. Cir. Theory, CT-7, 128–136. (1960).

[2] P. M. BROWN, K. W. JOHNSTON, M. KOSSAN, R. S. C. COBBOLD, *A Critical Study of Ultrasound Doppler Spectral Analysis for Detecting Carotid Disease*, Ultrasound In. Med. Biol., **8**, 5, 551–523 (1983).

[3] J. ETIENNE, A. NOWICKI, M. PIECHOCKI, W. SECOMSKI, *A trial of visualizing the blood flow in the carotid artery with the application of a laboratory ultrasonic arterioscopy system*, Proc. 5th Country Conf. Biocyb. Biomed. Eng., Warsaw 1981 (in Polish).

[4] J. ETIENNE, L. FILIPCZYŃSKI, A. NOWICKI, T. POWAŁOWSKI, M. PIECHOCKI, A. WLECIAŁ, M. BARAŃSKA, *Ultrasonic arterioscope and its application in the diagnostics of carotid arteries*, Proc. 6th Country Conf. Biocyb. Biomed. Eng., Warsaw 1983, Arch. Acoust., **9**, 1–2 (1984).

[5] F. Mc LEAD Jr., *A Directional* DOPPLER *Flowmeter Digest*, 7th Int. Conf. Med. and Biol. Eng. p. 71, Stokholm 1971.

[6] J. H. NIPPA, *Phase Rotation for Separating Forward Reverse Blood Velocity Signal*, IEEE Trans-Sonic. and Ultr., SV-22, 5. (1975).

[7] A. NOWICKI, *Ultrasonic methods of visualizing blood vessels and blood flows* (dissert.), IFTR Reports, Warsaw 1979 (in Polish).

[8] A. NOWICKI, P. KARŁOWICZ, M. PIECHOCKI, W. SECOMSKI, *Estimation of the maximal flow velocity on the basis of* DOOPLER *signal histograms*, Proc. 6th Country Conf. Biocyb. Biomed. Eng., Warsaw 1983 (in Polish).

[9] M. PIECHOCKI, G. ŁYPACEWICZ, T. POWAŁOWSKI, K. ŁUKAWSKA, *Examen des Tumeurs des seins a l'aide de la methode ultrasonore bidirectionalle de* DOPPLER, II Colloque sur les Ultrasonics, Warszawa 1980.

[10] J. M. REID, M. P. SPENCER, *Ultrasonic Doppler Technique for Imaging Blood Vessels*, Science, 1976, 1235–1236 (1972).

Received on 22 August, 1984; revised version on 6 November, 1985.

ARCHIVES OF ACOUSTICS
11, 1, 89-96 (1986)

HYDRATION OF NUCLEIC ACIDS AND NUCLEOTIDES IN AQUEOUS ETHANOLIC SOLUTIONS DETERMINED BY ULTRASONIC METHOD*

ADAM JUSZKIEWICZ

Faculty of Chemistry, Jagiellonian University
30-060 Kraków, Karasia 3

Hydration numbers of mono-and disodium salts of nucleotides as well as of sodium and potassium salts of *DNA* and *RNA* were determined from ultrasonic velocity measurements. For comparative purposes hydration numbers of monosodium and monopotassium phosphates were also determined.

1. Introduction

Hydration of nucleic acids is a subject of numerous experimental and theoretical investigations [1] – [22].

According to Jacobson [23] – [25] the structure of water surrounding macromolecules of DNA is similar in its order to that of ice. The double helix of DNA fits very well into the volume of empty cages in the quasicrystalline tetrahedral structure of water and being built into water lattice it stabilizes this structure. These long-range icelike structures around DNA, however, have not been confirmed by other investigations [7], [26]. NMR studies as well as dielectric constant measurements suggest rather local influence of DNA on the structure of water and bounding some amount of water in hydration sheath in which water molecules form a different structure and have different properties from those in the bulk. Another concept considers two- and three-state models of water. Despite richness of experimental and theoretical material reported so far, neither of the concept has been proved right. Both structure of aqueous sloutions of nucleic acids and the role of each

* This work was partially financed by the Polish Academy of Science (Problem MR. I. 24).

fragment of polinucleotide chains in hydration of macromolecules of DNA have not been clarified yet.

Our studies on the structure of aqueous solutions of various biologically active substances are aimed at the determination of hydration of these substances and of the contribution of the ionic and non-ionic group of such a substance in total hydration.

Our results of measurements of hydration numbers of sugars [27], dextran [28], nucleosides [29], amino acids and oligopetides [30] as well as of 1 : 1 electrolytes [31] were presented previously. This paper presents the results of measurements of hydration numbers of nucleic acids and nucleotides. The preliminary data on this subject were reported previously [32]. In order to examine the role of phosphate groups in the hydration of nucleic acids and nucleotides, the measurements of hydration numbers of monobasic sodium and potassium phosphates were also performed.

2. Experimental

The hydration numbers were determined from the measuerments of ultrasonic velocity in the aqueous ethanolic solutions. The method was described in details elsewhere [27, 33]. Sodium and potassium salts of nucleic acids DNA and RNA, and mono- and disodium salts of nucleotides were used. Sodium and potassium salts of nucleic acids as well as monosodium salts of nucleotides were prepared by slow neutralization of the acids with a 0.1 n base solution, using a slight excess of base. DNA $(C_{39}\ H_{51}\ N_{15}\ O_{25}\ P_4)_n$, *RNA* and 5′-citidine monophosphoric acid (CMP) were from Fluka AG; (5′-adenylic acid) 5′-adenosine monophosphoric acid (AMP) from Centrum Badań Medycznych, Łódź, Poland; disodium derivatives of nucleotides $AMPNa_2$, $UMPNa_2$, $CMPNa_2$, $GMPNa_2$ and $IMPNa_2$ from Fluka AG; 2(3′) -citidine monophosphoric acid from which 2(3′) $CMPNa_2$ was obtained, from Loba, Austria; inorganic phosphates from POCh, Gliwice, Poland.

Hydration of solute H (expressed in grams of water per gram of the solute) was determined from the relation:

$$H = W_x d_0/m, \tag{1}$$

where W_x is the volume, in cm^3, of water bound to m grams of solute and d_0 is the density of water. W_x is determined from the position of maximum of ultrasound velocity in the water-ethanol-solute system using the relation of YASUNAGA [34, 35]:

$$A_0/W_0 = A_1/(W_1 - W_x), \tag{2}$$

where A_0 and W_0 are the volumes of alcohol and water, respectively, at the point of maximum of velocity in the water-ethanol system; A_1 and W_1 are

the volumes of alcohol and water at the piont of maximum in the water-ethanol-solute system.

The hydration number n_t (in moles of H_2O per mole of solute) is determined by the formula:

$$n_t = HM/M_0, \tag{3}$$

where M_0 is the molecular weight of water and M is the molecular weight of the solute.

In the case of nucleic acids n_t was related to the mean molecular weight of nucleotides in DNA and RNA.

The results are presented in Table 1 and 2. For comparative purposes hydration numbers of nucleosides and ribose [29], are placed in Table 2. The values of n_t were measured at 25° C. Assuming that the temperature depen-

Table 1

	M_w	H [g/g]	$n_t\left[\frac{\text{mole}}{\text{mole}}\right]$	$n\left[\frac{\text{mole}}{\text{mole}}\right]$	Error n_t
2/3′-CMPNa$_2$	367	1.09	22.2	20.4	±1.0
5′-CMPNa$_2$	367	1.04	21.2	19.4	±1.0
5′-AMPNa$_2$	391	0.98	21.3	19.5	±1.0
5′-UMPNa$_2$	368	1.04	21.3	19.5	±1.5
5′-IMPNa$_2$	392	1.02	22.2	20.4	±1.5
5′-GMPNa$_2$	407	0.95	21.5	19.7	±1.5

Table 2

	M_w	H [g/g]	$n_t\left[\frac{\text{mole}}{\text{mole}}\right]$	$n\left[\frac{\text{mole}}{\text{mole}}\right]$	Error n_t
AMPNa	369	0.68	14.0	12.2	±1.0
CMPNa	345	0.73	14.0	12.2	±1.0
DNANa	335	0.77	14.3	12.5	±1.5
DNAK	351	0.67	13.1	11.3	±1.5
RNANa	343	0.73	13.9	12.1	±1.5
RNAK	359	0.62	12.6	10.8	±1.5
NaH_2PO_4	120	2.22	14.8	13.0	±1.5
KH_2PO_4	136	1.81	13.7	12.0	±1.5
D-ribose [29]			4.1	2.3	
uridine [29]			2.7	0.9	
cytidine [29]			2.4	0.6	

dence of n_t is similar to that found for 1 : 1 electrolytes, sugars, dextran, carboxylic acids, amino acids and peptides [27]–[33] the hydration number was extrapolated to 0° C using the relation:

$$n = n_t - At - Bt^2, \tag{4}$$

where n is the number of water moles per mole of solute at 0° C, A and B are experimental coefficients equal, respectively, to 0.0383 and 0.0013 and t is the temperature in °C.

3. Discussion

The studies on hydration of sugars [27] revealed that the values of n for various sugars are nearly equal to the average numbers of equatorial groups in cyclic forms of these sugars. According to a model of "specific hydration of sugars" [36], the position and orientation of equatorial —OH groups facilitate hydration interactions of these groups with the molecules of water. If only equatorial groups —OH are hydrated, from the data reported previously [27, 29, 36] it follows that each of these groups is hydrated by one water molecule.

Hydration number of D-ribose $n = 2.3$ (Table 2) is approximatly equal to an average number of equatorial —OH groups. Uridine and cytidine nucleosides have identical hydration numbers, $n = 1$. In nucleosides one equatorial —OH group of the sugar is replaced by a basic pyrimidine group. Hydration number of deoxyuridine deficient in one equatorial hydroxyl group as compared to uridine is equal to zero. Consequently, it can be stated that specific interactions of basic parts of nucleosides with water do not exist; if they exist then in an aqueous ethanolic solution they must be much weaker than water-water or water-ethanol ones. Thus in hydration of nucleosides the main part is played by the sugar component of nucleosides; the basic component is not hydrated. Basic components of nucleosides are not hydrated above all because of their inability to fit into the water lattice since rings of pyrimidine bases are located perpendicularly to the ribofuranose ring which, according to the model of "specific hydration" is built into octahedral water lattice. This inability to fit into the water lattice may result in the process of autcassociation of basic components of nucleosides.

The foregoing conclusions are fully confimed by the obtained results. As shown in Table 1 the obtained values of hydration numbers of $UMPNa_2$, $AMPNa_2$, $CMPNa_2$, $GMPNa_2$ and $IMPNa_2$ are identical within the limits of experimental error ($n = 20$). Therefore hydration numbers of nucleotides are independent of the type of the basic group in the compound. Identical hydration numbers $n = 12$ of CMPNa and AMPNa lead to the same conclusion. Subsequently, comparison of hydration numbers of CMPNa and AMPNa to those of NaH_2PO_4 and KH_2PO_4 indicates that the monovalent cations and phosphate anions of these substances interact with water in a similar way. This also confirms the thesis that basic components of nucleotides are not hydrated. Comparison of hydration numbers of DNANa, DNAK, RNANa and RNAK to those of CMPNa and AMPNa as well as to those of inorganic phosphates sug-

gests the same conclusion. Assuming that sugar components of nucleotides are hydrated in the same way and in the same number ($n = 1$) as in nucleosides it may be concluded that in disodium salts of nucleotides ca. 19 water molecules are bound to sodium ions and the phosphate group $-PO_4^{-2}$. Analogically the number of water molecules bound to the sodium ion and phosphate group $-PO_4H^-$ in CMPNa and AMPNa is equal to 11. Assuming that the hydration number of the sodium ion is equal to 5 [31], the calculated hydration numbers of $-PO_4H^-$ and $-PO_4^{-2}$ are 6 and 9, respectively, and that of the $H_2PO_4^-$ ion is 8 (assuming that the hydration number of Na^+ is the same and that of K^+ is 4 [31]). Similar calculations performed for DNANa and DNAK give the hydration number of the phosphate group equal to 7. For RNANa and RNAK, having taken into account water bound to sugar component, the hydration number of the $=PO_4^-$ group equal to 6 is obtained.

Analysing the obtained results and comparing them with those obtained by others it must be stated that the lack of information about the quality of samples, about the degree of denaturation of DNANa, RNANa, DNAK and RNAK samples obtained by neutralization of the acids with the bases as well as about the structures of DNA and RNA in a mixed ethanol-water solvent does not allow us to draw far reaching conclusions about the structure of water in the vicinity of these macromolecules. Nothwithstanding, by comparing the hydration numbers of alkali metal salts of nucleotides with those of alkali metal salts of phosphoric acid certain observations on interactions of these substances with water can be made:

1° Low values of hydration numbers of DNA and RNA alkali metal salts, similar to those of monobasic sodium and potassium phosphates, indicate that these numbers take into account the water which is bound to primary hydration centers ($=PO_4^-$, Me^+) [37].

2° Nearly indentical values of hydration numbers of DNANa, RNANa as well as of CMPNa and AMPNa suggest that the same concept of their building-in into water lattice should be assumed. According to this concept metal ions, phosphate groups and equatorial $-OH$ groups (if present) orient themselves towards the cages of the icelike structure of water, while pyrimidine bases rings located perpendicularly to ribofuranose rings undergo autoassociation.

As it results from our calculations, a phosphate group binds 6–7 water molecules. This result is in good agreement with the results obtained from experimental studies carried out with the use of other techniques as well as from theoretical calculations. The hydration number of the phosphate group of *DNA* determined by infrared spectroscopic analysis is 4–6 [5, 37, 38]. WOLF and HANLON [39] found this number to be equal to 6. Quantum-mechanical calculations performed by PULLMAN et al. [6, 7, 10] give the number of water molecules in the first hydration layer of phosphate group as equal to 6. The same number for the first hydration layer was obtained by CLEMENTI et al.

[12] from the calculations carried out by means of the Monte Carlo method. The latest NMR studies of DNA [40] show that 5 water molecules are bound to a phosphate group. The experimental data concerning the hydration of phosphate groups also come from the studies of phospholipides. KLOSE et al. [41, 42] established the hydration number of a phosphate group to be 5 by the ^2D NMR method applied for aqueous solutions of dipalmitylphosphatidylcholine. CEVC [43] determined hydration numbers of the $=PO_4H$ group and the $=PO_4^-$ ion as equal to 5 and 7–8, respectively, by studying a group of various phospholipids.

The presented measurement results of hydration numbers of alkali metal salts of nucleic acids are also in agreement with theoretical models given in [44, 45], which explain the role of alkali metal ions in hydration and structure stabilization of DNA. On the basis of the data concerning 1 : 1 electrolytes it was suggested that the hydration number of a sodium ion is equal to 5, not to 6, assuming that similarly to inorganic salt solutions the hydrated sodium ions dispose around the phosphate groups forming with them ionic pairs through one or more polarized water molecules. Mixed alcohol-water solvent of a dielectric constant about 60–70 is undoubtedly a factor facilitating such interactions. The value of the hydration number of a sodium ion lower by 1 results from the assumed principle [31] that a common water molecule binding cation to anion is ascribed to hydration layer of anion. The same values of the hydration number of a sodium ion (5–6) are assumed in [44, 45] and a hydrated sodium ion is thought to locate in a narrow fissure of DNA bihelix, forming a hydrogen bond with phosphate groups.

References

[1] J. L. KAVANAU, *Water and solute-water interactions*, Holden-Day Inc., San Francisco-London-Amsterdam 1964.

[2] D. EAGLAND, *Water — a comprehensive treatise*, F. FANKS Ed., Plenum Press, New York 1975, vol. 4, chapt. 5.

[3] B. LUBAS, *The characteristics of hydration of the DNA macromolecules and the methods of its determination*, Post. Biochem., **18**, 31–57 (1972).

[4] B. LUBAS, *The hydration and the stabilization of the structure and of the conformation states of the DNA macromolecules*, Problems of Modern Biophysics, **6**, 131–200 (1981) (in Polish).

[5] K. A. HARTMAN, R. C. LORD, G. J. THOMAS, *Physico-chemical properties of nucleic acids*, Duchensne J. Ed., Academic Press, New York-London 1973, vol. 2, pp. 18–33.

[6] B. PULLMAN, A. PULLMAN, H. BERTHOD, N. GRESH, *Quantum-mechanical studies of environmental effects of biomolecules VI.* Ab *initio studies on the hydration scheme of the phosphate group*, Theoret. Chim. Acta, **40**, 93–111 (1975).

[7] D. PERAHIA, M. S. JHON, B. PULLMAN, *Theoretical study of the hydration of B-DNA*, Biochim. Biophys. Acta, **474**, 349–362 (1977).

[8] A. PULLMAN, B. PULLMAN, H. BERTHOD, *An SCF ab initio investigation of the "through-water" interaction of the phosphate anion with the Na^+ cation*, Theoret. Chim. Acta (Berl.), **47**, 175–192 (1978).

[9] R. LAVERY, B. PULLMAN, *The molecular electrostatic potential, steric accessibility and hydration of Dickerson's B-DNA dodecamer d(CpGpCpGpApApTpTpCpGpCpGp)*, Nucleic Acids Res., **9**, 3765–3777 (1981).

[10] A. PULLMAN, *Direct versus through-water binding of cations to the phosphate anion*, Stud. Biophys., **84**, 17–18 (1981).

[11] E. CLEMENTI, G. CORONGIU, F. LELJ, *Analytical potentials from ab initio computations for the interaction between biomolecules. V. The phosphate group in nucleic acids*, J. Chem. Phys., **70**, 3726–3729 (1979).

[12] G. CORONGIU, E. CLEMENTI, *Simulations of the solvent structure for macromolecules. I. Solvation of B-DNA double helix at T = 300 K*, Biopolymers, **20**, 551–571 (1981).

[13] V. I. POLTEV, V. I. DANILOV, M. R. SHARAFUTDINOV, A. Z. SHVARTSMAN, N. V. SHULYUPINA, G. G. MALENKOV, *Simulation of the interaction of nucleic acid fragments with solvent using atom-atom potential functions*, Studia Biophys., **91**, 37–43 (1982).

[14] L. A. KOZLOVA, B. I. SUKHORUKOV, *O gidratatsi dezoksyribonukleinovoj kisloty*, Zhur. Fiz. Khim., **48**, 2063–2065 (1974).

[15] P. L. PRIVALOV, G. M. MRIEVLISCHVILI, *Issledovanie sostojania vody v rastvorakh kalorimetriczeskim metodom*, Biofizika, **11**, 951–955 (1966).

[16] P. L. PRIVALOV, G. M. MRIEVLISCHVILI, *Gidratasia makromolekul v nativnom i denaturirovannom sostojani*, Biofizika, **12**, 22–29 (1976).

[17] S. H. SADYKHOVA, F. I. BRAGINSKAJA, *Izutchenie gidratatsi nukleinovykh kislot (DNK i RNK) i ikh proizvodnykh ultrazvukovym metodom*, Biofizika, **20**, 20–22 (1975).

[18] A. P. SARVAZYAN, V. A. BUCKIN, P. HEMMES, *Ultrasonic investigation of solute-solvent and solute-solute interactions in aqueous solutions of bases, nucleosides and nucleotides. 1. Dependence of solute-solvent interactions on the chemical structure of bases, nucleosides and nucleotides*, J. Phys. Chem., **84**, 692–696 (1980).

[19] V. A. BUCKIN, A. P. SARVAZYAN, E. I. DUDCHENKO, P. HEMMES, *Ultrasonic investigation of solute-solvent and solute-solute interactions in aqueous solutions of bases, nucleosides and nucleotides. 2. pH-dependent solute-solvent interactions*, J. Phys. Chem., **84**, 696–699 (1980).

[20] P. HEMMES, A. A. MAYEVSKI, V. A. BUCKIN, A. P. SARVAZYAN, *Ultrasonic investigation of solute-solvent and solute-solute interactions in aqueous solutions of bases, nucleosides and nucleotides. 3. Solute-solute interactions: studies of base stacking by ultrasonic velocity measurements*, J. Phys. Chem., **84**, 699–703 (1980).

[21] P. BENDEL, J. MURPHY-BESCH, T. L. JAMES, *Deuterium NMR in the solid-state and in solution of the molecular motion oi the bases in poly (I) and poly (I) poly (C)*, Biochim. Biophys. Acta, **759**, 205–213 (1983).

[22] J. H. WANG, *The hydration oi deoxyribonucleic acid*, J. Amer. Chem. Soc., **77**, 258–260 (1955).

[23] B. JACOBSON, *Hydration structure oi deoxyribonucleic acid and its physico-chemical properties*, Nature, **172**, 666–667 (1953).

[24] B. JACOBSON, *On the interpretation of dielectric constants of aqueous macromolecular solutions. Hydration of macromolecules*, J. Amer. Chem. Soc., 77) 2919–1926 (1955).

[25] B. JACOBSON, W. A. ANDERSON, J. T. ARNOLD, *A proton magnetic resonance study of the hydration of deoxyribonucleic acid*, Nature, **173**, 772–773 (1954).

[26] H. J. C. BEREDSEN, *Nuclear magnetic resonance study of collagen hydration*, J. Chem. Phys., **36**, 3297–3305 (1962).

[27] A. JUSZKIEWICZ, *Ultrasonic velocity measurements of hydration numbers of sugars in alcohol-water solutions*, Archives of Acoust., **6**, 307–319 (1981).

[28] A. JUSZKIEWICZ, J. POTOCZEK, *Investigations of* the *hydration of dextran using an acoustic method*, Archives of Acoust., **6**, 401–408 (1981).

[29] J. ANTOSIEWICZ, A. JUSZKIEWICZ, D. SHUGAR, *Ultrasonic studies on hydration of pyrimidine nucleosides in aqueous ethanolic solutions*, J. Phys. Chem., **86**, 4831–4834 (1982).

[30] A. JUSZKIEWICZ, *Ultrasonic studies on hydration of carboxylic acids, amino acids and peptides in aqueous ethanolic solutions*, Archives of Acoust., **10** (1985) — in press.

[31] A. JUSZKIEWICZ, *Hydration numbers of electrolytes determined by ultrasonic method*, Polish J. Chem., **10**, 1115–1124 (1984).

[32] A. JUSZKIEWICZ, *Determination of the hydration of DNA and its subunits: nucleosides and nucleotides using acoustical method*. Akustyka molekularna i kwantowa, **3**, 37–43 (1982) (in Polish).

[33] A. JUSZKIEWICZ, J. RANACHOWSKI, *Ultraschallmessungen zur Untersuchung verschiedener physikalisch-chemischer Prozesse in Flüssigkeiten und Lösungen*, Wiss. Zeit. TH Leuna-Merseburg, **24**, 275–286 (1982).

[34] T. YASUNAGA, Y. HIRATA, Y. KAWANO, M. MIURA, *Ultrasonic studies of the hydration of various compounds in an ethanol-water mixed solvent. Hydration of inorganic compounds*, Bull. Chem. Soc. Japan, **37**, 867–871 (1964).

[35] T. YASUNAGA, I. USUI, K. IWATA, M. MIURA, *Ultrasonic studies of the hydration of various compounds in an ethanol-water mixed solvent. II. The hydration of organic compounds*, Bull. Chem. Soc. Japan, **37**, 1658–1660 (1964).

[36] A. SUGGETT, *Water — a comprehensive treatise*, F. FRANKS Ed., New York 1975, vol. 4, chapt. 6.

[37] M. FALK, K. A. HARTMAN, R. C. LORD, *Hydration of deoxyribonucleic acid. II. An infrared study*, J. Amer. Chem. Soc., **85**, 387–391 (1963).

[38] M. FALK, K. A. HARTMAN, R. C. LORD, *Hydration of deoxyribonucleic acid. III. A spectroscopic study of the effect of hydration on the structure of deoxyribonucleic acid*, J. Amer. Chem. Soc., **85**, 391–394 (1963).

[39] B. WOLF, S. HANLON, *Structural transitions of deoxyribonucleic acid in aqueous electrolyte solutions. II. The role of hydration*, Biochemistry, **14**, 1661–1670 (1975).

[40] M. T. MAI, D. E. WEMMER, O. JARDETZKY, *Effects of hydration on the dynamics of deoxyribonucleic acid*, J. Amer. Chem. Soc., **105**, 7149–7152 (1983).

[41] K. GAWRISCH, K. ARNOLD, T. GOTTWALD, G. KLOSE, F. VOLKE, *^2D NMR studies of the phosphate-water interaction in dipalmitoyl phosphatidylcholine-water systems*, Stud. Biophys., **74**, 13–14 (1978), Microfische 1/36–49.

[42] G. KLOSE, K. GAWRISCH, *Lipid-water interaction in model membranes*, Stud. Biophys., **84**, 21–22 (1981).

[43] G. CEVC, *Water and membranes: the interdependence of their physico-chemical properties in the case of phospholipid bilayers*, Studia Biophys., **91**, 45–52 (1982).

[44] V. B. ZHURKIN, J. P. LYSOV, V. I. IVANOV, G. G. MALENKO, *Prostrastviennaja model kompleksa DNK-gidrat Na^+, Molek.* Biologia, **9**, 95–104 (1975).

[45] L. P. DIAKONOVA, G. G. MALENKOV, V. I. DIAKONOV, *Izutchenie vsaimodiejstvia molekul DNK so sredoj methodom Monte Carlo*, Dokl. Akad. Nauk SSSR, **252**, 479–482 (1980).

Received on 26 November, 1984; revised version on 31 May, 1985.

ARCHIVES OF ACOUSTICS
11, 1, 97-116 (1986)

ASSESSMENT OF ULTRASONIC WELDING PROCESS OF POLYCARBONATE BY EMPLOYING THERMAL EMISSION ANALYSIS

JANUSZ ŁOZIŃSKI

Institute of Fundamental Technological Research Polish Academy of Sciences
00-049 Warsaw, Świętokrzyska 21

The thermal effects of ultrasonic welding of polycarbonate foil were considered. A contactless method of measuring temperature was developed, applying the emission of infrared radiation from the zone welded ultrasonically. The distributions of the thermal emission in the weld zone were observed on the oscilloscope screen and registered by a 16-mm camera, by recording the stages of the process every 1/32 sec.

Measurements were performed of the maximum temperature of the ultrasonic welding zone of the polycarbonate foil for three vibration amplitudes of the wave-guide instrument: 30, 35 and 40 μm. The wave-guide instrument was under static pressure ranging from 4.21 MPa to 9.64 MPa. The tensile strength of the weld was measured. It was shown that the static pressure and the vibration amplitude influence strongly on the contributions of the internal friction and the friction between the faces of welded polymer to the thermal emission observed.

1. Introduction

Despite many investigations undertaken in various scientific centres, polymers ultrasonic welding up to now has not been fully described and explained. The character of the process caused by a strong ultrasonic field is the main difficulty. These effects are nonlinear and the general ultrasonic wave propagation laws in elastic media can not be applied.

Many scientists have applied thermocouples and other thermo-sensitive elements. They introduced them into the weld zone, what falsified the measured values due to a strong ultrasonic field. An additional temperature rise at the boundry of both media was the cause of the falsification.

Due to a mismatch of the acoustical impedance of the detector and the studied medium, absorption and diffraction effects occur, forming a thermal

energy source wich adds up with the heat emitted during the propagation of an ultrasonic wave in the investigated polymer. Therefore the readings of the temperature detector are indeterminate resultants falsifying the measurement results.

According to S. S. WOŁKOW [11], the process of joint forming during ultrasonic welding of plastics can be divided into two stages. In the first stage the materials are heated up, and in the second, joints are formed between the surfaces heated up to a temperature ensuring a visco-fluid state. The forming of these joints condition a uniform connection.

The mentioned above author states, that the maximum welding temperature of polyethylene is 473 K. This author also adds that at this temperature the sample with a thermocouple placed in it was extruded from the weld zone during ultrasonic welding.

WOŁKOW considers the amplitude damping coefficient β, and not the modulus of elasticity E, as the decisive factor of the ultrasonic welding of polymers. This coefficient characterizes the absorption effect of mechanical vibrations propagating in the medium, and can be defined by the formula:

$$\xi_x = \xi_0 e^{-\beta x}, \tag{1}$$

where ξ_0 and ξ_x – displacement amplitudes for $x = 0$ and a wave propagating along the x axis.

In the above reasoning the author completly overlooks the fact that formula (1) can be applied only for very small amplitudes and for plane waves,

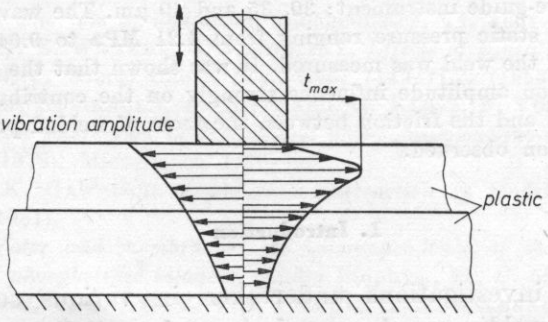

Fig. 1. Distribution of temperature and vibration amplitude in plastic during the process of ultrasonic welding, according to W. A. NEITZERT [19]

what is not the case during welding, which is a markedly non-linear process. WOŁKOW also does not pay any attention to the falsification of the temperature measurement results, what was explained at the begining of the paper.

A very interesting diagram of the temperature distribution in an ultrasonically welded plastic was included in W. A. NEITZERTS paper [15]. As it can

be seen the greatest temperature rise occurs near the welding instrument.

This work would have been of great significance, because it was a trial of a quantitive localization of thermal emission sources in a polymer under an ultrasonic field. Unfortunately the author does not mention the method of deriving this relation and does not motivate in detail the suggested temperature distribution.

B. MENGES and H. POTENTE [18] have conducted very detailed studies on the ultrasonic field and the energetic processes occuring during ultrasonic welding of thermoplastics. Their paper brings results of experiments on the propagation of an ultrasonic wave in bars made from cold hardened epoxy resin. The photo-elastic method was applied. The geometry of the models was so designed, that a standing wave was formed in them. A significant influence of the length of the bars on the vibration amplitude and the amount of transferred acoustical energy, was found.

The same authors in another paper [14] stated the theoretical foundations, supported by experiments, maintaining that energy transfer in thermoplastic bars depends signiticantly on the length of the system: welded element, support.

Owing to the applied contactless measurement method, the obtained results are objective and constitute a valuable information source for acoustic theory, as well as for designers of thermoplastic fittings appropriate for ultrasonic welding.

The work does not include heat measurements, which would allow the determination of the source position of transfer of ultrasonic wave energy into thermal energy, which is the direct cause of polymer melting and the formation of a stable connection.

Basing on the fundamental dependences of wave motion, J. G. STEGER [19] proves that the air at the end of a wave-guide bahaves as an acoustical isolator for an ultrasonic wave propagating in metals.

Through existing surface roughness, two media adjoin, but the contacting surfaces do not lie perpendicularily to the direction of propagation of the ultrasonic wave. These quantities of the ultrasonic field, acting on every point, have two components. One in the direction tangent to the element surface, the second — perpendicular to it. This effect is summed up on the whole boundary surface, giving a motion component of this surface. This component gives rise to a friction force, called the friction of the boundary surfaces. According to the author, this friction is of a fundamental importance the conversion of the ultrasonic energy into heat. H. POTENTE [16] carried out an analysis of the existing state of information on energy conversions occuring in thermoplastic polymers during ultrasonical welding and reached a conclusion that there is no uniformity of views on this problem. Therefore, theoretical trials of estimating the ultrasonic weldability of thermoplasts should be conducted.

H. POTENTE criticizes the measurements of the temperature of the weld zone done with the application of thermocouples, as not reproducible. To this aim he uses a set of sensitive to heat points.

His work is particularily valuable, because it contains temperature measurements of the weld zone, done with the application of a more objective method. The shortcoming of this method is the impossibility of conducting temperature measurements in dynamic conditions, i. e. investigating the temperature growth in the weld zone in the course of a 1–2 sec process. But we have to admit, that this method gives much more credible measurement results then those obtained with the application of detectors sunk into the bulk of the welded polymer.

Those, interested in a more detailed discussion of the literature in this domain, may find it in the authors doctors thesis [12].

1. 1. Conclusions of the critical literature survey

On the basis of the mentioned papers it can be concluded that investigating thermal effects in the welded zone are a very important source of information on the process of ultrasonic welding of thermoplasts. But these methods were most frequently based on the temperature measurements done with the aid of thermocouples placed directly in the polymer, being under the influence of an ultrasonic field. Moreover it can be found, that up to now there is no uniform view on the thermal effects taking place during ultrasonic welding of thermoplasts. On one hand, there are trials of explaining thermal energy formation on the basis of sound absorption, namely mechanical losses due to internal friction; on the other hand, some authors consider that the effect consists in the friction of the boundary surfaces in the joint point.

The experimental problem resolves itself into the development of a proper method of measuring the temperature of the weld zone during the welding process. This is a rather difficult problem, because it has to be solved considering the following fundamental conditions:

a) Temperature measurements will be conducted by the contactless method.

b) The reaction of the detector to temperature changes should be possibly immediate.

c) The measurement will be done by succeeding, linear searching of the whole weld zone.

In the last years research has been conducted at the IFTP on the application of infrared radiadion detection in temperature measurements in the zone of ultrasonic welding [1]–[4], [7]–[11] and also the process of welding of thermoplasts was investigated [5], [6].

The method allowed the observation of the thermal effects taking place during the welding process, without an adverse effect of the meter on the studied object.

The intention of the author was to analyse experimentaly the thermal effects occuring in the ultrasonic weld zone and to study the influence of fundamental physical parameters on the technological process of welding of a chosen amorphous polymer on the basis of the obtained results. Furthermore, the author wanted to undertake a trial of explaining the reasons of melting of the polymer during the process of welding. A polycarbonate, i. e. poly (4,4 dioxidiphenyl-2,2 propanocarbonate) was chosen as the subject of investigation. It is a typical amorphous polymer [17], what minimalizes the thermic disturbances, resulting from phase changes of the individual crystalline forms.

In the investigations of the process of ultrasonic welding of a polycarbonate, a polymer in the form of a foil, produced by BAYER, and called *Makrofol N*, was chosen. The thickness of the foil was 0.2 mm.

2. Temperature measurement on the basis of infrared radiation detection

Every body which has a temperature above O K radiates electromagnetically. The intensity and spectrum of this radiation is determined by the Planck law:

$$m_{\lambda cc} = \frac{2\pi hc^2}{\lambda^5 (e^{hc/(\lambda kT)} - 1)}, \tag{2}$$

where $m_{\lambda cc}$ – the power of radiation to a hemisphere of a unit surface, adequate to a unitary interval of wave length, for a given wave length, λ – radiation wave length, h – Planck constant $= 6.6\ 10^{-34}$ Js, T – temperature in K, c – light velocity $= 3 \cdot 10^8$ ms^{-1}, k – Boltzmann constant $= 1.4 \cdot 10^{-23}$ JK^{-1}.

In a general form, the radiation distribution function of a black body, is an equation with three coordinates: λ, $m_{\lambda cc}$ and T.

The total radiation power emitted to a hemisphere by an unitary surface of a black body equals:

$$M_{cc} = \int_0^\infty m_{\lambda cc} d\lambda = \sigma T^4, \tag{3}$$

where σ – Stefan constant $= 5.67 \cdot 10^{-8}$ Wm^{-2}K^{-4}.

The power of the emitted radiation is a temperature function, so its measurements can be applied in the contactless method of determining the temperature of the studied object.

Usually the studied object is a real body, in which apart from absorption, transmission and reflection, occur.

Therefore, a method of applying a spectrum, where the thermoplastic foil behaves as a black body, i. e. where the reflection and transmission effects practically do not occur, was chosen. In order to find such a range, a characteristic of the infrared absorption spectrum for a *Makrofol N* polycarbonate foil was made. This spectrum is presented in Fig. 2. There is a narrow range in this spectrum, where the absorption equals 100%, so transmission is 0. According to the KIRCHOFF law, the material will behave as a black body in this range.

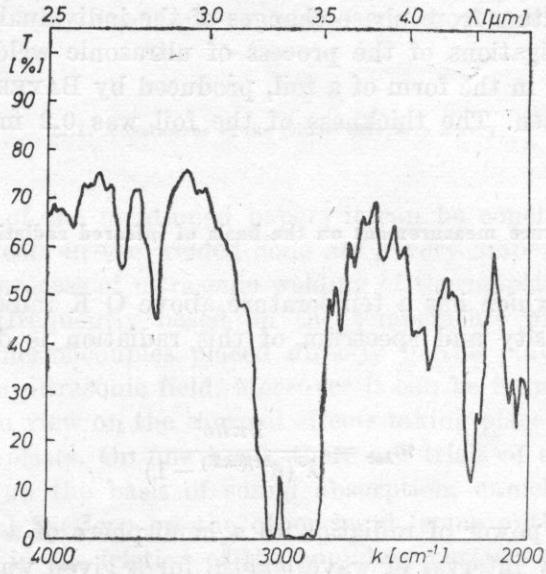

Fig. 2. Characteristic of the *Macrofol N* polycarbonate foil absorption spectrum; T — transmission in %; λ — wave length in μm; k — wave number in cm^{-1}. Beckman Instruments Inc. spectrophotometer

The mentioned conditions are fulfilled for a polycarbonate by the radiation of wave length $\lambda = 3.43$ μm. A signal generated by such radiation on the output of the detector is a function of only the surface temperature of the studied polymer

$$S = F(T_0), \tag{4}$$

where S is the value of the output signal from the detector.

The application of a selective filter, passing the radiation of wave length $\lambda = 3.43$ μm, allowed us to consider the material under research to be a black body.

3. Experimental ultrasonic apparatus and research set-up

The instrument for ultrasonic welding consisted of high frequency ultrasonic lamp generator, which generated a continuous wave of frequency 18.7 kHz, with maximum power of 600 W. The generator with an ultrasonic transducer worked in a feedback loop, securing an automatic tuning during the frequency changes of the free vibrations of the instrument.

The constant time of welding foil samples, equaling 1.3 sec, was ensured by an electronical time-measurer included in the circuit of the generator. It measured time with the accuracy of 0.1 sec.

A nickelic magnetostrictic transducer, connected to a transformer of acoustical vibrations of a sixtuple degree of amplitude transformation, was used as a vibration source.

An aluminium instrument wave-guide was fastened to the acoustical transformer. This wave-guide had a cylindrical section changing into a wegde and with a point at the end, which enables us to obtain a weld of dimensions 1.6×10.2 mm.

The process of welding was carried out on a steel support provided with special holders, making spontaneous movement of the foil during the process impossible.

The transfer of the static pressure to the instrument was done with the aid of weights with the accuracy of ± 10 g.

The amplitude of the vibrations of the wave-guide tip was accepted as an indicator of the ultrasonic energy supplied to the instrument wave-guide. The amplitude was measured by a capacitive meter of the vibration amplitude [18]. The amplitude was maintained at a constant level for every series of measurements.

In the generator of ultrasonic vibrations an electronic system was applied, which stabilized the amplitude of the vibrations of the welding instrument under load changes of the instrument [20].

4. Experiment methods leading to the determination of the temperature distribution in the weld zone in dynamic conditions

Results of experiments conducted on a model set-up have given rise an idea of adapting a serial thermograph "AGA" for the measurements of thermal emission from the weld zone.

The Swedish thermograph – "AGA" 680, enables, the visualization of the surface distribution of the radiation emitted by the investigated zone.

The characteristic of the spectral transmission of the "AGA" thermograph optic system allows to measure the temperature of the weld in the polycarbonate. In order to take advantage of this feature a special filter was designed and produced. Its pass band lied in the range of total absorption of

the polycarbonate. Fig. 3 presents the spectral characteristic of this filter.

The signal at the detector output in the "AGA" thermograph, proportional to the intensity of the infrared radiation, is amplified and utilized to modulate the electron flux in the picture tube. This permits us to obtain on the tube screen the image of the intensity of the infrared radiation emitted by the investigated surface.

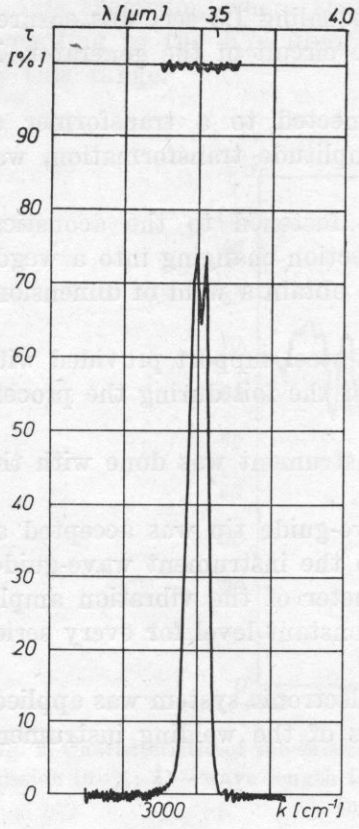

Fig. 3. Characteristic of an infrared filter, being applied in the measurements of the maximal temperature of the ultrasonically welded polycarbonate zone: λ — radiation wave length; k — wave number; τ — radiation transmission

The temperature of the zone very near the object changes in an uncontrol able manner.

This has a significant influence on the signal amplitude at the output of the detector, because the amplitude is a function of the difference between the temperature of the investigated surface of the object and the temperature of the region next to the object. In order to slove this problem, a resistance wire with a constant temperature is introduced in to the field of view of the camera. A holder for the resistance wire is fastened to the support appropriated for sample welding. A signal from the thermistor, fixed to the surface of the wire, controlled the supply source of the wire in such a manner, that the temperature of the wire was constant during temperature changes

of the surroundings – negative feedback. The wire can be deflected, what secures a constant distance of the edge of the foil mounted in the holders. In a position ready for measurement, the wire was 0.4 mm away from the bottom edge of the foil layer lying on the anvil. The measuring system is shown in Fig. 4.

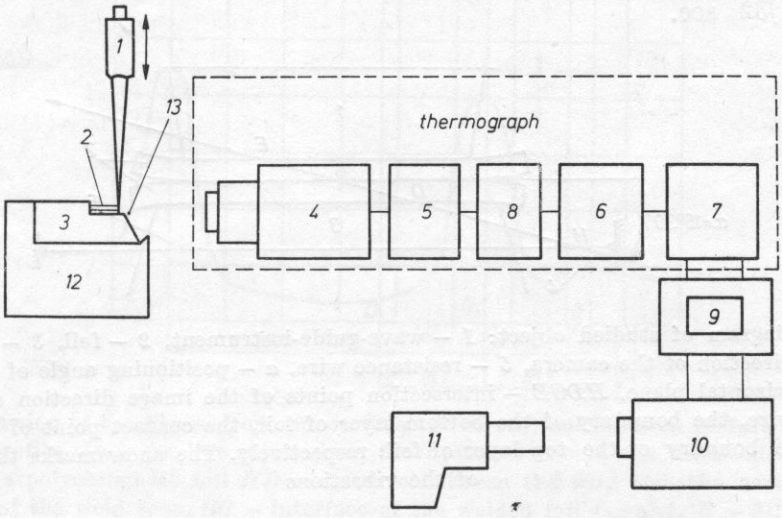

Fig. 4. Measuring system accomodated to the measurement of the temperature distribution in the weld zone in dynamic conditions: *1* – wave-guide instrument, *2* – foil, *3* – anvil, *4* – microscope, *5* – mechanic-optical analyser, *6* – detector, *7* – amplifier, *8* – filter, *9* – monitor, *10* – oscilloscope, *11* – film camera, *12* – support, *13* – resistance wire

4. 1. Description of the weld zone and method of its localization on the osciloscope screen

The tip of the wave-guide was a plaue in the shape of a rectangle, 0.16 cm^2 of surface and with dimentions: 1.6×10.2 mm. Therefore, the investigated object was a thickness weld zone 0.4×10.2 mm in dimention. The process required microscope optics.

Temperature changes in time were determined through the analysis of the amplified signal generated by the radiation emitted from points of the investigated surface, lying on a chosen line, i. e. the signal of the thermovision image line. Positioning the camera suitably in relation to the studied object, the line was chosen in such a way, that it intersected the weld zone, like it is shown in Fig. 5.

Due to the positioning of the camera under an angle of 15°30′, a rectangular zone along the diagonal 1.5 mm in length, was analyzed.

In such a case the output signal of the detector was proportional to the radiation emitted by points lying on the contact of two welded foils, and between the weld line and the foil surface, a like. By switching out a prism with

a horizontal axis of rotation a signal of a 1600 Hz frequency is obtained. This signal was observed on the oscilloscope screen. To register signal changes during the welding process a photographic camera was used.

The film moved with the speed of 32 frames per second. On following film frames the signal corresponding to the temperature profile was registered every 1/32 sec.

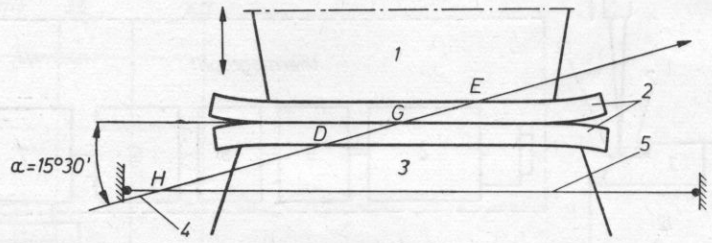

Fig. 5. Diagram of studied object: *1* — wave-guide-instrument, *2* — foil, *3* — anvil, *4* — analysis direction of the camera, *5* — resistance wire, α — positioning angle of the camera in the horizontal plane, *HDGE* — intersection points of the image direction and the resistance wire, the boundary of the bottom layer of foil, the contact point of the welded layers, the boundry of the top layer of foil, respectively. The anow marks the direction of the vibrations

The confrontation of the temperature profiles, registered on following frames of the film show, how, both the value and the distribution of the temperature, change in the foil during the process. On the basis of the optical system parameters of the thermograph and the camera, each point of the temperature profile was assigned to a point in the weld zone. This permitted the determination of the position of the heat source in relation to the boundary surfaces of the welded layers.

The described above method refers of course only to those cases, when both of the welded edges of the welded foil are optically accessible. In a general case, when the weld zone is surrounded from all sides by the welded material, a slight distortion in the temperature pattern may occur, due to a difference of the heat conduction of the material and air. However in the authors opinion, these errors are reduced to minimum and can be neglected, because of the instant reaction of the detector of thermal radiation, which has a propagating velocity uncomparably greater than the heat conduction velocity of the polymer.

4. 2. Determining the value of temperature in the weld zone

The temperature value of the wire did not have to be known. It only served as a constant reference level. A typical temperature profile along the line intersecting the heated wire and the foil weld zone is presented in Fig. 6.

The left side of the diagram corresponds to the heated wire, the right side – to the foil. The difference between the left peak and the other points of the right part of the profile, expressed in volts, is a temperature measure in the individual points of the weld.

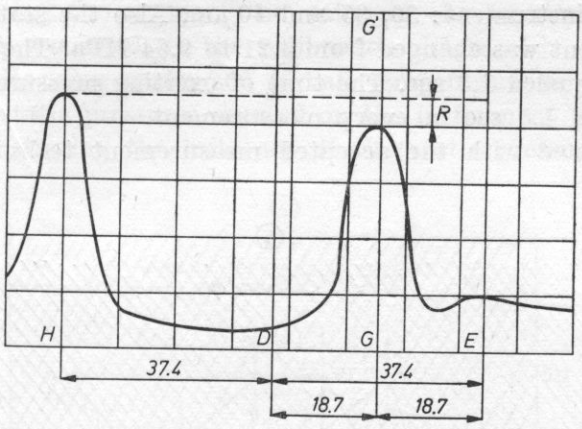

Fig. 6. Drawing of the filmed from the oscilloscope screen thermovision picture of the temperature profile along the line intersecting the heated wire and the ultrasonically welded zone of the polycarbonate foil *HD* – distance between the wire and the sample, DE – thickness of the weld zone, *GG* – interface of the welded foil samples, *R* – difference between the signal level from the heated wire, and a chosen point of the welded zone is the measure of the maximal temperature in a given profile; a difference *R* of 1 mm corresponds to 13.5 mV on the oscilloscope scale HDGE line dimensioning in mm. Sample boundries, broken line, dimensioning and letter denotation have beee drawn in for easier interpretation

In order to determine the absolute temperature value of the foil, the calibration of the mentioned difference *R* was conducted. The error of determining the temperature did not exceed 7 K.

5. Measurement results

5. 1. Strength measurements

An optimization of the technological parameters of the ultrasonic welding process was done on the basis of the strength measurements of the obtained joints. Tensile failure strength was the fundamental strength criterion of the weld for plastic foils.

The strength was measured on testing machine INSTRON, model 1115. Its measurement accuracy is $\pm 0.5\,\%$. Research results were registered by a recorder on paper fed with the velocity of $v_p = 30$ cm/min. The action velocity of the tensile force was $v_z = 5$ cm/min. The tensile strength of the foil was 177 N.

5. 2. Measurement of the maximum temperature value of the weld zone of the polycarbonate foil, as a function of the vibration amplitude and static pressure

Measurements were conducted for three amplitudes of the vibrations of the welding instrument: 30, 35 and 40 μm. Also the static pressure acting on the instrument was changed from 4.21 to 9.64 MPa. The welding time was constant and equaled 1.3 sec. The time of exerting pressure was slightly longer and equaled 1.5 sec in every measurement.

In accordance with the accepted measurement technique, the thermal

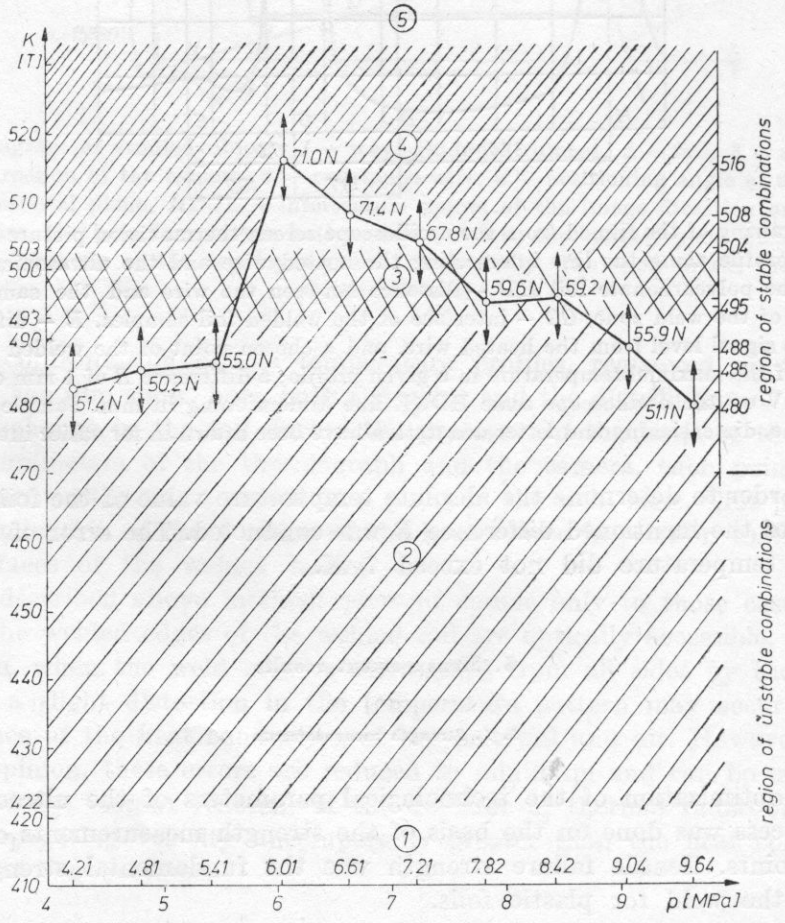

Fig. 7. Influence of static pressure P on the value of the maximal temperature T of the ultrasonically welded zone of the polycarbonate foil, at a vibration amplitude of 30 μm. Digits at the measuring points determine the weld tensile strength: 1) to 422 K — vitrification state, 2) to 493 K — highly elastic state, 3) to 503 K — visco-fluid state, 4) to 533 K — fluid state, 5) above 533 K — decomposition

emission of the wire and the weld zone was visualized at the same time on the oscilloscope screen. These images were documented by a film camera.

The weld zone difference between the peak temperature of the wire and the peak point on the curve of the temperature profile, was measured by employing the previously described measurement method.

After calculating the voltage, the value of the maximum temperature of the weld zone was read of the calibration diagram.

These activities were performed for all temperature profiles, corresponding to different static pressures exerted on the instrument wave-guide. This way diagrams illustrating the influence of the static pressure on the value

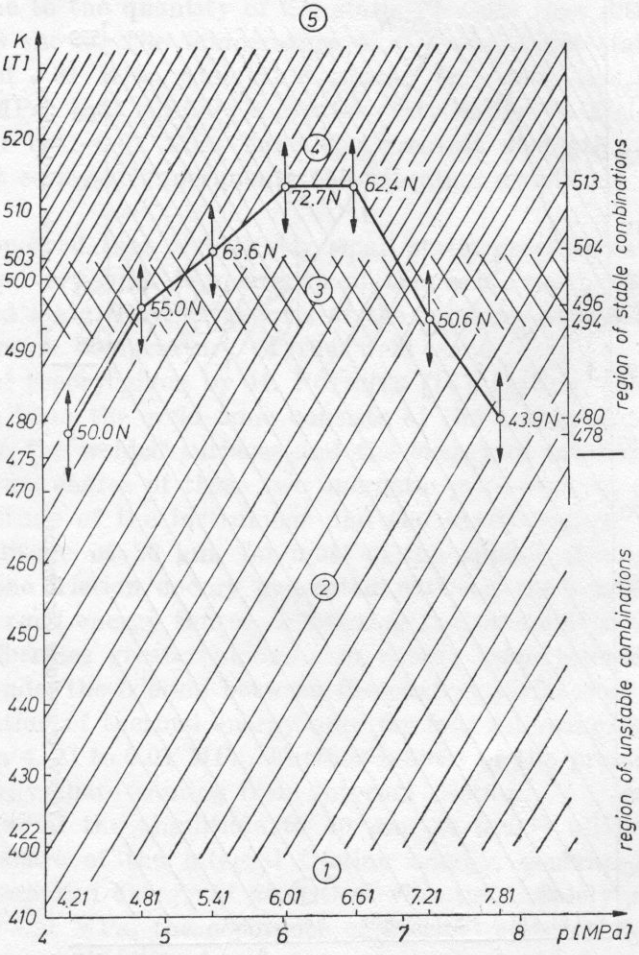

Fig. 8. Influence of static pressure P on the value of the maximal temperature T of the ultrasonically welded zone of the polycarbonate foil, at a vibration amplitude of 35 μm. Digits at the measuring points determine the weld tensile strength: 1) to 422 K — vitrification state, 2) to 493 K — highly elastic state, 3) to 503 K — visco-fluid state, 4) to 533 K — fluid state, 5) above 533 K — decomposition

of the maximum temperature of the weld zone, were obtained and are shown in Figs. 7–9.

On the basis of the measurements performed for an amplitude of 30 μm, it can be seen, that durable welding also takes place in a temperature below the visco-liquid state 3, yet in the top region of the highly elastic state 2 of the investigated polymer. This effect has also been observed for the amplitude of 35 μm. However, the strength of the joints obtained below the 3 state is low. It can be observed particularily when the welding temperature falls below 490 K.

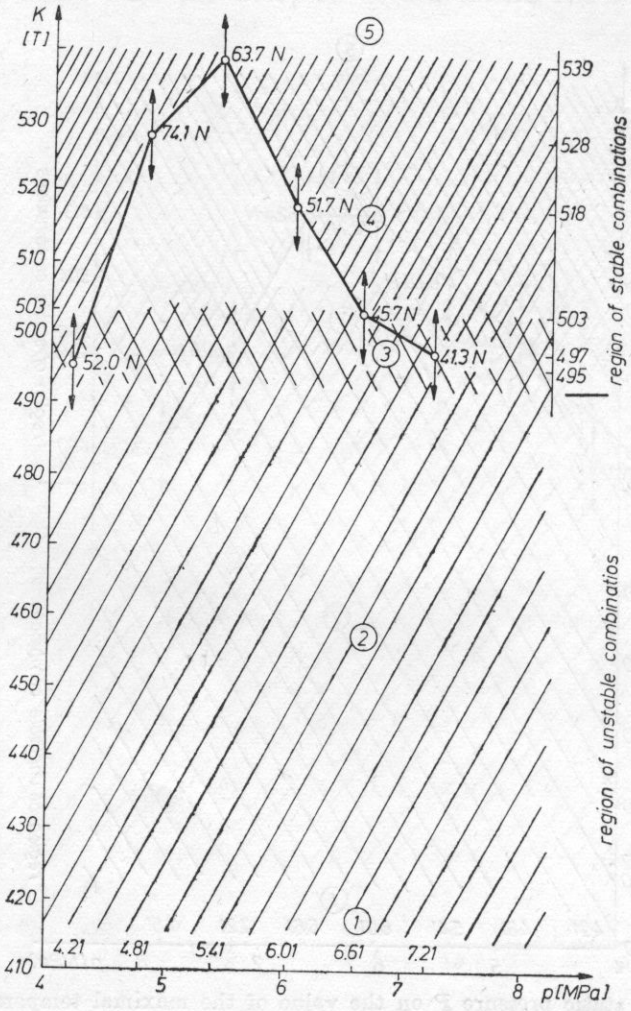

Fig. 9. Influence of static pressure P on the value of the maximal temperature T of the ultrasonically welded zone of the polycarbonate foil, at a vibration amplitude of 40 μm. Digits at the measuring points determine the tensile strength of the weld: 1) to 422 K — vitrification state, 2) to 493 K — highly elastic state, 3) to 503 K — visco-fluid state, 4) to 533 K — fluid state, 5) above 533 K — decomposition

As it can also be seen from Fig. 7, the increase of the pressure initially results in a very small rise of the maximum temperature of the weld and a small strength of the joints. This effect is characteristic for smaller vibration amplitudes. Pressures above 9 MPa cause a distinct deterioration of the joints strength in the latter part of the curve.

This is due to the braking of the amplitude by the pressure. Under pressures above 9.64 MPa the joints was not formed, in spite of the temperature of the weld zone exceeding the point of softening of the polymer.

As it can be seen the figure, in order to reach the highest strength of the welds the pressure must be 6.01–6.61 MPa for an amplitude of 30 μm.

At a higher amplitude the "sensitivity" of the maximum temperature of the weld zone to the quantity of the static pressure rises distinctly, as the curve in Fig. 8 shows. The temperature of the visco-fluid state is achieved at a pressure of 4.81 MPa, while at a smaller amplitude this effect occured at about 5.60 MPa; that is under a greater static pressure. Welds done under the pressure of 5.41–6.61 MPa have the greatest strength.

In the last series of experiments the vibration amplitude was increased to 40 μm.

Then it appeared that a relatively small static pressure causes a sudden attainment of a very high temperature of the weld, much above the state of the visco-fuid state. Further increas of the pressure over 5.40 MPa decreases the maximum temperature of the weld zone.

The general theory given by H. POTENTE [16], stating, that the thermal energy emitted from the weld zone consists of the energy coming from the friction between the welded surfaces and the energy of internal friction, was confirmed. Mutual shares of these two energetic processes yet depend on the vibration amplitude of the instrument and the exerted static pressure. And so, at the amplitude of 30 μm, for most of the applied pressures from 4.21 to 8.42 MPa, the friction energy generated between the contacting surfaces is the main thermal energy source. Increasing the pressure to 9.04, and then to 9.64 MPa liberates greater amounts of energy from internal friction. At a higher amplitude, the friction between the contact surfaces of the foil, cause now the generation of thermal energy only for four following increasing pressures, i. e. from 4. 21 to 6.01 MPa. Further increas of the pressure causes the rise of the energy share coming from internal friction.

The increase of the amplitude to 40 μm, at nearly all pressures, gives the dominant share of the internal friction energy, generated through the change of the supplied energy of acoustical vibrations. Solely under the lowest pressure of 4.21 MPa, the occurence of thermal emission due to the friction between the welded surfaces, was observed.

According to the theory of J. STAGER at al. [19], the heat causing ultrasonic welding of plastics is generated only from friction between the welded surfaces. The results of conducted by the author investigations on the distribution of the thermal energy in the weld zone, prove, that both the energy

from the friction between the contacting surfaces and the internal friction energy take part in the welding process.

Due to a quick attainment of a high temperature, the process of welding is shorter and thanks to smaller pressures the thickness of the joints differ less from the thickness of the welded material. The highest strengths are obtained at a pressure of 4.81 to 5.41 MPa.

5. 3. Influence of the static pressure on the thermal emission distribution in the weld zone and its dependency on the vibration amplitude of the instrument wave-guide

The investigations of the thermal emission in the weld zone were conducted through the analysis of following thermographs of the temperature profiles. The weld zone, marked on the thermographs, shows the position of

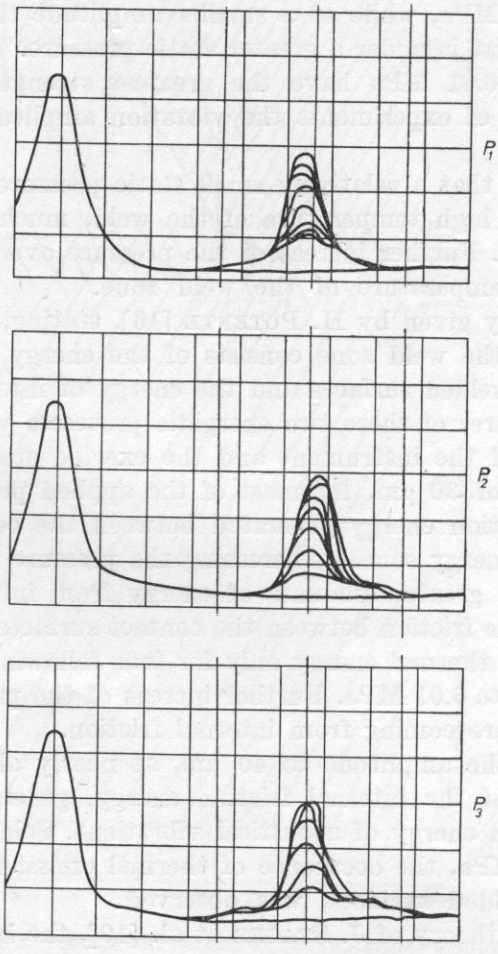

Fig. 10. Examples of thermograph of a temperature profile obtained at an amplitude of 30 μm. The zone enclosing the welded foils has been marked by three vertical lines: P_1 – pressure 4.21 MPa; P_2 – pressure 4.81 MPa; P_3 – pressure 5.41 MPa

the heat emission sources in relation to the contact surface of the welded foil samples.

At the amplitude of 30 μm, the first 8 following thermographs Fig. 10 showed, that the heat was generated in the region of contact of the welded samples. Only at pressures of 9.04 and 9.64 MPa, the heat source moves away from the contact surface.

The thermal emission from the sample joints points to a big share of the energy generated by friction of the two adjoining surfaces. At an adequatly high pressure, the share of the energy generated by internal friction of the polymer macromolecules, in the emitted thermal energy increases.

Welding at an amplitude of 35 μm presented a similar distribution of the thermal energy. However, at a higher amplitude the energy generated

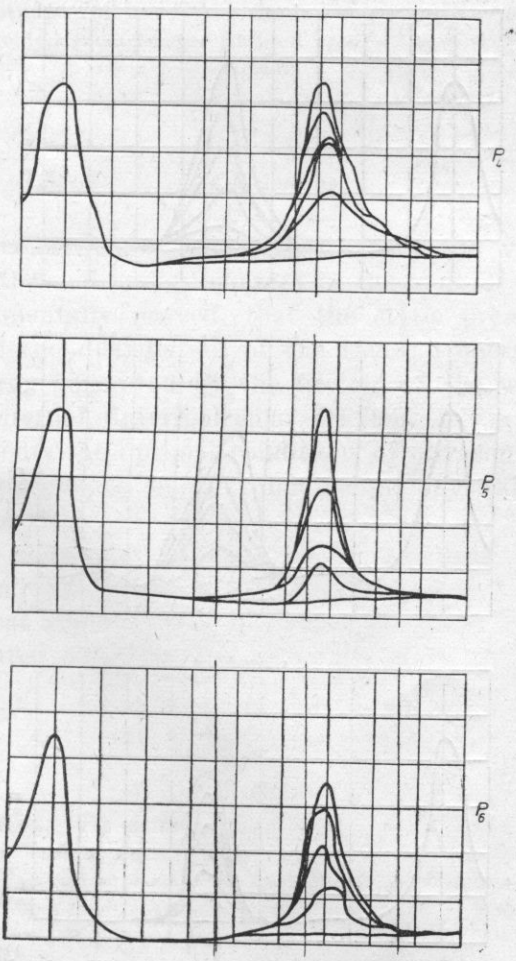

Fig. 11. Examples of thermograph of a temperature profile obtained at an amplitude of 35 μm. The zone enclosing the welded foils has been marked by three vertical lines: P_4 – pressure 6.01 MPa; P_5 – pressure 6.61 MPa; P_6 – pressure 7.21 MPa

by the friction of the welded surfaces has a dominating influence in the first four thermographs. Higher pressures, i. e. 6.61, 7.21 and 7.82 MPa, cause the increase of the share of the thermal energy generated by internal friction (Fig. 11).

Thermographs of the thermal energy distribution at the amplitude of 40 μm, showed that the thermal energy sources were moved away from the contact surface of the foil samples (Fig. 12). Solely thermograph P_1 done at the smallest pressure, i. e. 4.21 MPa, proved a certain share of the heat coming from the friction between the welded surfaces of the foil.

Fig. 13 presents a comparison of the shares making up the total thermal emission from the weld zone in dependence on the vibration amplitude and the static pressure on the instrument wave-guide.

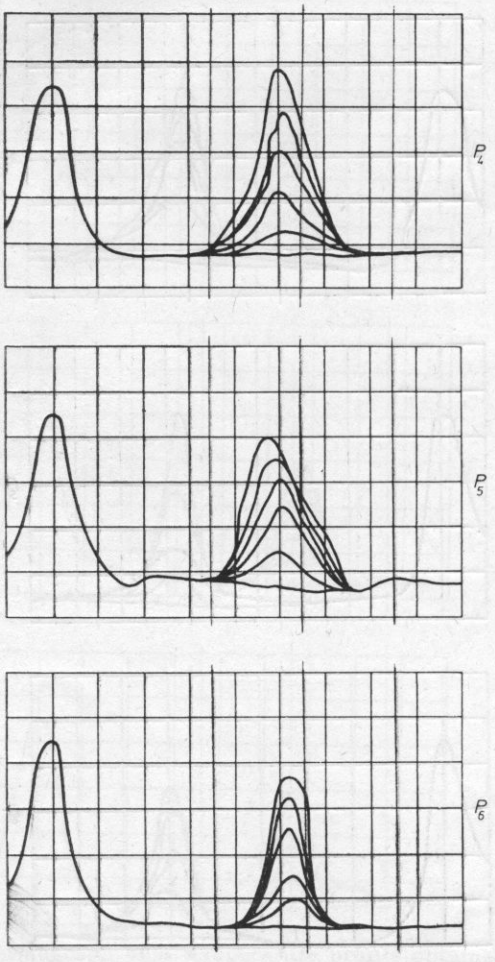

Fig. 12. Examples of thermograph of a temperature profile obtained at an amplitude of 40 μm. The zone enclosing the welded foils has been marked by three vertical lines: P_4 – pressure 6.01 MPa; P_5 – pressure 6.61 MPa; P_6 – pressure 7.21 MPa

The experiment results presented above confirm the theory of H. POTENTE [16], saying that the heat generated during the ultrasonic welding of polymers partially comes from the losses due to internal friction.

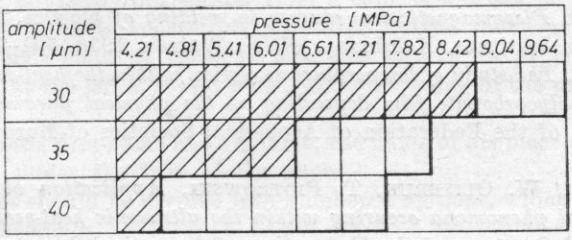

Fig. 13. Influence of static pressure on thermal emission from the weld zone, in dependence on the vibration amplitude. The lined area shows the part of the energy arising from the friction between the welded surfaces, the unlined area — the energy coming from internal friction

6. Conclusions

Conducted thermographic studies have given the visualization of the localization of the thermal energy sources in the zone of ultrasonic welding. It has been experimentally proved, that the static pressure and vibration amplitude influence the distribution of the thermal energy emission, which consists of the energy generated by the friction of the welded surfaces and the engrated by internal, intermolecular friction.

The paper presents the optimal conditions of ultrasonic welding of polycarbonate foil, in dependance on the fundamental physical and technological parameters of the process.

The developed contactless method of investigating thermal effects in the zone of ultrasonic welding with the use of infrared radiation, proved to be useful and of great applicatibility. The absence of the influence of the meter on the investigated object is the main advantage of this method.

References

[1] J. ŁOZIŃSKI, *Contactless method of measuring the temperature of the ultrasonic weld zone*, Proc. of XX Open Seminar on Acoustics, Poznań 1973, 189–190, (in Polish).

[2] J. ŁOZIŃSKI, *Contactless method of temperature distribution monitoring in ultrasonic welded polymers*, The Seventh International Conference on Nondestructive Testing, IFTR, Warsaw 1973, 315–319.

[3] J. ŁOZIŃSKI, T. PIOTROWSKI, *Kinetic and static studies of the temperature distribution in the ultrasonic weld zone in thermoplastic foil*, Proc. of XXI Open Seminar on Acoustics, Rzeszów 1974, 242–243, (in Polish).

[4] J. Łoziński, *Ultrasonic welding oi polyethylene in the view of the observations of the physical parameters of the process*, Proc. of XXII Open Seminar on Acoustics, Wrocław 1975, 517–521, (in Polish).

[5] J. Łoziński, *Ultrasonic welding of thermoplasts*, Polimery – Tworzywa Wielocząsteczkowe, **6**, 294–297 (1975) (in Polish).

[6] J. Łoziński, *Piezomagnetic transducers in welding of plastics*, Proc. of IV Spring School of the Physics Institute, Kołobrzeg, PWN, Warsaw 1978, 751–761, (in Polish).

[7] J. Łoziński, *The study of temperature variation within the heat-seal zone of the ultrasonic heatsealing of polycarbonate film depending on the physical parameters of the process*. The Second Congress of the Federation of Acoustical Societies of Europe, IFTR, Warsaw 1978, 207–211.

[8] J. Łoziński, W. Oliferuk, T. Piotrowski, *Application oi infrared radiation to studying the thermal phenomena occuring within the ultrasonic heat-seal zone of polycarbonate film*, The Second Congress of the Federation of Acoustical Societes of Europe, IFTR Warsaw 1978, 213–218.

[9] J. Łoziński, *Termiczeskije jawlenija w zonie sojedinienja pri ultrazwukowoj swarkie polikarbnatnoj folgi*, Sbornik: Informacionnyje Materiały SEW Instytuta Swarki im. Patona, **1**, 58–72 (1981).

[10] J. Łoziński, W. Oliferuk, T. Piotrowski, *Determination of the temperature distribution in the ultrasonic weld zone in thermoplastic foil, with the application of infrared* radiation detection, Pomiary, Automatyka, Kontrola, **7**, 247–249 (1979), (in Polish).

[11] J. Łoziński, *Study of the influence of static pressure of the thermal emission distribution in the ultrasonic weld zone in thermoplastic foil* in Polish, Proc. of VII Winter School on Molekular and Quantum Acoustics and Sonochemistry, Institute of Fundamen. Technolog. Research, Warszawa 1978, 76–82.

[12] J. Łoziński, *Doctors thesis*, Institute of Foundamental Technological Research, Polish Academy of Sciences, Warsaw 1983, (in Polish).

[13] G. Menges, H. Potente, *Schallfelder und Energieumsetzung beim Ultraschallschweissen von Kunststoffen*, Kunstotoffe, **6**, 369–374 (1969).

[14] G. Menges, H. Potente, *Neue Erkenntnisse beim Schweissen von thermoplastichen Kunststoffen-Ultraschallschweissen*, Plastverarbeiter, **5**, 1–11 (1970).

[15] W. A. Neitzert, *Ultraschall-Verbindungen an Kunststoffen*, Plastverarbeiter, 5, 337–343 (1971).

[16] H. Potente, *Zur Frage der Energieumwandlung beim Ultraschallschweissen von Thermoplasten*, Plastverarbeiter, **8**, 556–562, (1971) and **9**, 653–658 (1971).

[17] D. W. Philips, A. N. North, R. A. Petrick, *Ultrasonic studies of polycarbonate, polysulfone, and polyethersulfone*, Journal of Applied Polymer Science, **21**, 1859–1867 (1977).

[18] B. Peńsko, Z. Toczyski, *The capacity method of distance measurements and its application in the meter of displacement amplitudes of a frequency to 40 kHz*, Proc. of XXII Open Seminar on Acoustics, Wrocław 1975, 565–568, (in Polish).

[19] J. G. Steger, *Einführung in die Ultraschalltechnik*, Kunststofftechnik, **10**, 9, 299–304 (1971).

[20] Z. Toczyski, *Detection oi vibrations of ultrasonic transducers in Polish*, Arch. Akust., **9**, 4, 403 (1974).

[21] S. S. Wołkow, Ju. I. Orłow, R. N. Astachowa, *Swarka i skleiwanie plastmass*, Maschinostrojennie, **52**, Moskwa 1972.

Received on 3 May, 1985; revised version on 21 November, 1985.